

UNIVERSITY OF SOUTHAMPTON  
FACULTY OF PHYSICAL SCIENCES AND ENGINEERING  
Department of Physics & Astronomy

# **Disc Winds Matter: Modelling Accretion and Outflow on All Scales**

by  
James Matthews

A thesis submitted for the degree of Doctor of Philosophy

May 2016



*“Here, on the edge of what we know, in contact with the ocean of the unknown, shines the mystery and the beauty of the world.*

*And it’s breathtaking.”*

Seven Brief Lessons on Physics, Carlo Rovelli

*“Good enough for government work.”*

Christian Knigge



UNIVERSITY OF SOUTHAMPTON

## ABSTRACT

FACULTY OF PHYSICAL SCIENCES AND ENGINEERING

Department of Physics & Astronomy

Doctor of Philosophy

### **DISC WINDS MATTER: MODELLING ACCRETION AND OUTFLOW ON ALL SCALES**

by James Matthews

Outflows are ubiquitous in accreting systems across 10 orders of magnitude in mass, and there is good evidence that mass-loaded winds are launched from the accretion discs of quasars and cataclysmic variables (CVs). Perhaps the most spectacular evidence for accretion disc winds is the blue-shifted, broad absorption lines (BALs) in UV resonance lines, seen in CVs and the BAL quasars. As well as imprinting absorption features on the spectrum, disc winds may also affect the line and continuum emission from accreting objects. They thus offer a natural way to *unify* much of the phenomenology of CVs and active galactic nuclei (AGN).

In this thesis, I use a state-of-the-art Monte Carlo radiative transfer (MCRT) code, PYTHON, to conduct a series of simulations designed to test simple biconical disc wind models. I provide a detailed outline of the MCRT techniques used, before describing a series of code validation exercises. Having tested my methods thoroughly, I explore whether the winds that are responsible for the UV BALs in high-state CVs could also have an effect on the optical spectrum. I find that the wind produces strong emission in the Balmer series, He II 4686 Å and a series of He I lines. The model shows the observed trends with inclination and in some cases produces sufficient recombination continuum emission to fill in the Balmer photoabsorption edge intrinsic to disc atmospheres. The results suggest that disc winds could have a significant impact on the optical spectra of high-state CVs.

The next step was to apply the techniques to quasar winds in a test of disc wind unification models. In previous efforts, the outflow tended to become ‘over-ionized’, and BAL features were only present if the X-ray luminosity was limited to around  $10^{43}$  erg s $^{-1}$ . The outflow also failed to produce significant line emission. Motivated by these problems, I introduce a simple treatment of clumping, and find that it allows BAL features to form in the rest-frame UV at more realistic X-ray luminosities. The fiducial model shows good agreement with AGN X-ray properties and the wind produces strong line emission. Despite these successes, the model cannot reproduce all emission lines seen in quasar spectra with the correct equivalent width (EW) ratios, and I find the emission line EWs have a strong dependence on inclination.

Informed by the quasar wind modelling, I examine the emission line EW distributions of quasars in the context of geometric unification. I find that the observed distributions are not consistent with a model in which an equatorial BAL outflow rises from a foreshortened accretion disc. I discuss this finding in the context of other observational orientation indicators. Finally, I summarise my findings and suggest avenues for future work. Overall, the work presented here suggests that *disc winds matter*. They not only act as a spectral ‘filter’ for the underlying accretion continuum, but may actually dominate the emergent spectrum from accreting objects. As a result, unveiling their

driving mechanisms, mass-loss rates, and ionization structure is an important goal for the astronomical community.

# Contents

<b>Abstract</b>	<b>iv</b>
<b>List of Figures</b>	<b>xi</b>
<b>List of Tables</b>	<b>xv</b>
<b>Declaration of Authorship</b>	<b>xvii</b>
<b>Acknowledgements</b>	<b>xix</b>
<b>Abbreviations</b>	<b>xxi</b>
<b>Physical Constants</b>	<b>xxiii</b>
<b>1 Introduction</b>	<b>1</b>
1.1 The Physics of Accretion . . . . .	3
1.1.1 Spherical Accretion and The Eddington Limit . . . . .	4
1.1.2 Accretion Discs . . . . .	5
1.1.2.1 Steady-state Accretion Discs: the $\alpha$ -prescription . . . . .	6
1.1.3 Boundary Layers, Black Hole Spin and the ISCO . . . . .	8
1.1.4 The Emergent Spectrum . . . . .	10
1.2 Accreting Compact Binaries . . . . .	12
1.2.1 Roche Lobe-Overflow . . . . .	14
1.2.2 Cataclysmic Variables . . . . .	15
1.2.2.1 Dwarf Novae and the Disc-instability Model . . . . .	16
1.2.2.2 Nova-like Variables . . . . .	16
1.2.3 Low Mass X-ray Binaries . . . . .	17
1.3 Quasars and Active Galactic Nuclei . . . . .	20
1.3.1 AGN Unification and the Dusty Torus . . . . .	23
1.3.2 X-ray Properties of AGN . . . . .	24
1.3.2.1 The Soft X-ray Excess . . . . .	26
1.3.3 The Broad Line Region: Connection to Winds and Unification . .	27
1.4 The Current Understanding of the Disc Continuum . . . . .	27
1.4.1 The Spectral Shape of CV Discs . . . . .	27
1.4.2 The Big Blue Bump in AGN . . . . .	29
1.4.2.1 The Accretion Disc Size Problem . . . . .	29
1.4.2.2 Fitting AGN Spectra and the 1000 Å Break . . . . .	29
1.5 The Universality of Accretion . . . . .	30
1.5.1 The RMS-flux relation . . . . .	30
1.5.2 Accretion states and disc-jet coupling . . . . .	31
1.5.3 A Global Picture . . . . .	32

<b>2 Accretion Disc Winds</b>	<b>33</b>
2.1 Observational Evidence . . . . .	33
2.1.1 Cataclysmic Variables . . . . .	34
2.1.2 X-ray Binaries . . . . .	37
2.1.3 AGN and Quasars . . . . .	38
2.1.3.1 Broad Absorption Line Quasars . . . . .	38
2.1.3.2 Warm Absorbers . . . . .	42
2.1.3.3 Ultra-fast Outflows . . . . .	43
2.1.4 Stellar Winds . . . . .	44
2.1.4.1 Clumping in Stellar Winds . . . . .	45
2.1.5 Outflow Physics . . . . .	46
2.2 Driving Mechanisms . . . . .	46
2.2.1 Thermal Winds . . . . .	47
2.2.2 Radiatively Driven Winds . . . . .	48
2.2.3 Line-driven Winds . . . . .	48
2.2.4 Magnetic Winds . . . . .	50
2.3 Accretion Disc Wind Models . . . . .	51
2.3.1 MCGV95: A Line-driven Wind Model for AGN . . . . .	51
2.3.2 De Kool & Begelman: A Radiatively Driven, Magnetically Confined Wind . . . . .	52
2.3.3 Elvis 2000: A Structure for Quasars . . . . .	53
2.3.4 Proga et al.: Line-driven Hydrodynamic Models for AGN and CVs . . . . .	53
2.4 A Kinematic Prescription for a Biconical Wind . . . . .	56
2.5 The big picture: AGN Feedback . . . . .	58
2.5.1 Observational evidence for feedback . . . . .	59
2.5.2 Alternative Explanations . . . . .	62
 <b>Bibliography</b>	 <b>65</b>

# List of Figures

1.1	The temperature profile of an accretion disc for three different classes of compact object. . . . .	8
1.2	Angular velocity as a function of radius in an accretion disc around a rotating compact object. . . . .	9
1.3	The radius of the ISCO, $R_{ISCO}$ , and the horizon, $R_H$ , is as a function of the BH spin parameter, $a_*$ . . . . .	10
1.4	Accretion disc SEDs for three different compact objects. . . . .	11
1.5	A comparison between an accretion disc spectrum computed with black-body and stellar atmosphere spectra. . . . .	12
1.6	Artists impression of an LMXB and CV. . . . .	13
1.7	The Roche potential in a binary system . . . . .	14
1.8	A year in the life of SS Cyg. . . . .	17
1.9	Spectra of SS Cyg during an outburst cycle . . . . .	18
1.10	Optical spectra of three nova-like variables. . . . .	19
1.11	UV spectrum of RW Tri in and out of eclipse. . . . .	20
1.12	Template spectra, from the AGN atlas, for four common types of AGN. .	22
1.13	A unified scheme for AGN. . . . .	24
1.14	Broadband SEDs for different AGN SEDs . . . . .	25
1.15	Occam's quasar . . . . .	28
1.16	Hardness-intensity diagrams for three types of accreting objects. . . . .	32
2.1	A disagram showing how P-Cygni profiles form. . . . .	34
2.2	UV spectrum of the DN TW Vir during outburst. . . . .	35
2.3	UV spectrum of Z Cam, compared to a synthetic spectrum from MCRT simulations. . . . .	35
2.4	The effect of a disc wind on a double-peaked line profile. . . . .	36
2.5	A cartoon illustrating the expected geometry of soft-state LMXB winds. .	37
2.6	Hardness-intensity diagram for four dipping LMXBs. . . . .	38
2.7	Top Panel: A comparison between the SDSS non-BAL, HiBAL and LoBAL composite spectra as presented in Reichard et al. (2003). Bottom Two Panels: Two individual examples of a HiBAL and LoBAL quasar spectrum, respectively. In all panels some of the more prominent lines are labeled and shaded, and the object name is given in the bottom two plots. .	39
2.8	X-ray spectrum of PDS 456 fitted with a P-Cygni profile. . . . .	44
2.9	UV spectrum of one of the O4 supergiant $\zeta$ Puppis. . . . .	45
2.10	Cartoon showing the geometry of the MCGV95 model. . . . .	51
2.11	A cartoon showing the components in the De Kool & Begelman model. .	52
2.12	A schematic showing the main features of the Elvis model. . . . .	54
2.13	Density snapshot of the PK04 model. . . . .	55

2.14 A schematic showing the geometry and kinematics of the SV93 model . . . . .	57
2.15 The SV93 velocity law for various values of the acceleration exponent, $\alpha$ . . . . .	58
2.16 The $M_{BH} - \sigma_*$ correlation. . . . .	60
2.17 The $M_{BH} - M_{bulge}$ correlation. . . . .	61
2.18 Chandra X-ray images showing two examples of X-ray cavities. . . . .	62
2.19 Results of Gaussian line profile fitting to integral field spectroscopy of Mrk 231. . . . .	63

# List of Tables

1.1 Approximate values of compactness and accretion efficiency for four different compact objects. . . . .	4
--	---



# Declaration of Authorship

I, James Matthews, declare that this thesis titled, ‘Disc Winds Matter: Modelling Accretion and Outflow on All Scales’ and the work presented in it are my own. I confirm that:

- This work was done wholly or mainly while in candidature for a research degree at this University.
- Where any part of this thesis has previously been submitted for a degree or any other qualification at this University or any other institution, this has been clearly stated.
- Where I have consulted the published work of others, this is always clearly attributed.
- Where I have quoted from the work of others, the source is always given. With the exception of such quotations, this thesis is entirely my own work.
- I have acknowledged all main sources of help.
- Where the thesis is based on work done by myself jointly with others, I have made clear exactly what was done by others and what I have contributed myself.

The first two chapters of this thesis provide a general introduction to the field, and thus are based on the relevant literature. Where a figure is not produced by me, I have acknowledged this clearly with a credit to the relevant publication. Chapter 3 contains a description of the methods used. This is partly a description of the radiative transfer code PYTHON, which was originally developed by Knox Long and Christian Knigge ([Long & Knigge 2002](#)), but also includes substantial detail on the ‘macro-atom’ technique, which was proposed by Leon Lucy and incorporated into PYTHON by Stuart Sim for a study on young-stellar objects ([Sim et al. 2005](#)). Although I have put significant effort into testing, fixing and developing this scheme, I did not write the original code to deal with macro-atoms in PYTHON.

Chapter 4, 5 and 6 were studies I led under the guidance of my supervisor. For these chapters I conducted all simulations and data analysis, produced all the figures and wrote the text. A publication based on chapter 6 is in preparation, and chapters 4 and 5 are based on the following papers:

- Chapter 4: Matthews J. H., Knigge C., Long K. S., Sim S. A., Higginbottom N., ‘The impact of accretion disc winds on the optical spectra of cataclysmic variables’, 2015, MNRAS, 450, 3331.
- Chapter 5: Matthews J. H., Knigge C., Long K. S., Sim S. A., Higginbottom N., Mangham S. W., ‘Testing quasar unification: radiative transfer in clumpy winds’, 2016, MNRAS, 458, 293.

The following additional publications are not included in this thesis, although some of the work presented here did contribute towards the respective results

- Higginbottom N., Knigge C., Long K. S., Sim S. A., Matthews J. H., ‘A simple disc wind model for broad absorption line quasars’, 2013, MNRAS, 436, 2.3
- Higginbottom, N., Proga D., Knigge C., Long K. S., Matthews J. H., Sim S. A., ‘Line-driven Disk Winds in Active Galactic Nuclei: The Critical Importance of Ionization’ and Radiative Transfer, 2014, ApJ, 789, 1.
- Shankar F., Calderone G., Knigge C., Matthews J. H., et al., ‘The OpticalUV Emissivity of Quasars: Dependence on Black Hole Mass and Radio Loudness’, 2016, ApJ Letters, 818, 1.

Signed:

---

Date:

---

## *Acknowledgements*

First and foremost, I would like to thank Christian Knigge, for being such an enthusiastic, helpful and stimulating supervisor throughout my PhD. Christian, I *always* left our meetings more positive than before – that speaks volumes – and I greatly enjoyed our conversations about science and Explosions in the Sky. I am also extremely grateful to Knox Long for all his assistance, writing the majority of the code and sharing some of his astronomy knowledge with me, and Stuart Sim for being immensely helpful throughout, especially when it comes to radiative transfer. I would also like to thank Nick Higginbottom for hours upon hours of assistance and friendship, and Sam Mangham for his help and input nearer the end of my PhD. To all of the above people; thank you for being part of a collaboration that does some great science, but also knew when to discuss a disastrous code bug with a knowing smile and ironic joke. I would also like to thank Daniel Proga, Omer Blaes, Ivan Hubeny, Shane Davis, Mike Brotherton, Mike DiPompeo, Frederic Marin, Daniel Capellupo, Dirk Grupe, Simo Scaringi, Adam Foster, Randall Smith, Chris Done and countless others for useful correspondence or stimulating scientific conversations.

Apart from those who I worked with, I am grateful to everyone who helped make Southampton a happy place to be over 3+ years. There are too many to name, but I will indulge a few. To my girlfriend Cat, thank you for being so patient with me and for so many lovely evenings. To Sam Connolly, you have been an ever-present and someone who I can always rely on for good beer, music and knowing looks. Sadie Jones, you were there when I needed you most for a cwtch or wanted to hear you pronounce year or ear. To Rob, Aarran, Juan, Georgios and Poppy, thanks for being true friends throughout the process, and big thanks to everyone else in the department for making it a super cool place to work, particularly my other office mates Mari, Judith, Stew and CFro. Thanks also goes to all the staff for being so friendly and approachable, particularly Poshak, Diego and Seb who have all helped me at various points through the PhD, and to Phil Charles for his sage advice since the early days.

There are also many people, outside of Southampton, who I must thank. Most of all, Mum, Dad, Beth and Nick, and the rest of my family. Thanks for supporting me throughout my studies and just being all round lovely people. Thank you Josh, James and Alex, and our now manager John, for allowing me to play music that I love in

Waking Aida. Eschaton and Full Heal were both released during my PhD, and in many ways they are each a thesis within themselves.

In this thesis, figures were produced using the `matplotlib` plotting library. This work made use of the Sloan Digital Sky Survey. Funding for the Sloan Digital Sky Survey has been provided by the Alfred P. Sloan Foundation, the U.S. Department of Energy Office of Science, and the Participating Institutions. I acknowledge the use of the IRIDIS High Performance Computing Facility, and associated support services at the University of Southampton, in the completion of this work.

# Abbreviations

AGN	Active galactic nuclei/nucleus
ADAF	Advection dominated accretion flow
BAL	Broad absorption line
BALQSO	Broad absorption line quasar
BBB	Big blue bump
BEL	Broad emission line
BH	Black hole
BI	Balnicity index
BL	Boundary Layer
BLR	Broad line region
CDF	Cumulative distribution function
CV	Cataclysmic variable
DN(e)	Dwarf nova(e)
EW	Equivalent width
HERG	High excitation radio galaxy
HMXB	High-mass X-ray binary
HSE	Hydrostatic Equilibrium
IP	Intermediate polar
IR	Infra-red
ISCO	Innermost stable circular orbit
LINER	Low ionization nuclear emission-line region
LMXB	Low-mass X-ray binary
LTE	Local thermodynamic equilibrium
MCRT	Monte Carlo radiative transfer
MRI	Magneto-Rotational Instability
NAL	Narrow absorption line

NEL	Narrow emission line
NLR	Narrow line region
NL	Nova-like variable
NS	Neutron Star
QSO	Quasa-stellar object / Quasar
RL	Radio-loud
RIAF	Radiatively inefficient accretion flow
RLOF	Roche lobe overflow
SA	Sobolev approximation
SED	Spectral energy distribution
SFR	Star formation rate
sSFR	Specific star formation rate
SMBH	Supermassive black hole
SXXS	Soft X-ray excess
UFO	Ultra-fast outflow
UV	Ultraviolet
WA	Warm absorber
WD	White dwarf
WHIM	Warm, highly ionized medium
XRB	X-ray binary
YSO	Young stellar object

# Physical Constants

Speed of Light	$c = 2.997\ 924\ 58 \times 10^{10} \text{ cm s}^{-1}$
Boltzmann Constant	$k = 1.380\ 648\ 52 \times 10^{-16} \text{ erg K}^{-1}$
Gravitational Constant	$G = 6.672\ 59 \times 10^{-8} \text{ cm}^3 \text{ g}^{-1} \text{ s}^{-2}$
Solar Mass	$M_{\odot} = 1.988\ 55 \times 10^{33} \text{ g}$
Solar Radius	$L_{\odot} = 6.957\ 00 \times 10^{10} \text{ cm}$
Thomson Cross-Section	$\sigma_T = 6.652\ 458\ 734 \times 10^{-25} \text{ cm}^2$
Planck Constant	$h = 6.626\ 075\ 5 \times 10^{-27} \text{ cm}^2 \text{ g s}^{-1}$
Stefan Boltzmann Constant	$\sigma = 5.670\ 367 \times 10^{-5} \text{ erg cm}^{-2} \text{ K}^{-4} \text{ s}^{-1}$
Parsec	$pc = 3.085\ 677\ 6 \times 10^{18} \text{ cm}$
Proton mass	$m_p = 1.672\ 621\ 58 \times 10^{-24} \text{ g}$
Electron mass	$m_e = 9.109\ 389\ 7 \times 10^{-28} \text{ g}$
Electron volt	$eV = 1.602\ 176\ 57 \times 10^{-12} \text{ erg}$
Charge of an electron	$q_e = 4.803\ 206\ 8 \times 10^{-10} \text{ esu}$
$\pi$	$= 3.141\ 592\ 65$
$e$	$= 2.718\ 281\ 828$



*Dedicated to my family.*



# Chapter 1

## Introduction

“And now you’re asking, I don’t know where to begin”

*Mike Vennart, Silent/Transparent*

The release of gravitational potential energy as mass falls towards a compact object is the most efficient energetic process in the universe, even more efficient than nuclear fusion. This *accretion* process is thought to power the huge radiative engines at the centres of many galaxies – accreting supermassive black holes known as active galactic nuclei (AGN). As the matter falls into the potential well of the black hole, it often forms an accretion disc. This disc is an efficient radiator of the gravitational potential energy released and can sometimes outshine the entire stellar population of the galaxy, appearing as a quasi-stellar object (QSO) or *quasar*. As well as powering AGN, accretion discs are present in X-ray binaries (XRBs), young-stellar objects (YSOs) and cataclysmic variables (CVs). Accretion is a universal process; broadly speaking, the physics is similar regardless of whether matter is falling on to a  $\sim 1 M_{\odot}$  neutron star or white dwarf, or a  $\sim 10^{10} M_{\odot}$  black hole.

Outflows are ubiquitous in accreting systems. We see collimated radio jets in AGN (Hazard et al. 1963; Potash & Wardle 1980; Perley et al. 1984; Marscher 2006) and XRBs (Belloni 2010), and there is even evidence of radio emission in CVs (Benz et al. 1983; Körding et al. 2008; Coppejans et al. 2015). These radio jets tend to appear in specific accretion states (Fender 2001; Fender et al. 2004; Körding et al. 2008), implying an intrinsic connection to the accretion process. Even more intriguing, less collimated,

mass-loaded outflows or *winds* are observed in XRBs in soft accretion states, possibly emanating from the accretion disc (Ponti et al. 2012). Evidence for disc winds is widespread across the mass range, but perhaps the most spectacular indication is the blue-shifted, broad absorption lines (BALs) in the rest-frame ultraviolet (UV) seen in high-state CVs (Heap et al. 1978; Greenstein & Oke 1982; Cordova & Mason 1982) and in the so-called broad absorption line quasars (BALQSOs) that make up 20% – 40% of quasars (Weymann et al. 1991; Knigge et al. 2008; Allen et al. 2011). BALs and ‘P-Cygni’ profiles (Struve 1935; Rottenberg 1952) are also seen in stellar winds (e.g. Cassinelli 1979) and sometimes even in the optical spectra of CVs (Patterson et al. 1996; Ringwald & Naylor 1998; Kafka & Honeycutt 2004). Broad, blue-shifted absorption is also observed in the Fe K $\alpha$  line in some AGN (Reeves et al. 2003; Pounds & Reeves 2009; Tombesi et al. 2010) – these are known as ultra-fast outflows or UFOs.

The astrophysical significance of AGN disc winds extends, quite literally, far beyond the accretion environment. They offer a potential mechanism by which the central accretion engine can interact with the host galaxy and interstellar medium via a ‘feedback’ mechanism (King 2003; Fabian 2012). Feedback is required in models of galaxy evolution (Springel et al. 2005) and may explain the famous ‘ $M_{BH} - \sigma_*$ ’ (Silk & Rees 1998; Häring & Rix 2004) and ‘ $M_{BH} - M_{bulge}$ ’ (Magorrian et al. 1998) relations. Winds also offer a natural way to *unify* much of the diverse phenomenology of AGN, CVs and XRBs. This principle of unification can be applied along more than one ‘axis’ of parameter space. For example, there exist elegant models that attempt to explain *all* of the behaviour of quasars with only a central black hole, a jet, an accretion disc, and an associated outflow, just by varying the viewing angle (Elvis 2000). Similarly elegantly, it has been shown that much of the behaviour of XRBs is directly analogous to AGN (McHardy et al. 2006), and models of outflows in CVs have been successfully ‘scaled-up’ and applied to quasars and AGN (e.g. Higginbottom et al. 2013).

Despite their importance and ubiquity, there are still many unanswered questions relating to the true impact of winds and their underlying physical origins. Here, I aim to address some of these questions and take steps towards building a more holistic picture of the impact of winds on the spectral appearance and accretion physics of disc systems. This thesis is structured as follows. In the remainder of this chapter, I will outline the background accretion theory and highlight the successes and failures of accretion disc models when compared to observations, as well as describing the different classes

of accreting objects in more detail. In chapter 2, I dedicate some time to specifically discussing the theory of, and observational evidence for, accretion disc winds. In chapter 3, I outline the Monte Carlo radiative transfer and photoionization methods I have used in order to investigate the impact of disc winds on the spectra of accreting systems. The next three chapters are based on two publications and one paper in preparation, in which I discuss the impact of disc winds on the spectra of CVs (Chapter 4), and test disc wind quasar unification models (Chapters 5 and 6). In chapter 7, I summarise my findings and their astrophysical significance, and discuss potential avenues for future work.

## 1.1 The Physics of Accretion

The basic phenomenon of accretion – matter falling into a gravitational potential well – is ubiquitous in astrophysics. The energy,  $\Delta E$ , released by a parcel of mass,  $\Delta m$ , falling from infinity onto an object of mass  $M$  and radius  $R_*$  is given by

$$\Delta E = \frac{GM\Delta m}{R_*}, \quad (1.1)$$

meaning that the power generated by mass accreting at a rate  $\dot{M}$  onto this object is given by

$$L_{\text{acc}} = \frac{GM\dot{M}}{R_*}. \quad (1.2)$$

We can also characterise the efficiency of any energetic process by relating the energy released to the rest mass energy of the parcel of mass, such that

$$\Delta E = \eta\Delta mc^2, \quad (1.3)$$

where  $\eta$  is the radiative efficiency. Similarly, in terms of luminosity,  $L$ ,

$$L = \eta\dot{M}c^2. \quad (1.4)$$

Nuclear fusion is one of the more efficient energetic processes in the universe, with an efficiency of  $\eta = 0.007$ . If we rearrange the above equations in terms of  $\eta$ , we find

$$\eta = \frac{G}{c^2} \frac{M}{R_*}. \quad (1.5)$$

Object	$M(M_\odot)$	$R_*(R_\odot)$	$M/R_*(M_\odot/R_\odot)$	$\eta$
White Dwarf	0.8	0.01	79.4	$1.6 \times 10^{-4}$
Neutron Star	1.4	$1.4 \times 10^{-5}$	$10^5$	0.2
Black Hole	10	$4.2 \times 10^{-6}$	$2.4 \times 10^5$	0.5
SMBH	$10^9$	4244	$2.4 \times 10^5$	0.5

TABLE 1.1: Approximate values of compactness and accretion efficiency for four different compact objects with typical parameters. Here,  $R_*$  for black holes is set to the event horizon for a Schwarzschild black hole, whereas values of  $\eta \approx 0.1$  in discs are more realistic due to the presence of an innermost stable orbit (see section 1.1.3). SMBH stands for supermassive black hole.

In other words, the efficiency of accretion is directly related to the *compactness*,  $M/R_*$ , of the central object. Values of compactness and the associated radiative efficiencies for four different compact objects are shown in table 1.1.

### 1.1.1 Spherical Accretion and The Eddington Limit

The simplest geometry one might propose for accretion would be one in which a central mass accretes matter in a spherically symmetric manner. The process of spherical accretion has come to be known as Bondi-Hoyle-Lyttleton accretion ([Hoyle & Lyttleton 1939](#); [Bondi & Hoyle 1944](#)). In particular, [Bondi \(1952\)](#) studied spherically symmetric accretion onto a point mass and derived the Bondi radius,

$$r_B = \frac{GM}{c_S^2}, \quad (1.6)$$

where  $c_S = c_S(r_B)$  is the sound speed as a function of radius. The Bondi radius represents a critical point inside which the material is supersonic and will accrete on the free-fall timescale.

When this timescale is long enough, the accreting matter can radiate away its potential energy, generating a luminosity  $L$ . This radiation will exert a force on the electrons at radius  $r$  in the cloud, given by

$$F_{\text{rad}} = \frac{L\sigma_T}{4\pi r^2 c}, \quad (1.7)$$

where  $\sigma_T = 6.65 \times 10^{-25} \text{ cm}^2$  is the Thomson cross-section. If this outward radiation force dominates over the inward pull of gravity, the material will no longer fall inwards. Consider radiation pressure acting on ionized hydrogen, for which the gravitational force is approximately given by  $F_G \approx GMm_p/r^2$ . Combining this expression with equation 1.7

gives a natural maximum accretion luminosity, known as the *Eddington limit*, of

$$L_{\text{Edd}} = \frac{4\pi GMm_p c}{\sigma_T}, \quad (1.8)$$

with an associated Eddington accretion rate of

$$\dot{M}_{\text{Edd}} = \frac{L_{\text{Edd}}}{\eta c^2}. \quad (1.9)$$

The Eddington limit depends on a number of assumptions, namely that the accretion flow is steady, spherically symmetric, ionized, and that its opacities are dominated by electron scattering. Clearly, there are many astrophysical situations where one or more of these assumptions do not hold. For example, the recent outburst of V404 Cyg showed wildly variable luminosities on short timescales (see, e.g., [Kuulkers et al. 2015](#); [Motta et al. 2015](#), among many, many ATels), and in any binary or disc dominated system the assumption of spherical symmetry will break down. Nevertheless, the Eddington limit provides a good order of magnitude estimate of the maximum luminosity of an accreting object, and also provides a useful way of parameterising accretion rates, as it scales linearly with mass. It can also be used to characterise the *state* of an accretion flow. In general, sources above  $\sim 0.1 L_{\text{Edd}}$  find themselves in a ‘soft’ or thin-disc state (see section 1.1.2.1), whereas for much lower Eddington fractions, sources are expected to harbour geometrically thick, advection-dominated accretion flows (ADAFs; [Narayan & Yi 1994, 1995](#)) or, more generally, radiatively inefficient accretion flows (RIAFs). It is also clear that, near the Eddington limit, radiation pressure must play a major role in determining the disc morphology (see section 2.2.2).

### 1.1.2 Accretion Discs

In many astrophysical situations – for example, in binary systems and gas clouds orbiting BHs – any accreting matter will possess some net angular momentum. If the medium is dense enough, collisions between particles will be frequent, but the total angular momentum vector of two colliding particles will always be conserved. This provides a mechanism for a gas cloud to relax to its minimum energy state – an accretion disc.

As well as losing gravitational potential energy as it falls towards the central mass, a parcel of matter must also lose its angular momentum. Crucially, accretion discs provide a way for this to happen. If the disc overall maintains the same total angular momentum,

it follows that angular momentum must be transported outwards within the disc. The mechanism for transporting angular momentum outwards is unknown, and this is one of the biggest weaknesses of current accretion disc theory. Traditional molecular viscosity is insufficient in this regard ([Pringle 1981](#)). The reasons for this are readily apparent when we consider that molecular viscosity operates over the Debye length,  $\lambda_D$ , and at the sound speed,  $c_s$ . This results in a viscous force density that is much lower than the inertial force density (or in other words, the Reynolds number is much greater than 1). The consequence is that molecular viscosity is dynamically unimportant in accretion flows.

An alternative mechanism for angular momentum transport is therefore necessary. The most commonly invoked candidate is the magnetorotational instability (MRI; [Balbus & Hawley 1991](#)), in which accretion discs are subject to a strong shearing instability even when the magnetic field is weak. Angular momentum could also be lost via a magnetohydrodynamic outflow ([Blandford & Payne 1982](#)) or transported by spiral shock waves ([Ju et al. 2016](#)), although in the former case the disc would actually be dark if a wind extracted all the angular momentum (e.g. [Spruit 1996](#); [Knigge 1999](#)). Given the uncertainty about the transport mechanism, it is convenient to simply parameterise the unknown physics in an *effective viscosity*.

### 1.1.2.1 Steady-state Accretion Discs: the $\alpha$ -prescription

The so-called  $\alpha$ -disc model developed by [Shakura & Sunyaev \(1973\)](#), hereafter SS73) and [Lynden-Bell \(1969\)](#) is a simple approximation for how energy and angular momentum are transported in an accretion disc and provides useful insights into the disc's expected observational appearance. The starting point for this model is a parameterisation of the viscosity,  $\nu'$ , using the simple form

$$\nu' = \alpha c_s H, \quad (1.10)$$

where  $H$  is the scale height of the disc,  $\alpha$  is a parameter  $\leq 1$ , and  $c_s$  is the sound speed. Viscous torques then allow the conversion of orbital kinetic energy into heat, which can be radiated away. If we make one further assumption, that the accretion rate is constant throughout the disc, we can write down a mass continuity equation valid at any radius,

given by

$$\dot{M} \equiv 2\pi R V_R \Sigma = \text{constant}, \quad (1.11)$$

where  $\Sigma$  is the surface density at that radius. The angular momentum equation then becomes

$$\nu' \Sigma = \frac{\dot{M}}{3\pi} \left[ 1 - \left( \frac{R}{R_*} \right)^{1/2} \right]. \quad (1.12)$$

The viscous torques throughout the disc cause a local loss of mechanical energy, allowing us to derive (see, e.g. Frank et al. 1992) a rate of viscous dissipation, per unit area, given by

$$D(R) = \frac{1}{2} \nu' \Sigma (R \Omega')^2. \quad (1.13)$$

Here,  $D(R)$  is proportional to the derivative of the angular velocity,  $\Omega' = d\Omega/dR$ . By combining equations 1.13 and 1.12, we can show that the viscous dissipation rate is

$$D(R) = \frac{G M \dot{M}}{8\pi R^3} \left[ 1 - \left( \frac{R}{R_*} \right)^{1/2} \right], \quad (1.14)$$

where we have also set the angular velocity to the Keplerian velocity. This expression is independent of viscosity – which is fortunate, because we do not know what value of  $\alpha$  to use in equation 1.10. This result comes about because of the implicit assumption that the viscosity regulates the mass accretion rate so as to achieve a steady state.

We can now integrate across both sides of the whole disc to obtain the disc luminosity,

$$L_{\text{disc}} = 2 \int_{R_*}^{\infty} D(R) 2\pi R dR = \frac{G M \dot{M}}{2 R_*} = \frac{1}{2} L_{\text{acc}}. \quad (1.15)$$

This result can also be shown by considering the difference in gravitational binding energy of gas in Keplerian rotation at  $R = R_*$  and  $R = \infty$ . From equation 1.14, an effective temperature distribution can be derived by setting

$$\sigma T_{\text{eff}}^4(R) = D(R), \quad (1.16)$$

which then gives

$$T_{\text{eff}}(R) = T_* \left[ 1 - \left( \frac{R}{R_*} \right)^{1/2} \right]^{1/4}, \quad (1.17)$$

where

$$T_* = \left( \frac{3 G M \dot{M}}{8\pi R_*^3 \sigma} \right)^{1/4}. \quad (1.18)$$

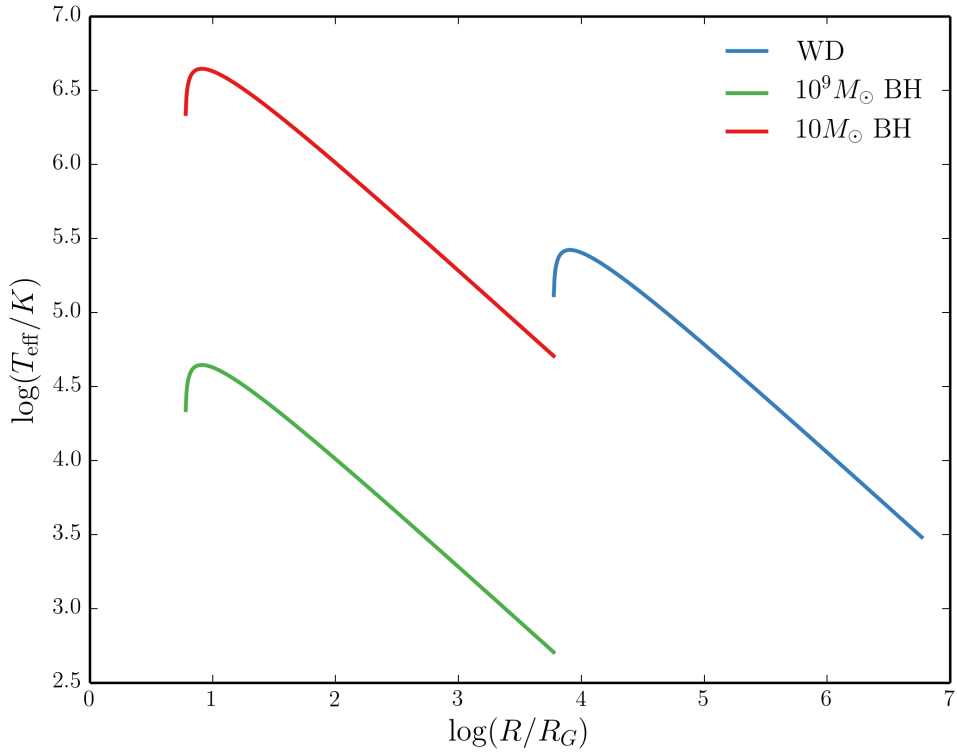


FIGURE 1.1: The temperature profile of an accretion disc for three different classes of compact object.

When  $R \gg R_*$  this simplifies to

$$T_{\text{eff}}(R) = T_*(R/R_*)^{-3/4}. \quad (1.19)$$

Now we have not only derived the total luminosity of an accretion disc, but also the effective temperature profile which will govern the shape of the emergent SED. This temperature profile is shown in Fig. 1.1 for three different compact objects, assuming an Eddington fraction of 0.2.

### 1.1.3 Boundary Layers, Black Hole Spin and the ISCO

In equation 1.15, we found that  $L_{\text{disc}} = 1/2 L_{\text{acc}}$ . One might then ask: where does the rest of the luminosity go? Alternatively, what happens to the kinetic energy the material has at the inner disc edge? The answer is dependent on the compact object in question. In an accreting WD, the rotating matter must eventually deposit itself on the surface of the WD. This is illustrated in Fig. 1.2, which shows the angular velocity as a function of radius in a disc around a compact object rotating with angular velocity  $\Omega_*$ .

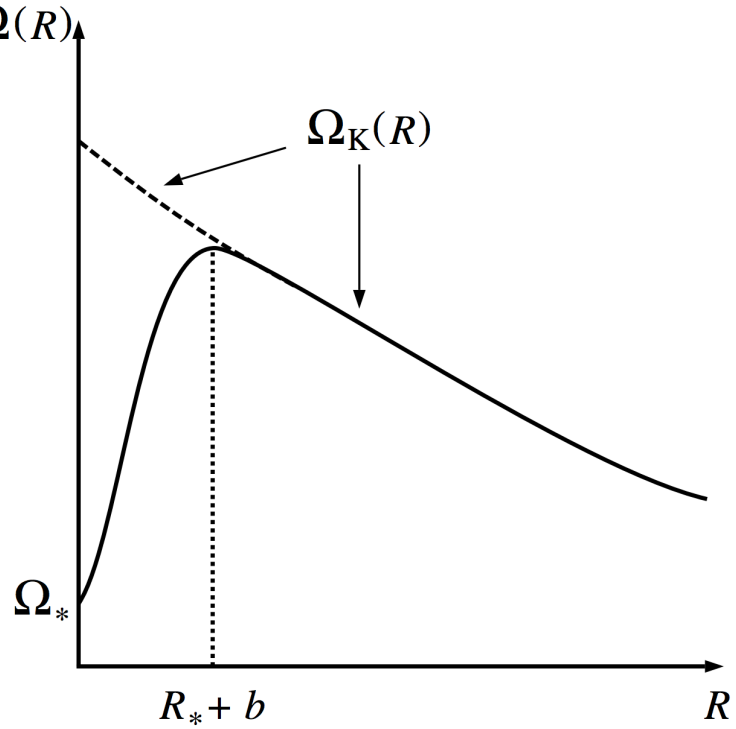


FIGURE 1.2: Credit: Frank et al. 2002. Angular velocity as a function of radius in an accretion disc around a rotating compact object with angular velocity  $\Omega_*$ .  $\Omega_K$  is the Keplerian angular velocity. This graph also helps explain why there is a turnover in the temperature-radius relation, as  $D(R)$  is proportional to the square of the derivative of this quantity.

The boundary layer (BL) is the region to the left of the dotted line, inside the maximum of  $\Omega$ , the angular velocity. The luminosity of the boundary layer is ([Frank et al. 1992](#))

$$L_{BL} = \frac{1}{2} \frac{GM\dot{M}}{R} \left[ 1 - \left( \frac{\Omega_*}{\Omega_K(R_*)} \right)^2 \right], \quad (1.20)$$

where  $\Omega_K(R_*)$  is the Keplerian angular velocity at  $R_*$ , assuming the thickness of the BL is small. When  $\Omega_K(R_*) \gg \Omega_*$ , this reduces to  $L_{BL} = 1/2 L_{\text{acc}} = L_{\text{disc}}$ .

In cataclysmic variables, BLs can be approximated with blackbodies and their temperatures estimated indirectly via the [Zanstra \(1929\)](#) method (e.g. [Hoare & Drew 1991, 1993](#)). However, they likely exhibit a variety of atomic features ([Suleimanov et al. 2014](#)). Extreme-UV (EUV) datasets have confirmed the existence of boundary layer emission in non-magnetic CVs ([Mauche 1996](#)), although these observations are limited in number.

Clearly, in BH systems a boundary layer cannot exist in the same way, due to the lack of a physical surface. Instead, the energy must either go into growing the BH, contributing to its angular momentum or being channeled into a jet or other radiative source (see section 1.5.2). The question of what happens at the inner disc edge is complicated

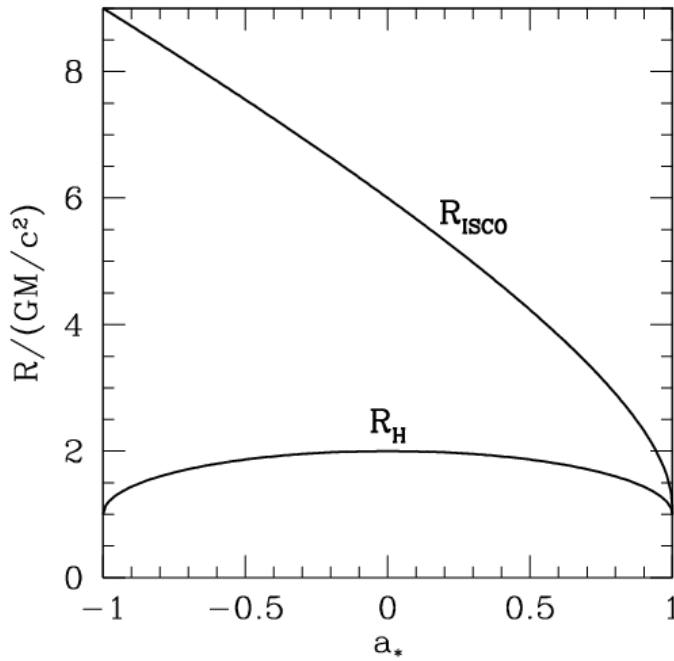


FIGURE 1.3: Credit: Narayan 2014. The radius of the ISCO,  $R_{ISCO}$ , and the horizon,  $R_H$ , is as a function of the BH spin parameter,  $a_*$ .  $a_* = 0$  corresponds to a Schwarzschild BH, and  $a_* = 1$  and  $a_* = -1$  to prograde and retrograde Kerr BHs respectively. Note that this figure ignores the counteracting torque of photons swallowed by the BH, which actually limits  $a_*$  to a value of around 0.998 (Thorne 1974).

further by the fact that the disc cannot extend to the event horizon of the BH. Instead, there is an ‘innermost stable circular orbit’ (ISCO) beyond which the accreting matter will simply fall into the BH along nearly radial paths. The radius of this orbit,  $R_{ISCO}$ , and the horizon radius,  $R_H$ , is shown for different values of the BH spin parameter,  $a_*$ , in Fig. 1.3, showing how matter can orbit closer to a prograde spinning BH. In estimating the luminosity of a Keplerian disc around a BH, we should really set  $R_* = R_{ISCO}$  in equation 1.5, giving the interesting result that rapidly spinning (Kerr) BHs ( $\eta \approx 0.32$ ) are more radiatively efficient than Schwarzschild BHs ( $\eta \sim 0.17$ ).

#### 1.1.4 The Emergent Spectrum

It is important to recognise that the steady-state disc treatment *does not specify the exact shape of the disc SED*. What it does do is say where energy is originally released. The simplest assumption is that each annulus emits as a blackbody with temperature

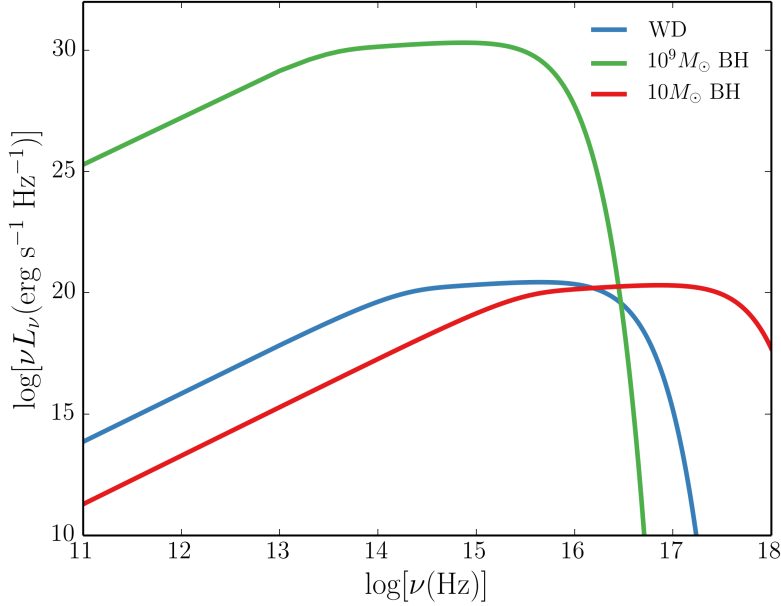


FIGURE 1.4: Accretion disc SEDs for three different compact objects, corresponding roughly to a quasar, an XRB and a CV. The SEDs are computed via an area-weighted sum of blackbodies with effective temperatures governed by equation 1.17, and the  $\nu^{1/3}$  shape in the middle of the spectra can be seen.

$T_{\text{eff}}(R)$ , i.e. that the specific intensity through the emitting surface follows Planck's law:

$$B_\nu(T) = \frac{2h\nu^3}{c^2} \frac{1}{\exp(h\nu/kT) - 1}. \quad (1.21)$$

Under this assumption, it is possible to show that at intermediate frequencies, where  $kT(R_{\text{max}}) \ll h\nu \ll kT_*$ , the spectrum appears as a 'stretched blackbody', with monochromatic flux,  $F_\nu$ , of the form

$$F_\nu \propto \nu^{1/3}. \quad (1.22)$$

Fig. 1.4 shows the blackbody SEDs expected for the same objects as in Fig. 1.1, in which the  $\nu^{1/3}$  portion can be clearly seen. A stellar atmosphere model with frequency-dependent opacity creates a somewhat different (and more realistic) spectrum. Fig. 1.5 shows a comparison between a disc spectrum computed with stellar atmosphere models and standard multi-temperature blackbody disc, showing how the two treatments can have a significantly different spectral shape when one includes frequency-dependent opacities in the atmosphere. It is of course possible that *neither* a blackbody treatment or the current stellar atmosphere models produce accurate disc spectra. I shall therefore devote a little time to discussing the observational appearance of accretion discs and reviewing the different classes of accreting objects.

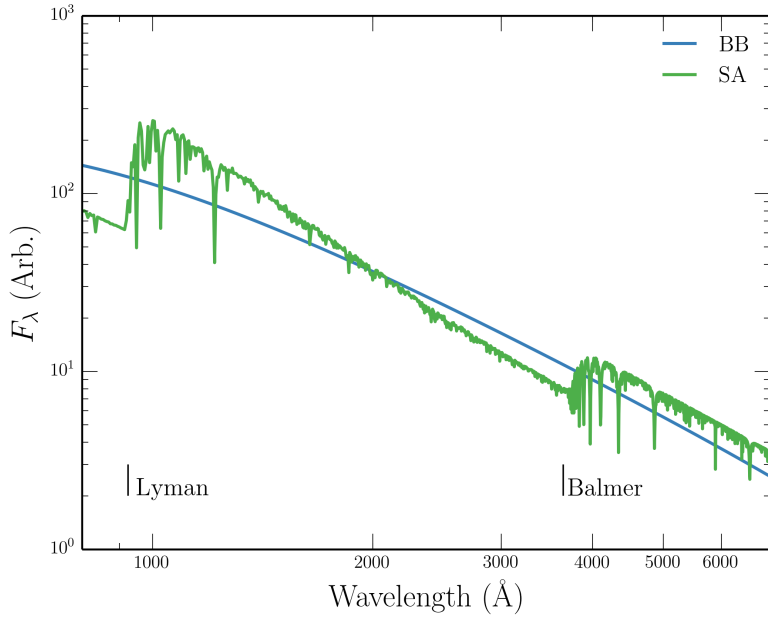


FIGURE 1.5: A comparison between a disc spectrum computed with stellar atmosphere models and standard multi-temperature blackbody disc. The major photoabsorption edges are marked. Flux is reprocessed into different wavelengths by bound-free opacities, and line blanketing also has a big effect on the spectrum. The Hydrogen and Helium lines also experience a degree of pressure broadening.

## 1.2 Accreting Compact Binaries

Accreting compact binaries form many different classes, but all are characterised by matter streaming from a donor onto a compact object. When the compact object is more massive than the donor, it is designated as the ‘primary’, and its companion as the ‘secondary’. In high-mass X-ray binaries (HMXBs), the opposite is formally true. There are only two ways by which matter can transfer from the secondary to the compact object. One is by Roche lobe-overflow (RLOF), where the donor star expands to fill its Roche lobe, a critical surface of equipotential around the star (see section 1.2.1). The alternative is that the donor may expel material in an outflow, some of which can be captured by the compact object. Although accretion from a wind or circumstellar disc is common in HMXBs (Bartlett 2013), here I will focus on RLOF as it is more common in the systems that possess high-state accretion discs and associated outflows. Two examples of these are shown in Fig. 1.6

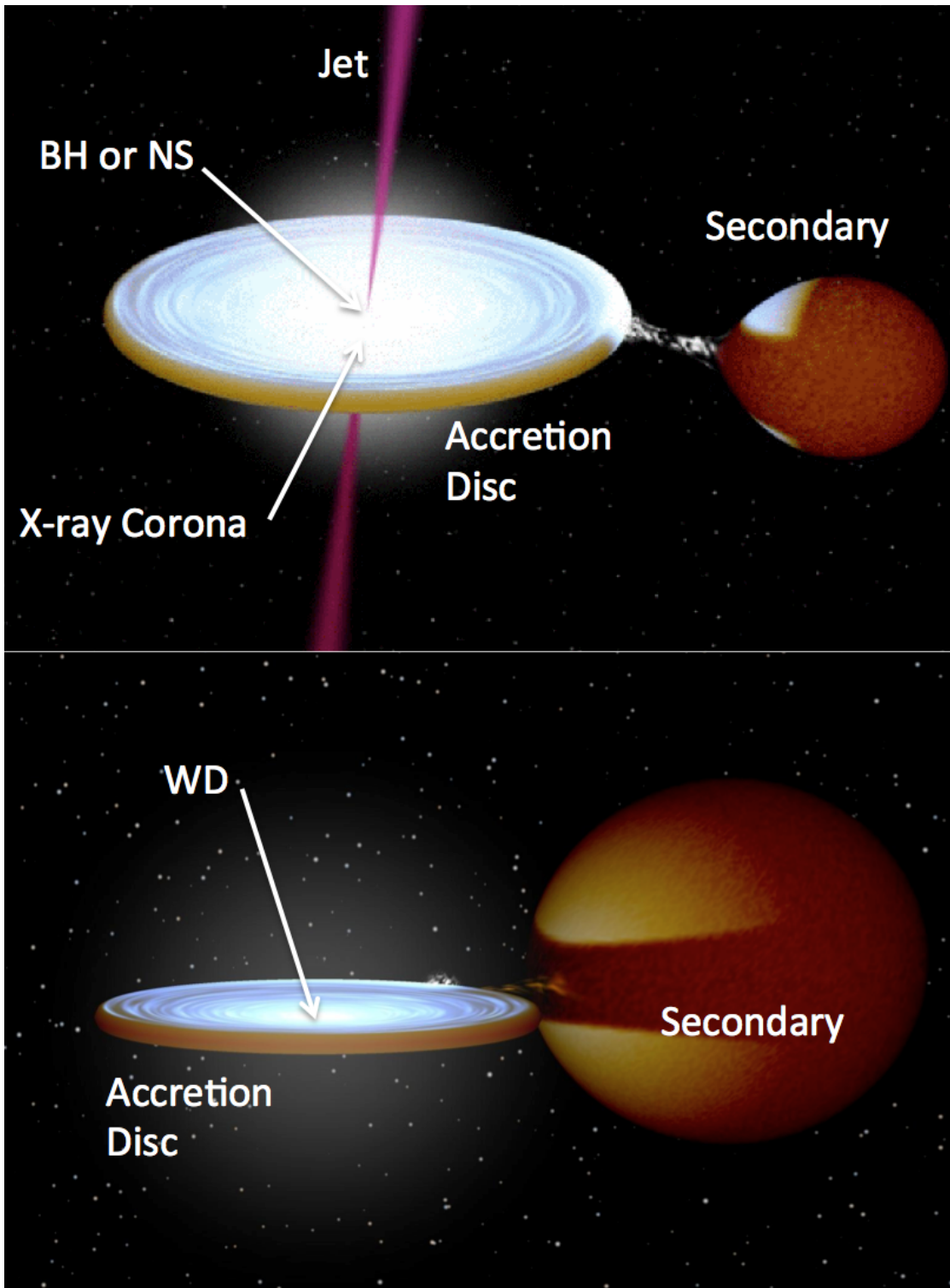


FIGURE 1.6: Credit: Rob Hynes. Artists impression of a low-mass X-ray binary (top) and cataclysmic variable (bottom). The key components are marked, and the clear similarity in overall structure is apparent.

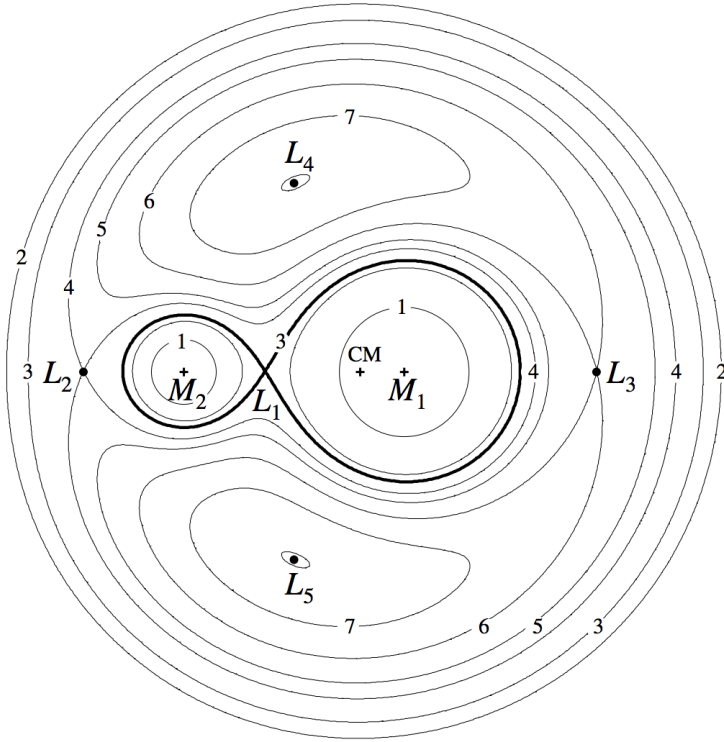


FIGURE 1.7: Credit: Frank et al. 2002. The Roche potential in a binary system for  $q_M = M_2/M_1 = 0.25$ . The Lagrangian points are marked, as are the locations of the individual and system centres of mass.

### 1.2.1 Roche Lobe-Overflow

Let us consider a binary system containing two point sources with masses  $M_1$  and  $M_2$  at positions  $\vec{r}_1$  and  $\vec{r}_2$ . The Roche potential,  $\Phi_R$ , in this system is then

$$\Phi_R = -\frac{GM_1}{|\vec{r} - \vec{r}_1|} - \frac{GM_2}{|\vec{r} - \vec{r}_2|} - 1/2(\vec{\omega} \times \vec{r})^2, \quad (1.23)$$

where  $\vec{\omega}$  is the angular velocity of the binary and is a vector normal to the orbital plane. This potential is plotted in Fig. 1.7 for a mass ratio,  $q_M = M_2/M_1 = 0.25$ .

In the context of semi-detached binary systems, the most important equipotential is the dumbbell-shaped region enclosing both masses. Each of these enclosed regions is known as the ‘Roche lobe’ of the object. A good approximation for the size of the Roche lobe takes the form (Eggleton 1983)

$$\frac{R_2}{a} = \frac{0.49q_M^{2/3}}{0.6q_M^{2/3} + \ln(1 + q_M^{1/3})}. \quad (1.24)$$

Here,  $R_2$  is the radius of a sphere with the same volume as the Roche lobe for the secondary star, which we can see depends only on  $q_M$  and the orbital separation,  $a$ . If this secondary expands enough to fill its Roche lobe, then matter will fall onto the other object through the  $L_1$  Lagrangian point. This process is known as Roche lobe overflow (RLOF) and is vitally important in astrophysics. Any accretion from RLOF will alter the mass ratio of the binary system and thus affects the evolution of binary systems. This is reflected in the orbital period distribution of binaries (e.g. Knigge et al. 2011) and also affects the delay time distribution of Type Ia Supernovae, for which CVs are one of the progenitor candidates (e.g. Wang & Han 2012). It is also worth noting that the existence of gravitational waves has been required in models to explain the orbital period evolution of CVs since the 1960s (Kraft et al. 1962).

### 1.2.2 Cataclysmic Variables

Cataclysmic variables (CVs) are systems in which a WD accretes matter from a donor star via Roche-lobe overflow (see the ‘CV bible’, Warner 2003). CVs are not always dominated by their accretion luminosity; for example, novae undergo dramatic eruptions caused by thermonuclear runaway, and the so-called ‘supersoft sources’ show evidence of nuclear burning on the WD surface. Accretion-dominated CVs – the focus here – can be classified according to the magnetic field strength of their WD primary ( $B_{WD}$ ) and their photometric activity. Magnetic systems are classified as either ‘Polars’ ( $B_{WD} \gtrsim 10^7$  G) or ‘Intermediate Polars’ (IPs;  $10^6 \lesssim B_{WD} \gtrsim 10^7$  G); in these systems the accretion flow inside the some critical radius (related to the Alfvén radius) is dominated by the WDs magnetic field. In polars, this radius is large enough, due to the strong magnetic field, that no disc forms at all (Liebert & Stockman 1985). In IPs the accretion disc is truncated at the magnetospheric boundary, and accretion ‘curtains’ channel the material onto the WD (e.g. Patterson 1994; Evans et al. 2004). When  $B_{WD} \lesssim 10^6$  G the accretion disc can extend all the way down to the WD boundary, and the CV is classified as non-magnetic. Here, I consider only non-magnetic CVs, which come in two flavours: dwarf novae and nova-like variables.

### 1.2.2.1 Dwarf Novae and the Disc-instability Model

Dwarf novae (DNe) are CVs that are characterised by repeated cycles of faint quiescence followed by a dramatic bright outburst. One of the most famous DNe is SS Cyg, whose light curve is shown in Fig. 1.8. The repeated outbursts can be clearly seen, and SS Cyg itself has been undergoing this behaviour over the full century for which it has been observed. A spectrum over the course of a typical outburst is shown in Fig. 1.9 and is characterised by the appearance of a blue, optically thick accretion disc continuum – note the similarity to the stellar atmosphere disc spectrum computed in section 1.1.2.1 and to the intermediate inclination nova-like variables discussed in the next section.

The leading scenario for explaining DN outbursts, and in fact also the outbursts in low mass X-ray binaries or ‘soft X-ray transients’, is the disc-instability model (DIM; [Osaki 1974](#); [Hōshi 1979](#); [Meyer & Meyer-Hofmeister 1981](#); [Lasota 2001](#)). In this model, the disc is in a cool, low viscosity state in quiescence, and H is mostly neutral. The constant mass supply from the donor causes a gradual build up of mass in the disc. Eventually, the disc hits a critical temperature, around 7000 K, and H becomes ionized. This causes an increase in viscosity and temporarily allows a higher accretion rate through the disc. In this state, the disc becomes geometrically thin and optically thick. It can now undergo efficient radiative cooling, meaning that a significant increase in brightness is observed. This state is relatively short-lived, as the accretion rate through the disc will be lower than the supply rate from the donor star, so eventually the disc will drop below the critical temperature and back onto the cool, low viscosity branch.

### 1.2.2.2 Nova-like Variables

Nova-like variables (NLs) are similar to DNe, except that the disc is always in a relatively high-accretion-rate state ( $\dot{M} \sim 10^{-8} M_{\odot} \text{ yr}^{-1}$ ). NLs are therefore one of the best ‘laboratories’ for testing the steady-state accretion disc theory described in section 1.1.2.1. In the optical, NLs generally exhibit a series of H and He emission lines superposed on a blue continuum. In many cases, and particularly in the SW Sex subclass of NLs ([Honeycutt et al. 1986](#); [Dhillon & Rutten 1995](#)), these lines are single-peaked. This is contrary to theoretical expectations for lines formed in accretion discs, which are predicted to be double-peaked ([Smak 1981](#); [Horne & Marsh 1986](#)). *Low-state* CVs (dwarf novae in quiescence) do, in fact, exhibit such double-peaked lines ([Marsh & Horne 1990](#)).

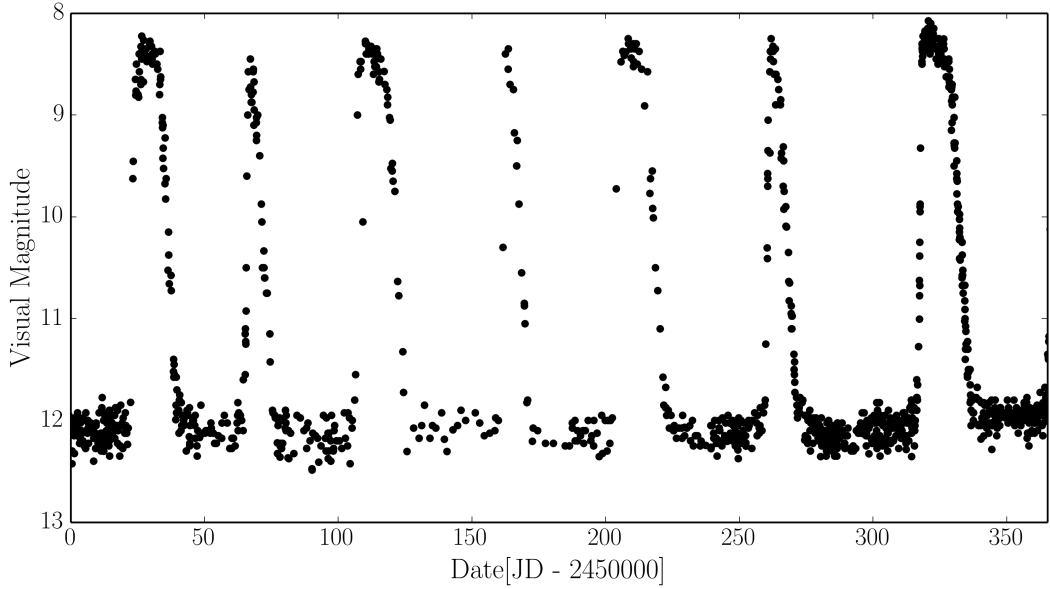


FIGURE 1.8: *Data: AAVSO.* A year in the life of SS Cyg, showing the characteristic repeated outbursts and periods of quiescence typical of a DN. SS Cyg has been undergoing this activity since it was first observed in 1896.

The UV spectra of NLs also show strong emission lines, and at low to intermediate inclinations dramatic blue-shifted absorption lines can be seen in some objects. The emission line equivalent widths in both the optical and the UV show clear trends with inclination (Hessman et al. 1984; Echevarria 1988; Noebauer et al. 2010). This can be seen clearly in Fig. 1.11 and is connected to the correlation between line strength and absolute magnitude found by Patterson (1984); that is, the decrease in equivalent width at low inclination is caused by an *increase* in continuum flux, rather than a decrease in line flux. This is discussed further in chapters 4 and 6, but also has relevance to AGN and quasar unification schemes mentioned later in this introduction. The optical and UV spectra of NL CVs are discussed further in the context of winds in chapter 2.

### 1.2.3 Low Mass X-ray Binaries

Although I do not study low-mass X-ray binaries (LMXBs) directly in this thesis, it is instructive to briefly discuss their observational appearance, as it is relevant to the connections between accretion and outflows. LMXBs are similar to CVs in structure (see Fig. 1.6), but the compact object is either a neutron star (NS) or a black hole (BH). The accretion disc emits in the soft X-ray regime, and an additional hard X-ray power law is also seen in the spectrum. This hard component is normally attributed to Compton up-scattering of seed disc photons by some kind of ‘corona’ of hot electrons close to the

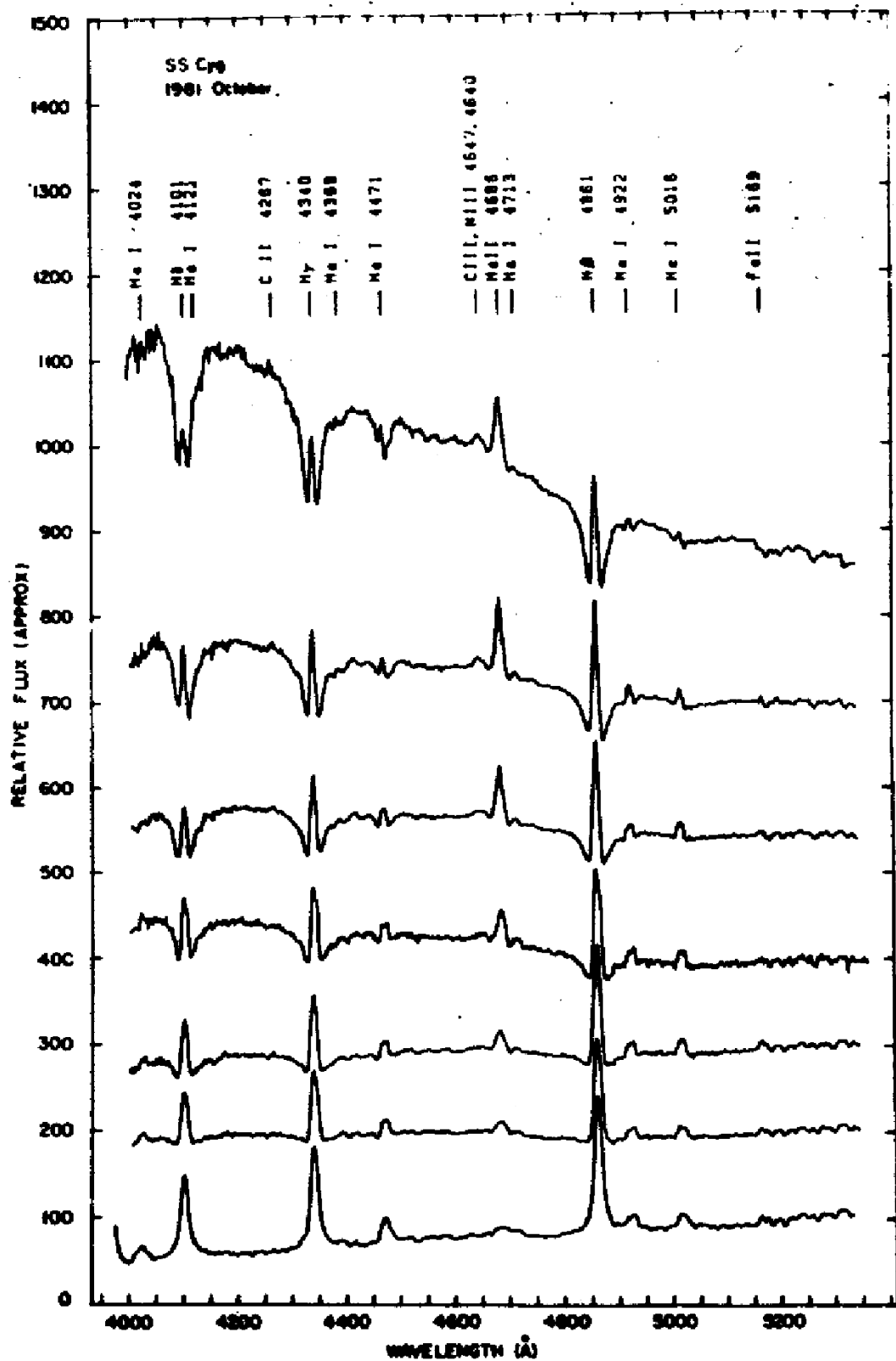


FIGURE 1.9: Credit: Hessman et al. 1984 / Dhillon et al. 1996. Spectra of SS Cyg during an outburst cycle, showing the evolution from minimum to maximum light. The rise is characterised by the appearance of an optically thick accretion disc spectrum. The flux scale is approximate.

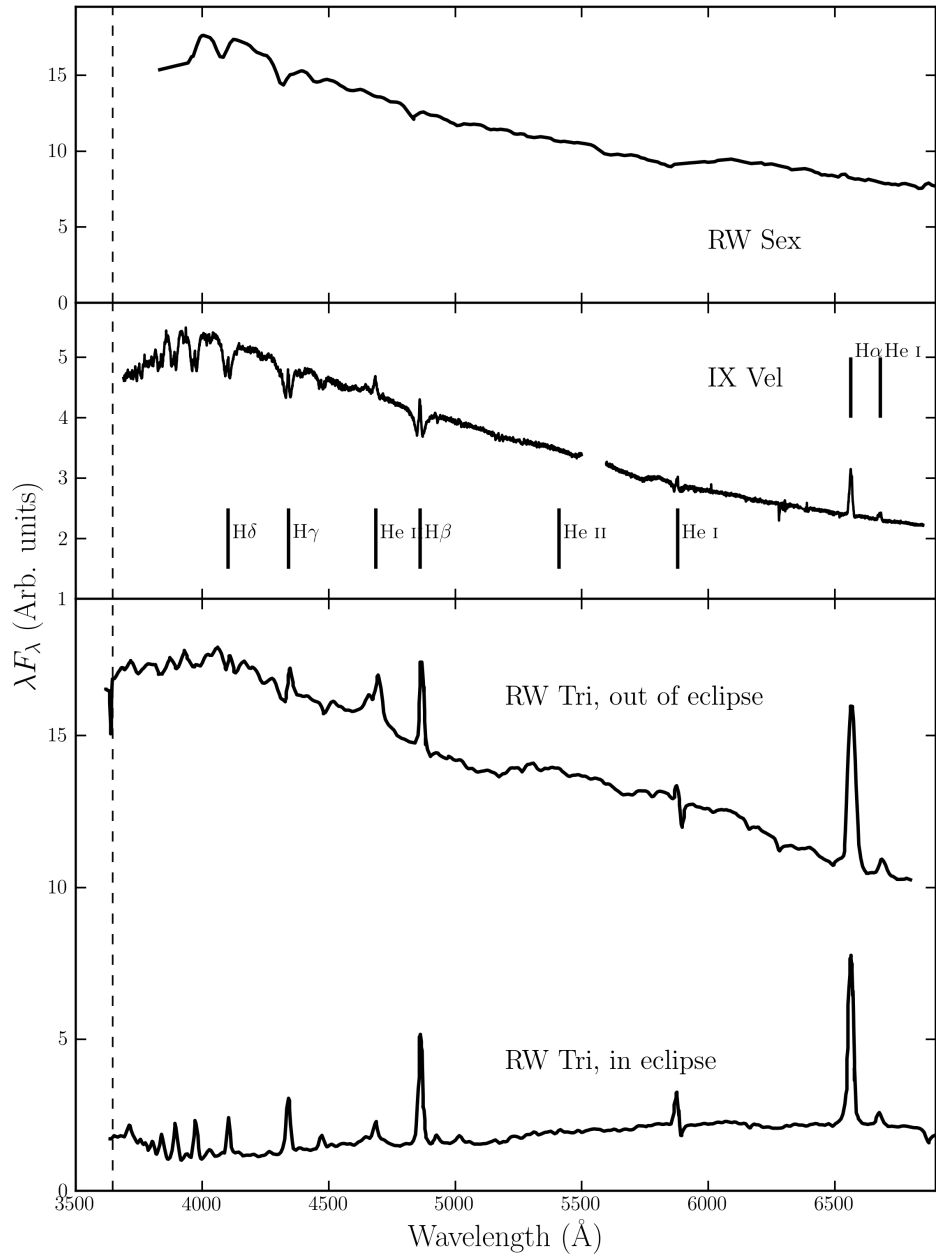


FIGURE 1.10: Optical spectra of three nova-like variables: RW Sex (top; Beuermann et al. 1992), IX Vel (top middle; A. F. Pala & B. T. Gaensicke, private communication) and RW Tri in and out of eclipse (bottom two panels; Groot et al. 2004). The data for RW Sex and RW Tri were digitized from the respective publications, and the IX Vel spectrum was obtained using the XSHOOTER spectrograph on the Very Large Telescope on 2014 October 10. These systems have approximate inclinations of  $30^\circ$ ,  $60^\circ$  and  $80^\circ$  respectively. The trend of increasing Balmer line emission with inclination can be seen. In RW Tri strong single-peaked emission in the Balmer lines is seen even in eclipse, indicating that the lines may be formed in a spatially extensive disc wind, and there is even a suggestion of a (potentially wind-formed) recombination continuum in the eclipsed spectrum. I have attempted to show each spectrum over a similar dynamic range.

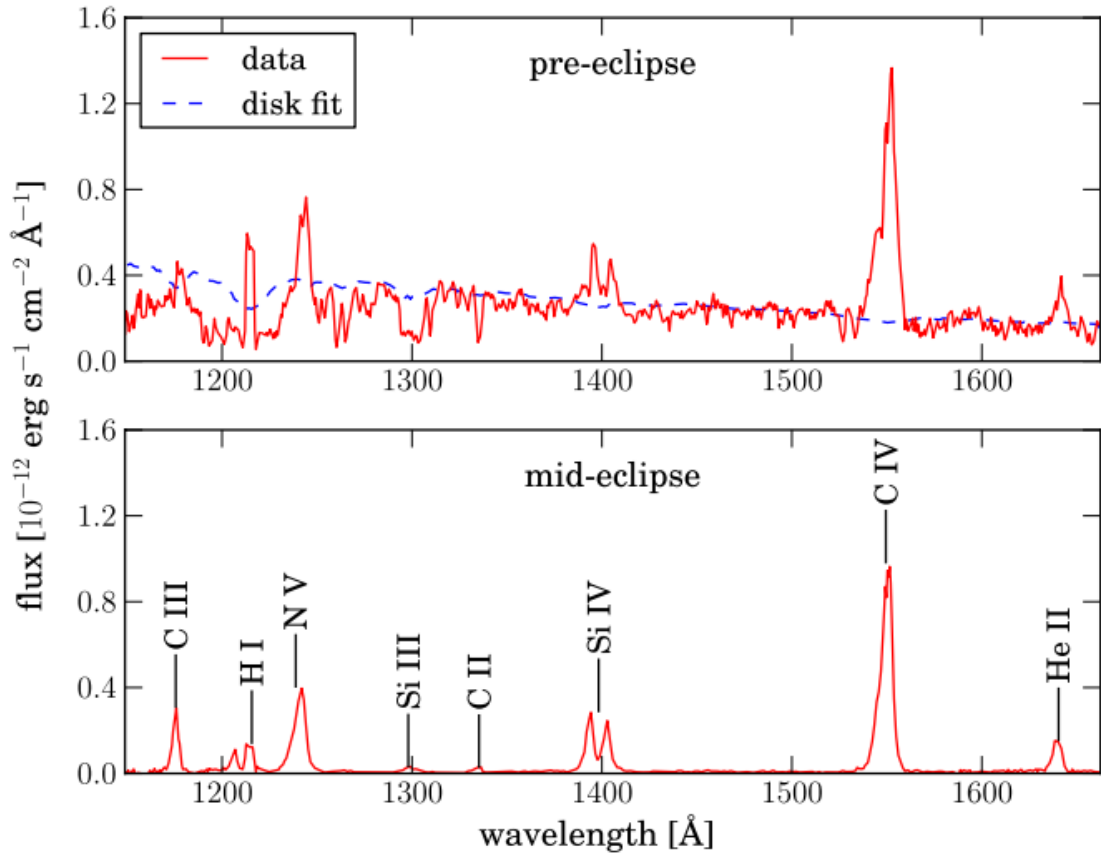


FIGURE 1.11: Credit: Noebauer et al. 2010. UV spectrum of RW Tri in and out of eclipse, showing strong lines in C IV 1550 Å and Ly $\alpha$ , among others.

BH (e.g. [White et al. 1988](#); [Mitsuda et al. 1989](#); [Uttley et al. 2014](#)). The discovery that XRBs and CVs follow similar tracks on a hardness-intensity diagram (HID; [Körding et al. 2008](#)) is particularly interesting, especially since [Ponti et al. \(2012\)](#) showed that broad Fe absorption lines are only seen in the soft-state high-inclination systems (see section 2.1.2). This implies that equatorial outflows may be intrinsic to the accretion process. Although the outflow driving mechanism is probably different to CVs (e.g. [Díaz Trigo & Boirin 2015](#)), the general structure of LMXBs – that of a disc around a compact object with an associated outflow – is strikingly similar to models for CVs and quasars.

### 1.3 Quasars and Active Galactic Nuclei

Spectra of AGN have now been studied for over 100 years, and we have known that they exhibit strong, broad emission lines since the first spectrum was taken by [Fath \(1909\)](#). However, it wasn't until the work of [Seyfert \(1943\)](#) that the systematic classification of AGN really began, leading to the phrase ‘Seyfert galaxy’. This label was applied to

galaxies possessing a bright nucleus, spectroscopically characterised by a blue continuum and a series of strong emission lines. The first real physical insight into the extraordinary nature of AGN was provided by [Woltjer \(1959\)](#), who noted that (i) the nuclei must have sizes  $< 100$  pc, based on the fact that they were unresolved, and (ii) the mass of the nucleus must be very high, based on virial estimates. While both of these observations were based on simple arguments, the fact that these ultra-luminous celestial objects are both *compact* and *supermassive* is perhaps the defining insight into the nature of AGN.

Although the study of AGN was established in the optical waveband, radio astronomy also significantly furthered our understanding of AGN in the mid-20th century. A number of surveys, such as the Cambridge ([Edge et al. 1959](#)), Parkes ([Ekers 1969](#)) and Ohio ([Ehman et al. 1970](#)) surveys discovered a great many bright radio point sources distributed isotropically across the sky. These sources eventually became known as ‘quasi-stellar radio sources’, or *quasars*, and were soon found to be coincident with bright optical sources or ‘quasi-stellar objects’ (QSOs) at high redshifts ([Schmidt 1963, 1965a,b](#)). Nowadays, the term quasar normally has very little to do with radio emission and is often used interchangeably with QSO. Indeed, throughout this thesis I shall use the term quasar simply to mean a bright, massive AGN; with a sufficiently high luminosity to dominate the emission from its host galaxy.

One of the main classification schemes for AGN is a spectroscopic one, based on whether an object possesses broad emission lines in its spectrum, such as C IV, H $\beta$  and Ly $\alpha$ , in addition to the narrow lines that are always present. If these broad lines are seen, then the AGN is classed as type 1; if not, it is classed as type 2 ([Fig. 1.12](#)). These designations were originally applied to Seyfert galaxies ([Seyfert 1943](#)), but can also be used to classify the more luminous quasar class, despite the apparent difficulty in finding the expected number of type 2 quasars ([Zakamska et al. 2003](#)). This classification scheme is complicated somewhat by the existence of two unusual types of AGN: narrow line Seyfert 1s (NLS1s), which may be explained by super-Eddington accretion ([Done & Jin 2015](#)) or perhaps simply an orientation effect ([Baldi et al. 2016](#)), and so-called ‘true type 2’ AGN, in which the broad line region is absent ([Tran 2001; Shi et al. 2010](#)) rather than obscured (see next section). Despite this muddying of the waters, what was originally a clear dichotomy in spectral type provided a profound motivation for attempting to *unify* AGN via geometric arguments.

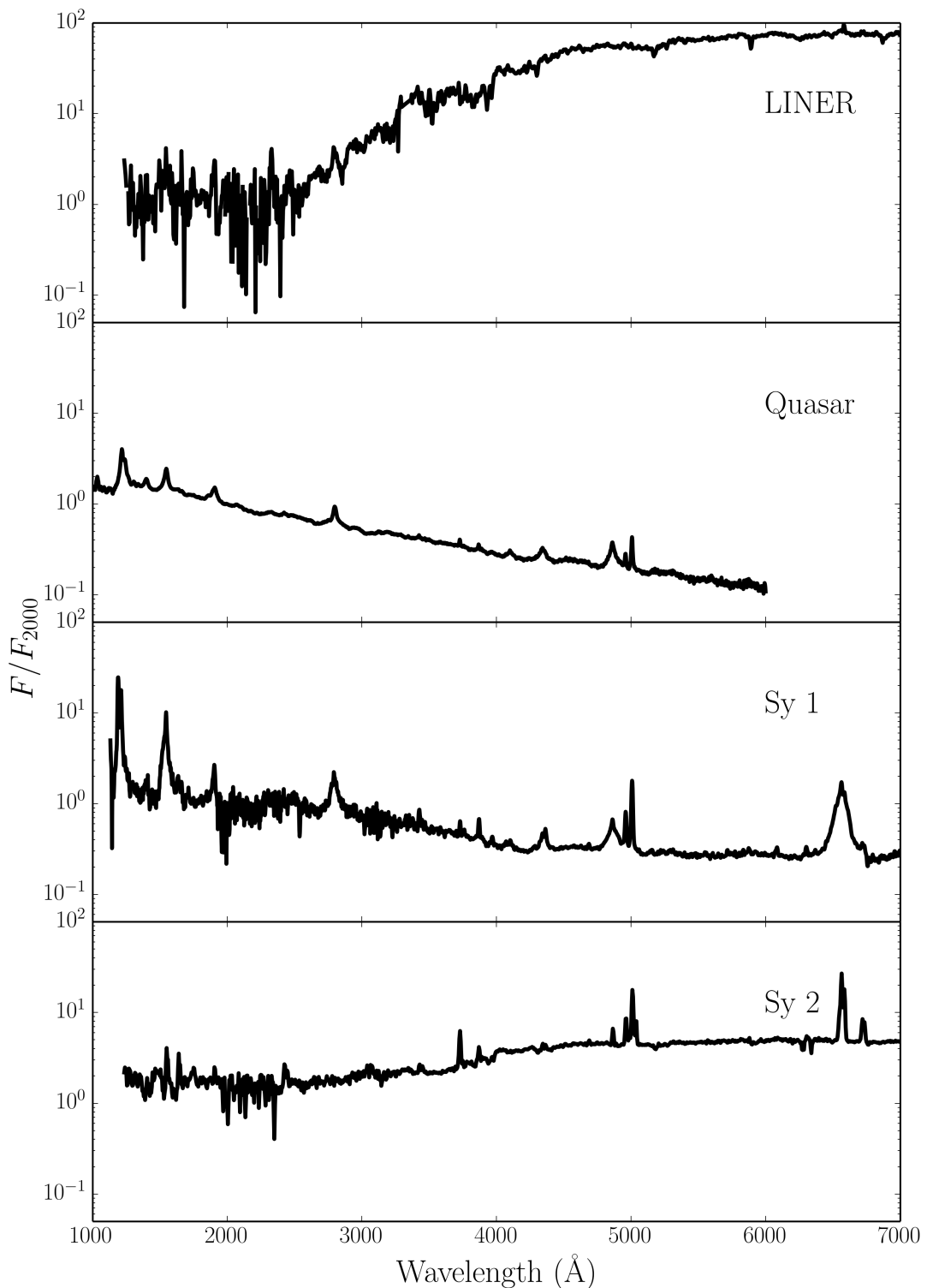


FIGURE 1.12: Template spectra, from the AGN atlas, for four common types of AGN.  
Obtained from [http://www.stsci.edu/hst/observatory/crds/cdbs\\_agn.html](http://www.stsci.edu/hst/observatory/crds/cdbs_agn.html).

### 1.3.1 AGN Unification and the Dusty Torus

Although Seyfert had identified type 1 and 2 AGN, a physical explanation for this dichotomy was not forthcoming until a study by [Antonucci & Miller \(1985, AM85\)](#). They showed unambiguously that the nearby Seyfert 2 NGC 1068 is simply an obscured type 1 AGN, by finding that broad emission lines appeared in the spectrum of *polarised* flux. This provided the basis for the first successful attempt to unify AGN behaviour, as it elegantly explained the apparent disconnect between the two types of AGN as simply a viewing angle effect: in type 1s, an observer can look directly into the broad line region (BLR) near the nucleus, but, in type 2s, this region is hidden from view. The obscuring structure became known as the ‘torus’ ([Krolik & Begelman 1986](#)), due to its proposed geometry, and it was soon realised that this structure may be made of dust, in which case it could also be responsible for the infra-red (IR) bump in AGN spectra ([Neugebauer et al. 1979](#)).

[Urry & Padovani \(1995, UP95\)](#) went further than the original unification model proposed by AM85, as they also tried to account for the dichotomy in AGN radio properties (radio-loud/radio-quiet). The picture they proposed is shown in Fig. 1.13. This model attempts to explain all types of AGN solely in terms of viewing angle and presence, or absence, of a radio jet. Models such as this also describe the series of ‘bumps’ observed in AGN – the portions of the spectrum that dominate the luminosity, shown in Fig. 1.14. In most models, the ‘Big Blue Bump (BBB)’ is ascribed to thermal emission from an accretion disc, and the ‘Small Blue Bump’ to optically thin Balmer continuum and Fe II emission from the BLR. The latter can just be seen between  $\sim 2000 \text{ \AA}$  and  $\sim 4000 \text{ \AA}$  in the Seyfert 1 and quasar templates in Fig. 1.12. Our understanding of the BBB is still unsatisfactory (see section 1.4).

Since the seminal works by AM85 and UP95, the picture has become somewhat more complicated. Variable X-ray absorption has been detected in so-called ‘changing look’ AGN ([Matt et al. 2003; Puccetti et al. 2007](#)), including even NGC 1068 itself ([Marinucci et al. 2016](#)). Changes in type have also been seen in the optical lines; the broad H $\beta$  component in some AGN can dramatically disappear or reappear (e.g. [Tohline & Osterbrock 1976; Cohen et al. 1986; Denney et al. 2014](#)). The explanation for this could be variable absorption ([Elitzur 2012](#)) or a change in the accretion state of the disc. In the latter case, it has even been suggested that a disc wind could be directly responsible for this switch ([Elitzur et al. 2014](#)). Furthermore, dusty *polar* outflows have been found

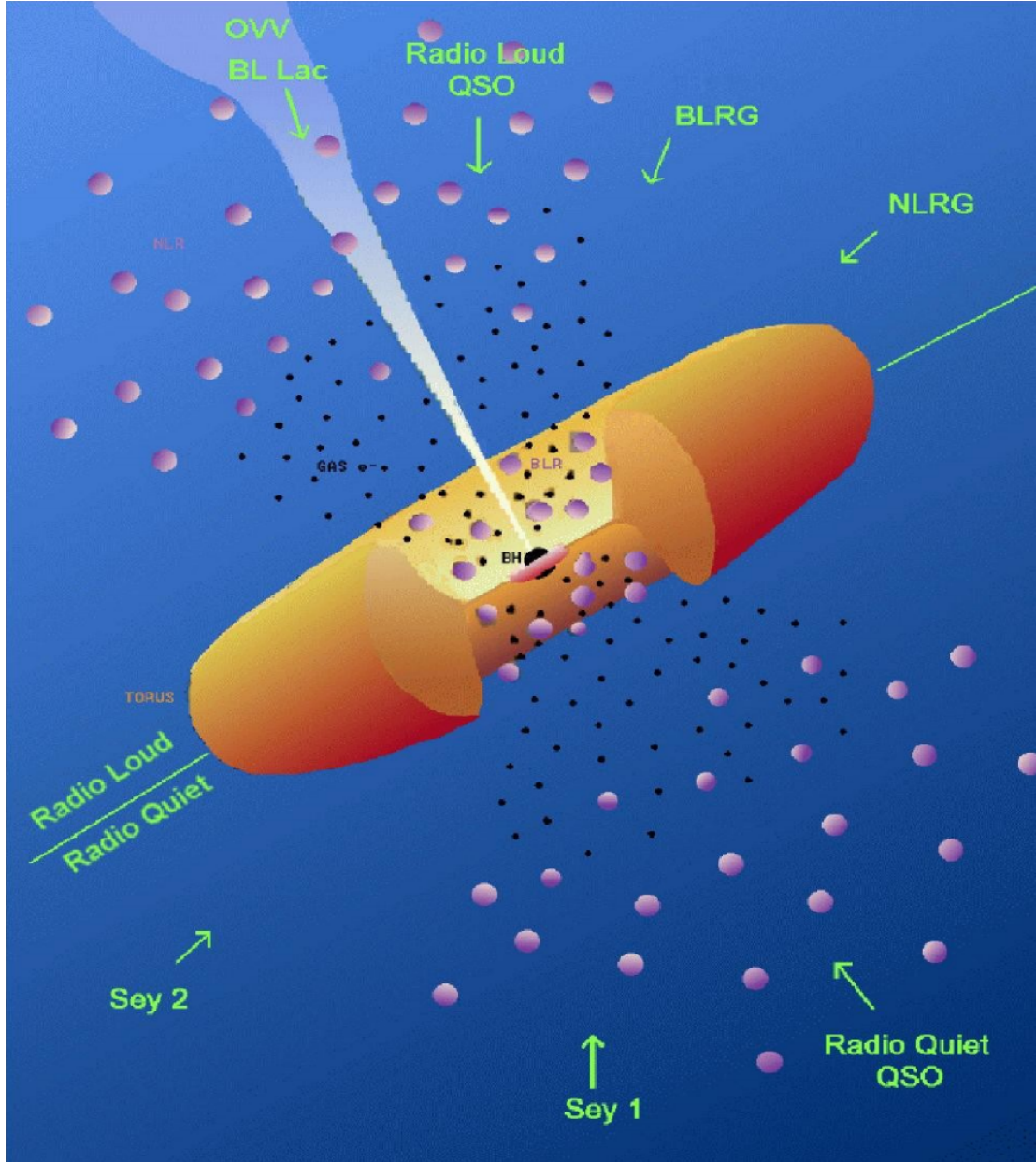


FIGURE 1.13: A unified scheme for AGN.

to be important IR emitters (Hnig et al. 2013), implying that, even when it comes to dust, the torus is not the whole picture. Despite these complications, the AGN torus unification picture still explains a lot of AGN phenomenology and represents a useful framework that can be tested with observations.

### 1.3.2 X-ray Properties of AGN

Approximately 10% of the bolometric luminosity of AGN comes out in the X-ray band, between  $\approx 0.1$  and  $\approx 100$  keV. Thus, AGN dominate the cosmic X-ray background

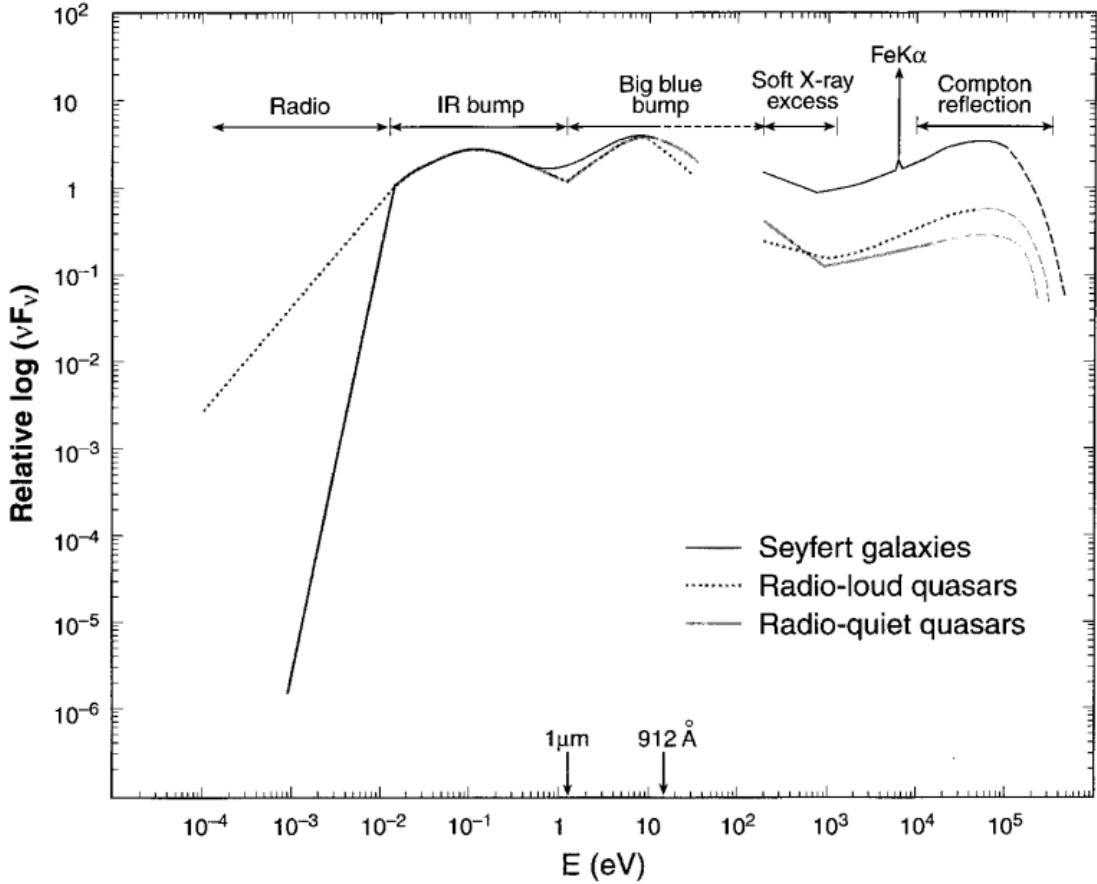


FIGURE 1.14: Credit: Koratkar & Blaes 1999 Approximate average broadband SEDs for a few types of AGN. The series of characteristic bumps can be clearly seen. The Soft-X-ray excess is also visible (see section 1.3.2.1).

(Madau et al. 1994). The hard X-ray emission typically follows a power law shape with spectral index -0.9 (e.g. Koratkar & Blaes 1999), widely considered, as in LMXBs, to come from a hot ‘corona’ of electrons close to the BH that upscatters disc seed photons (e.g. Haardt & Maraschi 1991). The compactness of this X-ray corona has been confirmed by microlensing (Chartas et al. 2009; Dai et al. 2010) and variability studies (Green et al. 1993; Crenshaw et al. 1996; Risaliti et al. 2007; Emmanoulopoulos et al. 2014). Indeed, X-rays in AGN can be highly variable, both in terms of their intrinsic X-ray emission, but also due to changes in the absorption characteristics (Risaliti et al. 2002; Miller et al. 2008; Connolly et al. 2014). I discuss X-ray absorption in more detail in chapter 2, particularly with respect to disc winds.

The hard X-ray spectra of AGN also tend to exhibit a number of reflection features. Typically, these consist of a strong Fe K $\alpha$  emission line and a ‘Compton hump’ at high energies. The latter is produced by Compton down-scattering of high energy photons (Pounds et al. 1989; Nandra & Pounds 1994). It is still unclear exactly where these

features originate, but a common interpretation is that they are caused by reflection off the inner parts of the accretion disc (Fabian et al. 1995; Iwasawa et al. 1996a; Reynolds 1999). If this is the case, and the broadening of the iron line is relativistic, this would allow for measurements of the BH spin (Laor 1991; Iwasawa et al. 1996b; Dabrowski et al. 1997). This hypothesis is somewhat controversial, as many of the relativistic features supposedly imprinted by BH spin can also be explained by Comptonisation or absorption (e.g. Misra & Kembhavi 1998; Miller & Turner 2013). In addition, an outflow can naturally produce the characteristic broad red Fe K $\alpha$  wing (Sim et al. 2010a).

In Compton-thick AGN, the intrinsic continuum is heavily absorbed by columns of  $N_H \gtrsim 10^{24} \text{ cm}^{-2}$  – this absorption is normally attributed to the dusty torus, but disc winds could also contribute. Compton-thick AGN are required in large numbers in order to explain the cosmic X-ray background (Setti & Woltjer 1989). In these sources, reflection features can actually dominate the X-ray spectrum (Alexander et al. 2011; Gandhi et al. 2013), but the Fe line is formed from low ionization stages of Fe on  $\sim 0.1 \text{ pc}$  scales (Gandhi et al. 2015).

### 1.3.2.1 The Soft X-ray Excess

If one interpolates between the  $\nu^{1/3}$  law from the BBB in the UV, and the power law in the hard X-rays, a curious excess of flux is often found in type 1 AGN (see Fig. 1.14, and Koratkar & Blaes 1999). This is known as the soft X-ray excess (SXXS), which is too hot to be explained by thermal disc emission, as a thin disc around an AGN should never approach the temperatures required. Many models have been proposed to explain this excess, including relativistically smeared photoabsorption (Gierliński & Done 2004, 2006), relativistically smeared line and free-free emission (Ross & Fabian 2005; Crummy et al. 2006) and a variety of cool Comptonised component geometries, such as an inner accretion flow (Magdziarz et al. 1998; Done et al. 2012) or a geometrically thin layer on top of the disc (Janiuk et al. 2001). While the SXXS poses a challenge to the simplest pictures of AGN, it may also solve some of the outstanding puzzles, since some of the geometries proposed may help to explain the accretion disc size problem discussed in section 1.4 (Gardner & Done 2016).

### 1.3.3 The Broad Line Region: Connection to Winds and Unification

In the UP95 unification model, the broad emission lines come from a series of virialised clouds close to the disc plane. As noted by Murray et al. (1995, hereafter MCGV95), there are a number of problems with the BLR ‘cloud’ model, perhaps most notably that there is no obvious physical origin for such virialised clouds. Testing alternative models for the BLR is therefore important. Indeed, MCGV95 proposed a disc wind model in order to explain both BALs and BELs in quasars. A disc wind model was also discussed by Elvis (2000), who proposed a structure for quasars that attempted to explain much of the behaviour of luminous AGN merely as a function of viewing angle. It is worth noting that there is observational support for the unification paradigm; for example, it has been suggested that orientation is a key driver of the so-called ‘Eigenvector 1’ relationship in quasars (Boroson & Green 1992; Sulentic et al. 2000; Marziani et al. 2001; Shen & Ho 2014). Disc wind unification models are discussed further in section 2. The philosophy of these models is that, before invoking additional degrees of freedom in a model, we should first test if known quasar phenomenology (disc winds) can explain other aspects of their observational appearance. I have illustrated this general principle with the ‘Occam’s quasar’ cartoon shown in Fig. 1.15. This is the picture that I will quantitatively test in the latter, quasar-focused sections of this thesis. The same general principle can also be applied to cataclysmic variables and other accreting objects.

## 1.4 The Current Understanding of the Disc Continuum

The SS73 model is still the most common way to fit accretion disc spectra and infer information about the underlying physics. However, a number of issues have been raised concerning the thin-disc model and its applicability to accreting systems.

### 1.4.1 The Spectral Shape of CV Discs

Attempts to fit the observed SEDs of high-state CVs with simple disc models have met with mixed success. In particular, the SEDs predicted by most stellar/disc atmosphere models are too blue in the UV (Wade 1988; Long et al. 1991, 1994; Knigge et al. 1998a) and exhibit stronger-than-observed Balmer jumps in absorption (Wade 1984; Haug 1987; La Dous 1989a; Knigge et al. 1998a). One possible explanation for these problems is

OCCAM'S QUASAR: THE PRINCIPLE THAT IN EXPLAINING A QUASAR NO MORE ASSUMPTIONS SHOULD BE MADE THAN ARE NECESSARY.

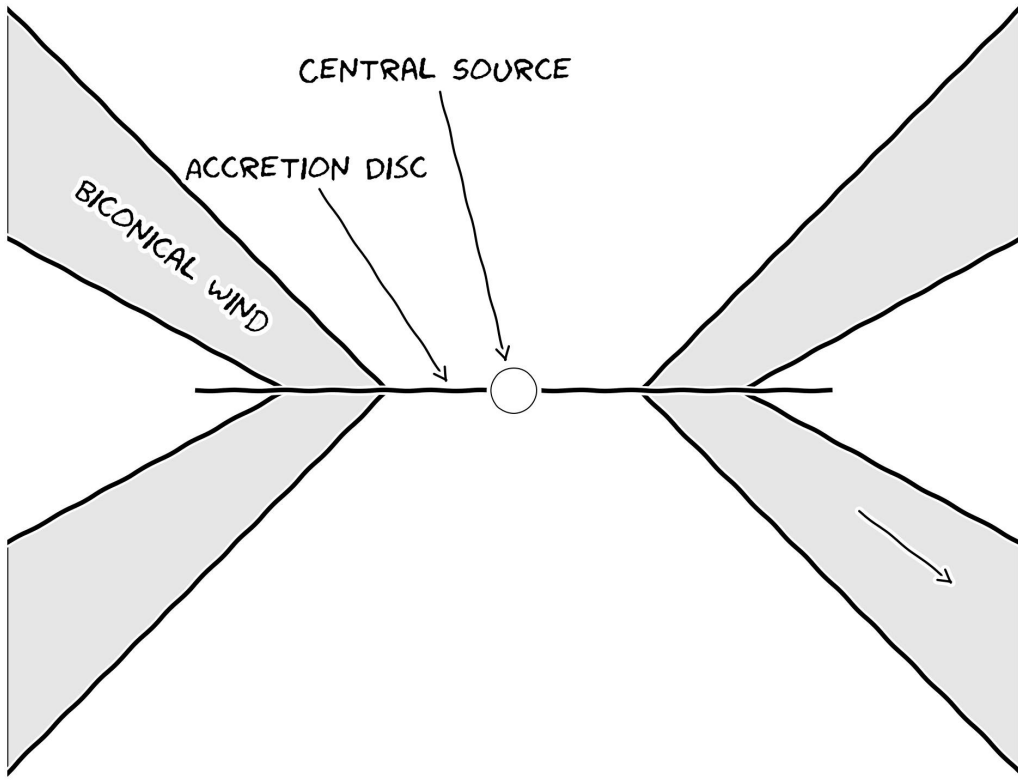


FIGURE 1.15: Occam's quasar. How far can this general picture take us when trying to explain the behaviour of quasars and other accreting compact objects?

that these models fail to capture all of the relevant physics. Indeed, it has been argued that a self-consistent treatment can produce better agreement with observational data (e.g. Shaviv et al. 1991; but see also Idan et al. 2010). However, an alternative explanation, suggested by Knigge et al. (1998b; see also Hassall et al. 1985), is that recombination continuum emission from the base of the disc wind might fill in the disc's Balmer absorption edge and flatten the UV spectrum.

Alternatively, it may just be that CV disks are never really in a steady state, and so we should only expect the  $R^{-3/4}$  temperature profile to hold in a limited portion of the disc. From eclipse mapping, it has been shown that the inferred accretion rate increases with radius in NLs (Rutten et al. 1992; Horne 1993). These results suggest that a non-radiative form of energy loss is present in the inner regions of the disc, of which potential forms may be advection or mass loss. This is yet another piece of evidence that the understanding of accretion and outflow are intertwined, although hopefully not

inextricably.

### 1.4.2 The Big Blue Bump in AGN

Does the SS73 model apply well to AGN spectra? There are contrasting views on the matter. On the one hand, [Antonucci \(2013\)](#) claims that “most of the AGN community is mesmerized by unphysical models that have no predictive power”. Yet a recent spectral fitting study by [Capellupo et al. \(2015\)](#) concludes that “altogether, these results indicate that thin accretion discs are indeed the main power houses of AGN”. So, what are the main problems when confronting thin disc models with observation?

#### 1.4.2.1 The Accretion Disc Size Problem

One of the most interesting results of recent years relating to AGN and accretion discs is the discovery that the continuum emission region size appears to be a factor  $\sim 3$  larger than predicted by standard thin disc theory. This result has been found independently in both microlensing ([Morgan et al. 2010; Dai et al. 2010](#)) and reverberation ([Edelson et al. 2015](#)) studies, and poses a challenge to the current best-bet model for the big blue bump in AGN. One proposed solution is that the discs in AGN are inhomogenous, consisting of individual clumps with independently varying temperatures ([Dexter & Agol 2011](#)), but this is very much still an active area of research. It is worth noting that the impact of winds on these results has not yet been properly quantified, something our team is currently trying to address ([Mangham et al. 2016](#)).

#### 1.4.2.2 Fitting AGN Spectra and the 1000 Å Break

AGN spectra do not, in general, exhibit the canonical  $\nu^{1/3}$  slope (e.g. [Koratkar & Blaes 1999; Davis et al. 2007; Shankar et al. 2016](#)) or colour-mass scalings ([Bonning et al. 2007](#)) expected from theoretical predictions. Furthermore, there is a characteristic break in AGN spectra at around 1000 Å ([Lusso et al. 2015](#)), which does not scale with BH mass or luminosity, as one might expect for a break associated with an accretion disc. There is also no evidence in AGN of the expected polarisation signatures from an optically thick disc atmosphere ([Stockman et al. 1979; Antonucci 1988; Antonucci et al. 1996](#)).

Despite these problems, recent work suggests that the thin disc model still has some potential. Capellupo et al. (2015) were able to fit a number of AGN spectra in the UV and optical with thin disc models, although successful fits were only found once they included effects such as Comptonisation and mass loss, as well as correcting for extinction. BH spin also had a reasonable effect on the spectral fits, although it is somewhat difficult to constrain from spectral fitting alone. The 1000 Å break has also been explained with mass-losing discs (Laor & Davis 2014), and Lusso et al. (2015) suggested that incorrect IGM corrections may be exacerbating the effect. So, while many problems exist, it may not be time to abandon the good ship “Shakura-Sunyaev” just yet.

## 1.5 The Universality of Accretion

Accretion appears to be an important physical processes across  $\sim 10$  orders of magnitude in mass. But is this process the same on all scales? Does any behaviour manifest in all accreting systems?

### 1.5.1 The RMS-flux relation

Broad-band variability is common in all types of accretion disc. It has been known for some time that there exists a linear relationship between the flux and absolute root-mean-square (rms) amplitude of this variability. This was discovered first in XRBs and AGN (Uttley & McHardy 2001; Uttley et al. 2005; Heil et al. 2012), but it has been shown more recently that the relationship extends to CVs and even YSOs (Scaringi et al. 2012, 2015). The relationship is also not limited to just one type of CV but is present in both NLs and DNe (Van de Sande et al. 2015).

The model that best reproduces this behaviour is the so-called ‘fluctuating accretion disc’ model (Lyubarskii 1997; Kotov et al. 2001; Arévalo & Uttley 2006; Hogg & Reynolds 2015). More generally, additive processes cannot reproduce this behaviour, and a multiplicative mechanism is required (Uttley et al. 2005). Regardless of the mechanism, the rms-flux relation is one of the most clear-cut examples of a universal accretion phenomenon. It tells us that at least some of the behaviour in CV discs is also present

in AGN and XRBs, strengthening the argument that CVs can be used as ‘accretion laboratories’.

### 1.5.2 Accretion states and disc-jet coupling

Variable and transient sources are common in astrophysics, particularly when the sources are accreting. It turns out that when one plots the colour and luminosity evolution over the course of an outburst cycle it follows very similar tracks in both CVs and XRBs (see Fig. 1.16, Körding et al. 2008). This colour-luminosity behaviour traces the accretion state of the system. The detection of radio jets is intrinsically linked to this accretion state (disc-jet coupling), as jets only appear in the ‘hard’ accretion state, to the right of the so-called ‘jet line’ (Fender 2001; Fender et al. 2004). Körding et al. (2008) showed that this behaviour also occurs in CVs, as radio emission in the DN SS Cyg is detected in the same region of colour-luminosity space. In addition, there is a well-known correlation between radio and X-ray luminosities in low-hard states (Gallo et al. 2003).

Clear connections between disc state and radio loudness have also been found in AGN. Perhaps the most obvious piece of evidence that disc-jet coupling is scale invariant is the so-called ‘fundamental plane of BH activity’ (Merloni et al. 2003), which extends from LMXBs right up to quasars. AGN have been shown to occupy similar regions of colour-luminosity space to the LMXBs (Körding et al. 2006), and simulations involving scaled-up LMXB discs have been successful in reproducing AGN accretion states (Sobolewska et al. 2011). Correlations in X-ray photon index are present in AGN and LMXBs; ‘softer when brighter’ behaviour is found at relatively high Eddington ratios (McHardy et al. 1999; Gu & Cao 2009), while ‘harder when brighter’ is observed in low states (Gu & Cao 2009; Emmanoulopoulos et al. 2012; Connolly et al. 2016).

Despite this apparently universal behaviour, the jet production mechanism in BHs is not well known. Theoretical work suggests that radio jets should be correlated with BH spin (Penrose & Floyd 1971; Blandford & Znajek 1977), but whether such a correlation exists in LMXBs is controversial (Fender et al. 2010; Narayan & McClintock 2012). This has significant implications for AGN; if powerful radio jets are associated exclusively with rotating BHs then the number of radio-loud AGN would imply a large fraction of them must be rapidly spinning, with high radiative efficiencies. Further evidence that radio jets are not simply produced by RIAFs onto spinning BHs is found when one considers

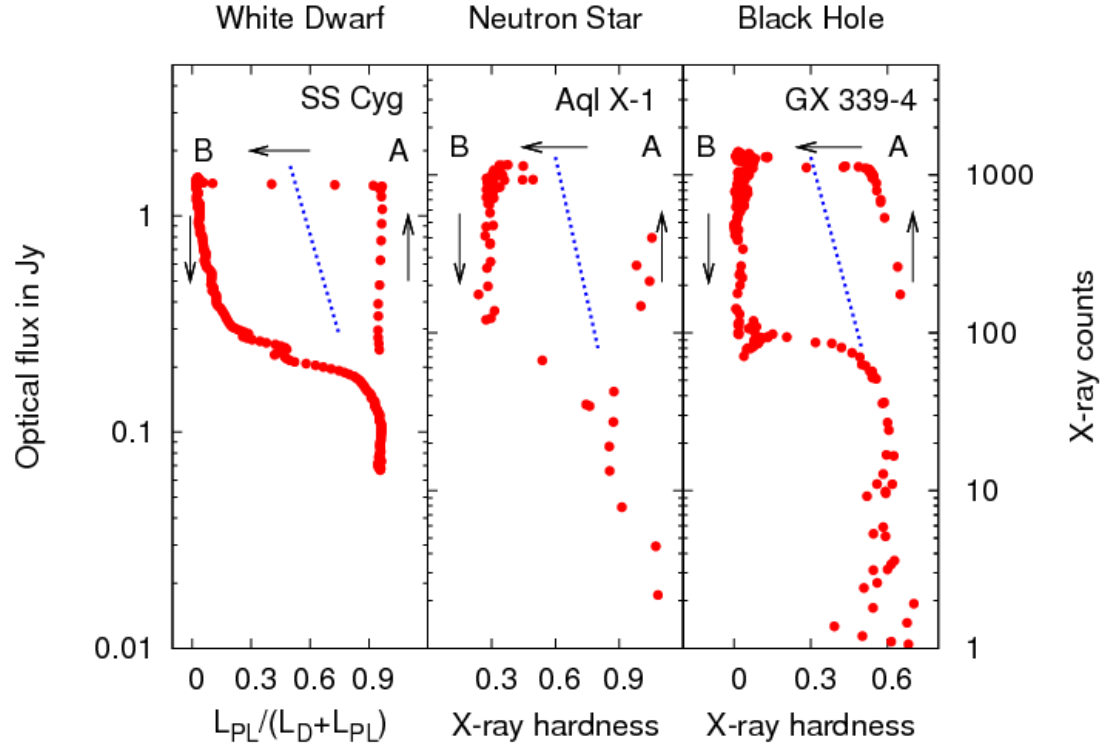


FIGURE 1.16: Credit: Kording et al. 2008. Caption.

that NLs show evidence of synchrotron radio emission ([Coppejans et al. 2015](#)). This important result suggests that our understanding of jets is incomplete, and that the links between accretion state and jet production are fundamental, but unsolved. Disc winds may complicate, or simplify, matters, depending on one's outlook (see chapter 2).

### 1.5.3 A Global Picture

Clearly, accretion physics is relevant to a plethora of astrophysical phenomena, and at least some of the physics of accretion is applicable to *all* classes of accreting object. It would also appear that the outflowing material observed in accreting systems has a profound effect on the accretion process itself, and possibly significantly affects the observational appearance of disc-accreting systems (c.f. Elvis' unification model). Hence, in the next chapter, I will review the evidence for winds and discuss some of the relevant background theory.

# Chapter 2

## Accretion Disc Winds

“A view of space, with an elephant  
obstructing it”

*Mike Vennart, Silent/Transparent*

### 2.1 Observational Evidence

Observational evidence for mass-loaded outflows or winds is widespread across the entire astrophysical mass range and most of the electromagnetic spectrum. Before exploring this evidence, it is pertinent to briefly discuss the ‘smoking gun’ used to unambiguously detect winds – the presence of blue-shifted BALs or ‘P-Cygni’ profiles in an object’s spectrum.

Fig. 2.1 shows how a spherical outflow presenting significant line opacity will cause these characteristic profile shapes to form, as scattering out of the line of sight causes a dip in the blue wing of the line, while scattering into the line of sight from other portions of the outflow causes an increase in flux in the red wing of the line. The situation is much more complex in most astrophysical situations; for example, the geometry is rarely spherically symmetric, and the line is rarely a pure scattering case. Indeed, the potential for complicated radiative transfer effects and the variety in line formation mechanisms (e.g. recombination, collisional excitation) is one of the reasons why 3D Monte Carlo radiative transfer simulations are necessary to effectively model disc winds (see chapter 3).

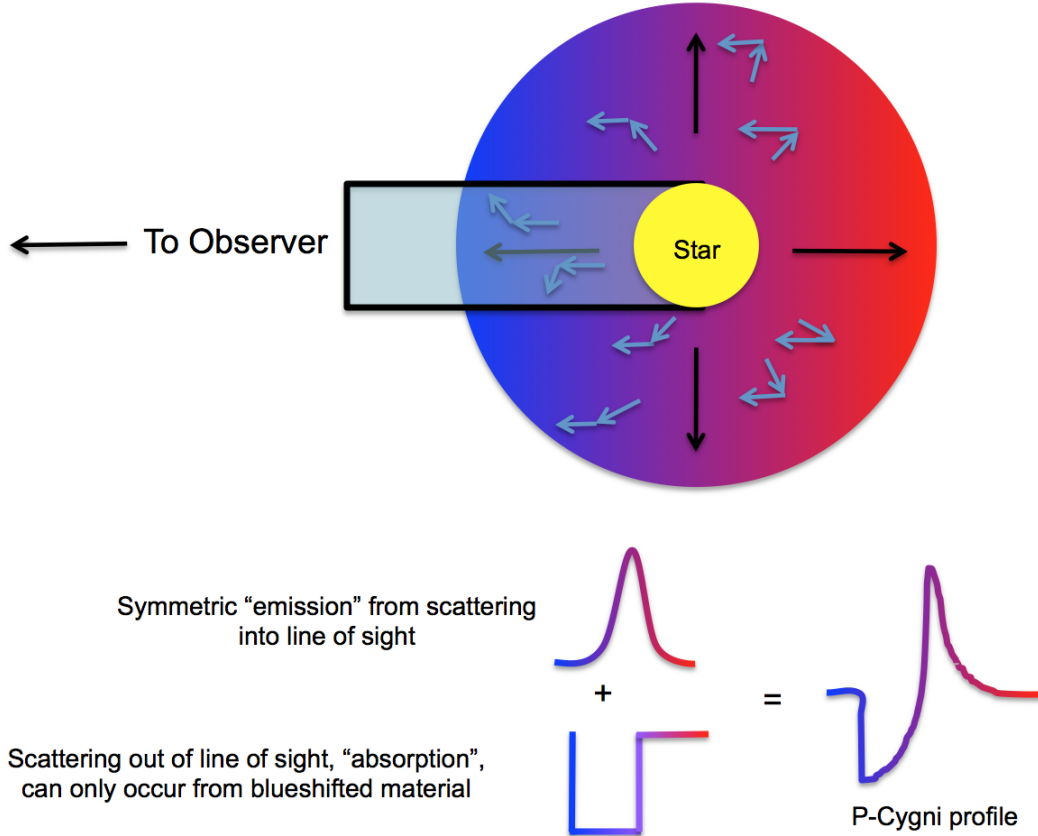


FIGURE 2.1: Diagram showing how an expanding envelope or wind presenting significant line opacity around a continuum source leads to the formation of P-Cygni profiles. The black arrows denote the outflow direction and the blue arrows typical scattering interactions.

### 2.1.1 Cataclysmic Variables

It has been known for a long time that winds emanating from accretion discs are important in shaping the ultraviolet (UV) spectra of high-state CVs (Heap et al. 1978; Greenstein & Oke 1982). The most spectacular evidence for such outflows are the P-Cygni-like profiles seen in UV resonance lines such as C IV 1550 Å (e.g. Cordova & Mason 1982, see Fig. 2.2). Considerable effort has been spent over the years on understanding and modelling these UV features (e.g. Drew & Verbunt 1985; Mauche & Raymond 1987; Shlosman & Vitello 1993; Knigge et al. 1995; Knigge & Drew 1997; Knigge et al. 1997; Long & Knigge 2002; Noebauer et al. 2010; Puebla et al. 2011). The basic picture emerging from these efforts is of a slowly accelerating, moderately collimated bipolar outflow that carries away  $\simeq 1\% - 10\%$  of the accreting material. State-of-the-art simulations of line formation in this type of disc wind can produce UV line profiles that are remarkably similar to observations, as shown in Fig. 2.3.

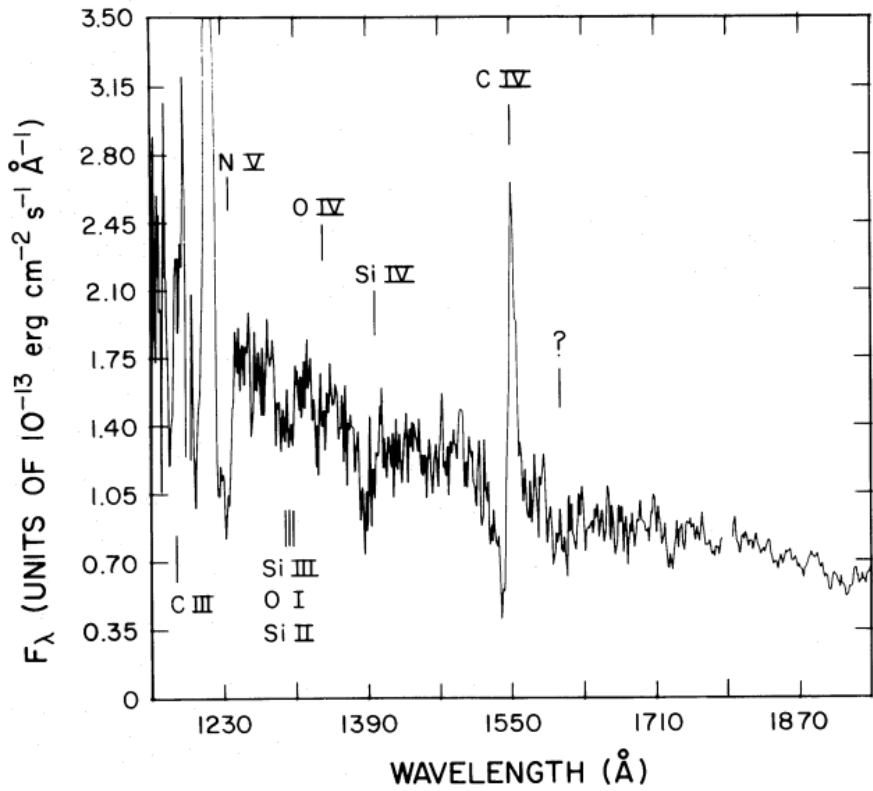


FIGURE 2.2: Credit: Cordova & Mason 1982. UV spectrum of the DN TW Vir during outburst. The P-Cygni profiles can be seen clearly, demonstrating that a strong, fast outflow is present in the system.

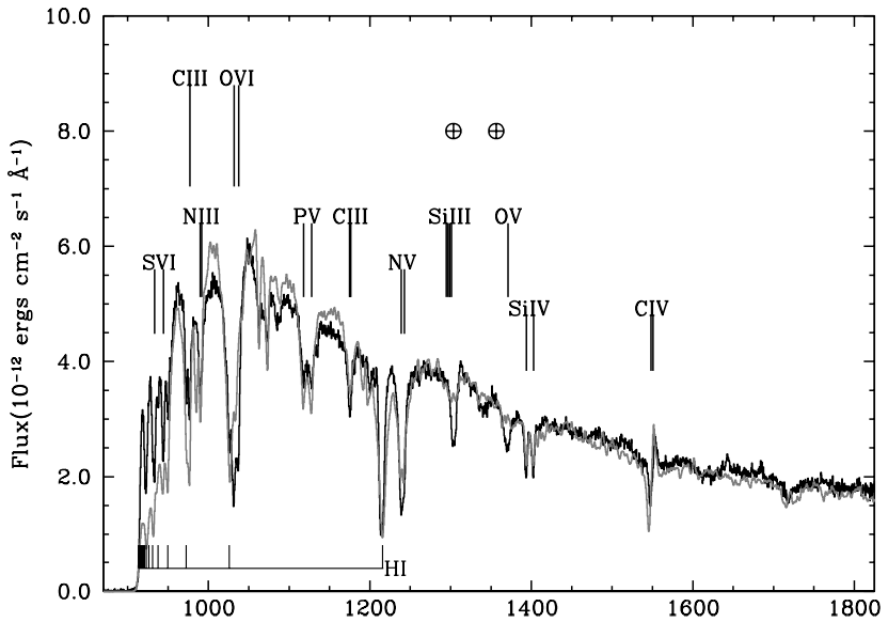


FIGURE 2.3: Credit: Long & Knigge 2002. UV spectrum of Z Cam (black), compared to a synthetic spectrum from MCRT simulations (grey).

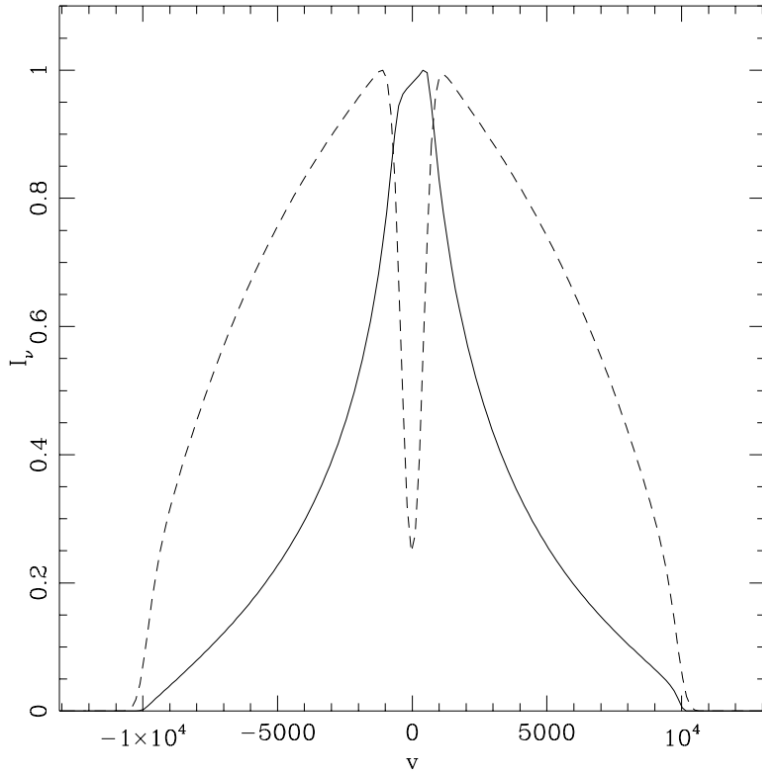


FIGURE 2.4: Credit: Murray & Chiang (1997). A comparison between a line profile, normalised to have peak intensity of 1, produced from a Keplerian disk (solid line) and the same model with an additional disc wind (dashed line). The radial velocity component of the disc wind modifies the escape probabilities across the disc, causing a single-peaked line to form.

Much less is known about the effect of these outflows on the optical spectra of high-state CVs. Direct evidence of wind-formed lines comes from isolated observations of P-Cygni-like line profiles in H $\alpha$  and He I 5876 Å, (Patterson et al. 1996; Ringwald & Naylor 1998; Kafka & Honeycutt 2004). However, the effect of a wind on the *emission* lines in the optical spectrum is unclear. Murray & Chiang (1996, 1997) have shown that the presence of disc winds may offer a natural explanation for the single-peaked optical emission lines in high-state CVs, since they can strongly affect the radiative transfer of line photons (Fig. 2.4; also see Flohic et al. 2012). Stronger support for a significant wind contribution to the optical emission lines comes from observations of eclipsing systems. There, the single-peaked lines are often only weakly eclipsed, and a significant fraction of the line flux remains visible even near mid-eclipse (e.g. Baptista et al. 2000; Groot et al. 2004). This points to line formation in a spatially extended region, such as a disc wind. It is also possible that a wind may affect the continuum emission of CVs, as described in section 1.4. The effect of an accretion disc wind on the optical line and continuum emission of CVs is addressed directly in chapter 4.

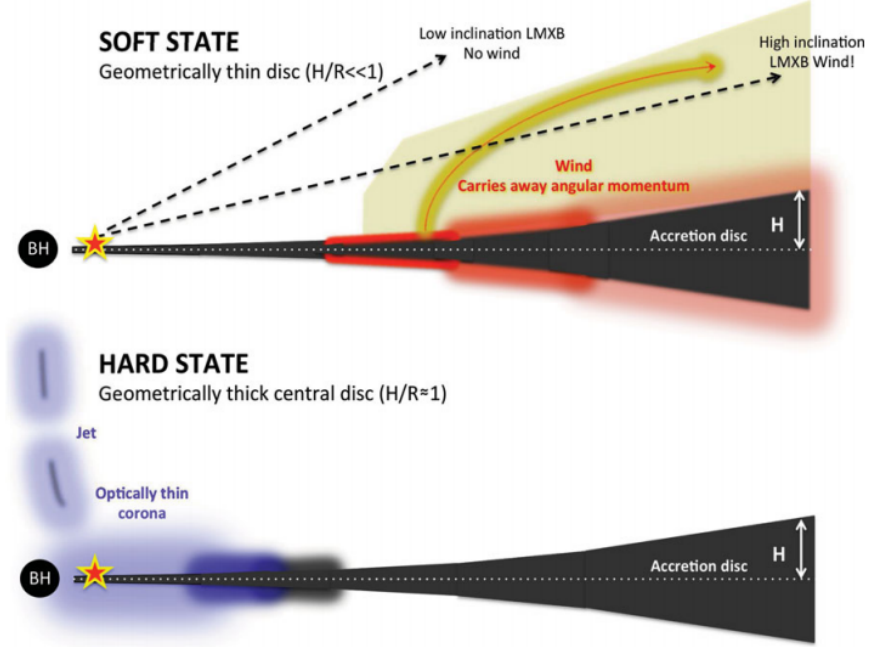


FIGURE 2.5: Credit: Ponti et al. 2012. A cartoon illustrating the expected geometry of soft-state LMXB winds.

### 2.1.2 X-ray Binaries

As in CVs, evidence for fast outflows in LMXBs is not constrained to a single waveband. UV absorption in outflows was detected when [Ioannou et al. \(2003\)](#) observed C IV 1550 Å P-Cygni profiles with blueshifts of  $\sim 1500 \text{ km s}^{-1}$  in the LMXB X2127+119. A series of studies also found X-ray absorption features in similar objects ([Ueda et al. 1998](#); [Kotani et al. 2000](#); [Parmar et al. 2002](#)). These absorption features appeared to be preferentially detected in high-inclination, ‘dipping’ LMXBs. This was confirmed by [Ponti et al. \(2012\)](#), who proposed an equatorial outflow geometry based on this association (see Fig. 2.5). The same study demonstrated that the winds only appeared in the soft, disc dominated accretion state, on the opposite side of the HID to the region where jets are common (Fig. 2.6). This exciting result illustrates how important winds are to our understanding of accretion and requires that we expand the discussion of accretion states from ‘disc-jet’ coupling to also include winds.

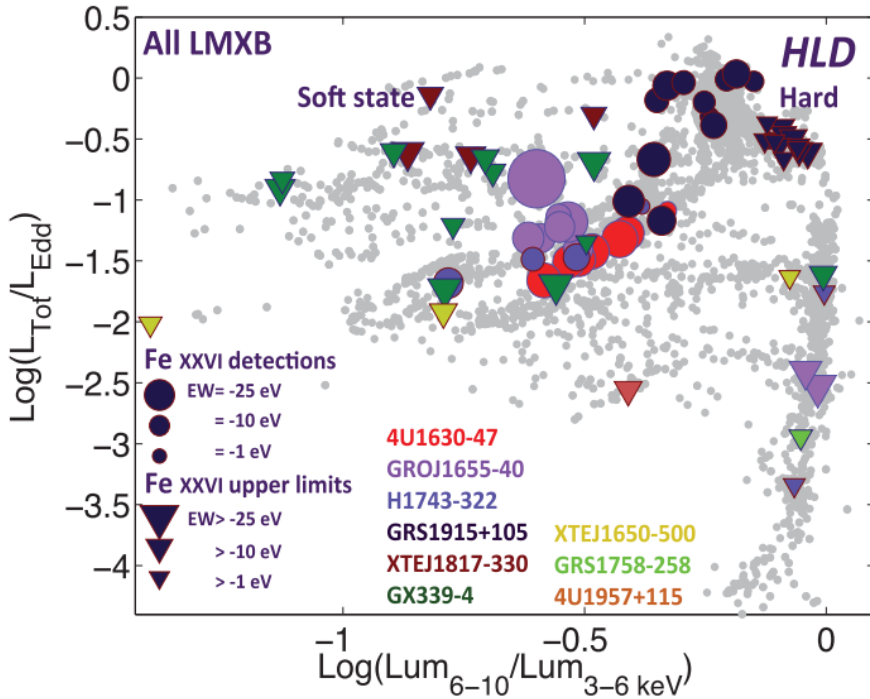


FIGURE 2.6: Credit: Ponti et al. 2012. Hardness-intensity diagram for four dipping LMXBs, demonstrating that winds appear only in the soft state.

### 2.1.3 AGN and Quasars

#### 2.1.3.1 Broad Absorption Line Quasars

Perhaps the clearest evidence of outflows in AGN is provided by the blueshifted ( $\sim 0.1 c$ ) ultraviolet BALs seen in approximately 20% of quasars (Weymann et al. 1991; Knigge et al. 2008; Dai et al. 2008; Allen et al. 2011). High-ionization BAL quasars (HiBALs) only show broad, blue-shifted absorption in species such as C IV, Si IV, N V and O VI, the most prominent BAL profile often being associated with the C IV 1550 Å line. In addition to the more common HiBALs, approximately 10% of BALQSOs also show absorption in lower ionization species such as Mg II and Al III (LoBALs; Voit et al. 1993; Gibson et al. 2009); an even smaller subset also show absorption in Fe II and III (FeLoBALs; Becker et al. 2000; Hall et al. 2002). Some example spectra of BAL quasars from the HST and SDSS archives are shown in Fig. 2.7, with important spectral lines marked.

The simplest explanation for the incidence of BAL quasars (BALQSOs) is in terms of an accretion disc wind viewed from different angles. This principle of geometric unification is very similar to the idea behind the UP95 and AM95 models discussed in Chapter 1. According to this paradigm, a biconical wind rises from the accretion disc so that the

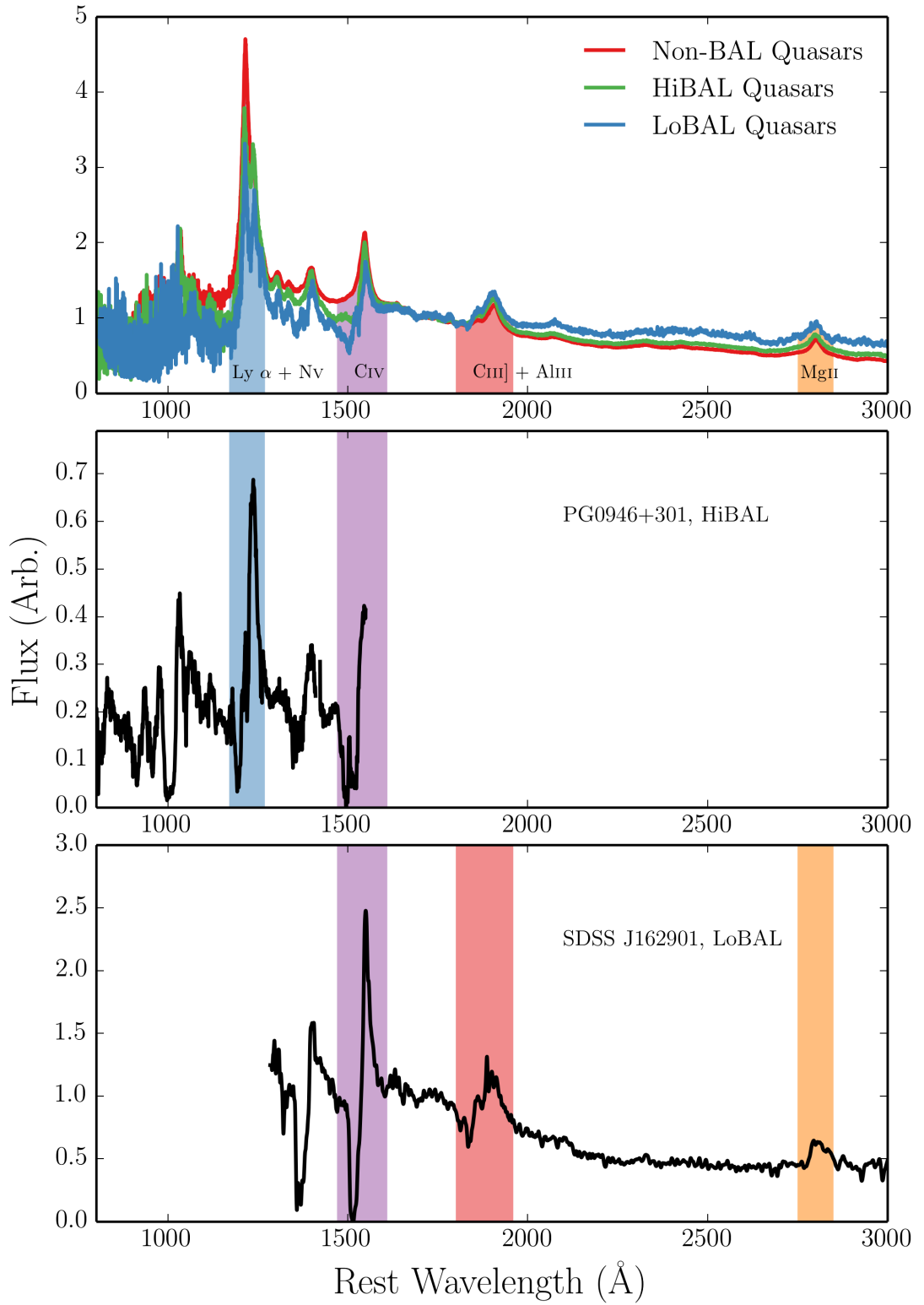


FIGURE 2.7: Top Panel: A comparison between the SDSS non-BAL, HiBAL and LoBAL composite spectra as presented in [Reichard et al. \(2003\)](#). Bottom Two Panels: Two individual examples of a HiBAL and LoBAL quasar spectrum, respectively. In all panels some of the more prominent lines are labeled and shaded, and the object name is given in the bottom two plots.

BALQSO fraction is associated with the covering factor of the outflow. This fraction has been estimated by various authors using different selection criteria, with values ranging between 10% and 40% depending on the treatment of selection effects and the classification scheme used (Weymann et al. 1991; Trump et al. 2006; Knigge et al. 2008; Dai et al. 2008; Allen et al. 2011)

BAL quasars can also be interpreted in an *evolutionary* context, in which quasars spend a certain proportion of their life in the ‘BAL phase’. Models generally put this phase near the start of the quasar lifetime (Hazard et al. 1984; Surdej & Hutsemekers 1987; Boroson & Meyers 1992; Zubovas & King 2013), after a dust-enshrouded phase, but before the main quasar period. It is perhaps more likely that *both* evolutionary and geometric effects are at work (Borguet & Hutsemékers 2010; Dai et al. 2012). One of the main problems with testing these two paradigms is that many of the properties of BAL quasars fit naturally into either picture, and so disentangling their true nature is challenging. The latter chapters of this thesis attempt to address this issue by testing the geometric unification model and seeing how close this simple picture can get to explaining the BAL phenomenon.

While the BAL fraction,  $f_{BAL}$ , is a very useful number and must be at least related to the covering factor of the outflow, continuum selection (Goodrich 1997; Krolik & Voit 1998) and reddening (Allen et al. 2011) effects could lead to significant underestimates of its true value. Unfortunately, accurately correcting for these effects is difficult. The degree of collimation of the BAL wind is also not well known. Polarisation studies suggest that the wind is roughly equatorial (Goodrich & Miller 1995; Cohen et al. 1995), as also found from hydrodynamical and radiative transfer simulations (Proga et al. 2000; Proga & Kallman 2004; Higginbottom et al. 2013; Borguet & Hutsemékers 2010). However, there is also evidence for polar BAL outflows in radio-loud (RL) sources (Zhou et al. 2006; Ghosh & Punsly 2007). In addition to these uncertainties, the physical scale of the BAL phenomenon is also disputed and may vary from object to object. A common assumption is that the BAL region is roughly co-spatial with the BLR, which is reasonable considering the similar velocity widths and ionization states in BELs and BALs. In this case, the radius of the absorbing material can be estimated as  $\sim 100 r_G - 1000 r_G$  from reverberation mapping and microlensing (e.g., for BLRs in BALQSOs, Sluse et al. 2015; O’Dowd et al. 2015). However, distances of  $\sim 0.1$  pc ( $\sim 10^4 r_G$ ) have been estimated in at least some objects from photonization modelling,

conducted using densities calculated from absorption line doublets (Borguet et al. 2013; Chamberlain et al. 2015).

BAL quasars display a wide variety of different trough shapes. The line profiles themselves often show complex structure (Foltz et al. 1987; Ganguly et al. 2006; Simon & Hamann 2010) and can be time variable (Hall et al. 2011; Capellupo et al. 2011, 2012, 2014; Filiz Ak et al. 2012). Furthermore, a subset of quasars show BAL-like absorption troughs with much smaller velocity widths. Depending on their width, these are known as narrow absorption lines (NALs) or ‘mini-BALs’ (Misawa et al. 2007, 2008; Nestor et al. 2008). While some of this behaviour can be explained once again as a viewing angle effect (e.g. Ganguly et al. 2001), the BAL profile variety and variability implies that BALQSOs are far from a homogenous population, and perhaps suggests the existence of dense substructures (clumps) in their flows. Such clumpiness has been invoked in several disc wind unification models for AGN and quasars (see section 2.3)

The X-ray properties of BAL quasars are particularly important due to the strong ionizing potential of the X-ray radiation. Observationally, BALQSOs are X-ray weak when compared to non-BAL quasars (Gibson et al. 2009). This X-ray weakness is often attributed to the presence of absorbing material with column densities of  $N_H \sim 10^{22-24} \text{ cm}^{-2}$  along the line of sight (Gallagher et al. 1999, 2002; Green et al. 2001; Grupe et al. 2003a; Stalin et al. 2011), although there is also evidence that BALQSOs are *intrinsically* X-ray weak (Sabra & Hamann 2001; Clavel et al. 2006; Morabito et al. 2013). The X-ray properties of BAL quasars are fundamentally coupled to the properties of the wind – the X-ray absorption may, in fact, be caused by the outflow, which in turn has its ionization state determined by the X-ray radiation. Furthermore, the true X-ray luminosities cannot be reliably inferred until the inclinations of BALQSOs are constrained, as gravitational lensing can significantly alter the emergent angular distribution of X-ray emission even for an intrinsically isotropic source (Chen et al. 2013a,b).

Although the observed X-ray emission in BALQSOs is weaker than in otherwise similar quasars, it still still possesses strong ionizing power. This leads to what has become known as the ‘over-ionization problem’ in BALQSOs: how is the moderate ionization state of the BAL gas maintained in the presence of ionizing X-rays? A number of potential solutions have been proposed, which can be broadly separated into ‘shielding’ models (Murray et al. 1995; Proga & Kallman 2004) and ‘clumpy’ models (de Kool &

Begelman 1995; Hamann et al. 2013). Some of these models are discussed further in section 2.3 and chapter 5.

### 2.1.3.2 Warm Absorbers

Warm absorbers (WAs) are regions of photoionized plasma responsible for some of the characteristic absorption features seen in the soft X-ray spectra of AGN (Reynolds & Fabian 1995). In particular, they produce photoelectric continuum absorption (e.g. Halpern 1984; Cappi et al. 1996; Kriss et al. 1996) and a series of narrow absorption lines in H-like and He-like ions of C, N, O, Si, Ne, and Fe (Kaastra et al. 2000). A wind origin is a common hypothesis for WAs (e.g. Krolik & Kriss 2001). Clear evidence for this comes from the measured blueshifts of the lines, typically on the order of  $\sim 100 \text{ km s}^{-1}$ . X-ray absorption and WAs are often variable (Fabian et al. 1994; Otani et al. 1996), which may be interpreted in terms of the changing kinematics of an accretion disc wind (Connolly et al. 2014). There is also evidence of contemporary and associated UV and X-ray absorption in NGC 5548 (Kaastra et al. 2014) and in mini-BALS (Giustini et al. 2011), and, as mentioned above, BALQSOs often show strong X-ray absorption. This suggests the same outflow may produce observational signatures across a large range of ionization states and line energies.

Some WAs can be modelled well with single absorbers (Kaastra et al. 2000), but most require multiple absorption components with different ionization states (e.g. Kriss et al. 1996; Orr et al. 1997; Krolik & Kriss 2001; Connolly et al. 2014). One common way to parameterise the ionization state of a plasma is via the ionization parameter, given by (e.g. Reynolds & Fabian 1995)

$$\xi = \frac{L_H}{n_H R^2}, \quad (2.1)$$

where  $L_H$  is the luminosity above 13.6eV, and  $n_H$  is the number density of H atoms. If the absorber is stratified and the SED subject to absorption, self-consistent ionization and radiative transfer models should really be used to model the spectrum (see e.g. chapter 3). This is because optically thin ionization parameter estimates will not properly capture the ionization physics due to the variation of the SED shape within the medium. The overall body of observations points towards an outflow with a stratified ionization structure ranging from  $\log \xi \sim 0 - 2$  and densities on the order of  $10^7 \text{ cm}^{-3}$ , located at around  $\sim 10^{16} \text{ cm}$ . These physical conditions or scales are not well constrained, and

the connection to other outflows, such as the ultra-fast outflows introduced in the next section, is unknown. Timing observations may help to shed light on the properties of the mysterious, but ubiquitous, AGN WAs (Silva et al. 2015).

### 2.1.3.3 Ultra-fast Outflows

In addition to acting as WAs, winds can also imprint clear absorption features in highly ionized Fe K $\alpha$  lines in AGN such as PDS 456 (Reeves et al. 2003; Gofford et al. 2014; Matzeu et al. 2016), MCG-5-23-16 (Braito et al. 2007) and PG 1211+143 (Pounds & Reeves 2009; Fukumura et al. 2015). These outflow signatures are fairly common in Seyfert galaxies (Tombesi et al. 2010; Gofford et al. 2013). One example of such a feature is shown in Fig. 2.8, along with a simple spherical outflow model fit (Nardini et al. 2015). The high velocities ( $\sim 0.1c$ ) inferred from the line blueshifts have lead to these winds becoming known as ultra-fast outflows, or UFOs.

UFOs are characterised by ionization parameters in the range  $\log \xi \sim 3 - 4$  and column densities  $N_H > 10^{22} \text{ cm}^{-2}$ . Their high mass-loss rates and large energy budgets mean that they are natural candidates for AGN feedback (see section 2.5). Measurements of their kinetic luminosities suggest that UFOs have sufficient energy to affect their host galaxy (Gofford et al. 2015). In fact, a large-scale molecular outflow has recently been detected in one UFO host, possibly driven by the UFO itself (Tombesi et al. 2015). As with WAs, many of the models used to constrain physical parameters are simplistic, and assume single ionization parameters, large covering factors and thin expanding shells of outflow. Under the assumption of a thin expanding shell, the mass-loss rate can be estimated using (e.g. Borguet et al. 2012)

$$\dot{M} \sim \Omega N_H m_p v_{out} R_{in}, \quad (2.2)$$

where  $\Omega$  is the solid angle covered by the outflow,  $N_H$  is the column density,  $m_p$  is the proton mass,  $v_{out}$  is the outflow velocity and  $R_{in}$  is the launch radius of the outflow. In reality, the absorber is probably much more complex, and full RT and photoionization simulations are required to accurately model the expected spectrum. In a series of papers, Sim et al. (2008, 2010b,b) carried out such calculations and found that reasonable verisimilitude with Fe line profiles could be achieved. However, as with many models of AGN, a holistic, broad wavelength range fit is still required.

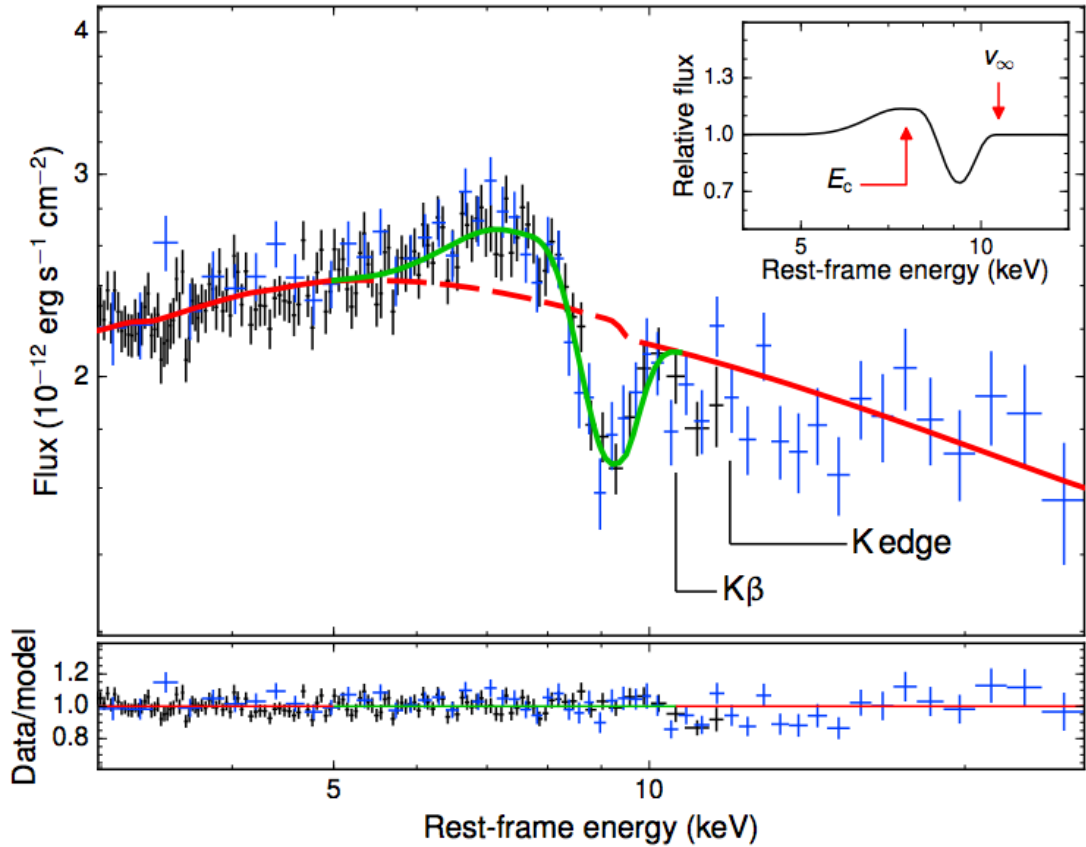


FIGURE 2.8: Credit: Nardini et al. 2015. X-ray spectrum of PDS 456 fitted with a P-Cygni profile from a spherical outflow model. *XMM-Newton* data is shown in black with two combined *NuStar* observations in blue.

#### 2.1.4 Stellar Winds

Although stellar winds are clearly not accretion disc winds, they provide a useful, and better understood, testing ground for much of the physics of radiatively-driven outflows. Wolf-Rayet (WR) stars and O-stars possess strong outflows with mass-loss rates of up to  $10^{-5} M_\odot \text{ yr}^{-1}$ , thought to be driven by radiation pressure mediated by spectral lines (see section 2.2.3). Over the typical lifetime of a massive star ( $\sim 10^6 \text{ yr}$ ), this can have a significant impact on the overall stellar mass, causing losses of around  $10 M_\odot$  of material.

As with the systems described previously, the P-Cygni profiles seen in hot, massive stars provide the key evidence for the presence of a strong wind (see Fig. 2.9). Mass-loaded winds are also thought to be responsible for the emission lines seen in hot star spectra (e.g. Pauldrach et al. 1994). Indeed, emission line diagnostics have been particularly important in determining the mass-loss rates of stellar winds and have also been used to demonstrate that line-driven stellar winds are clumpy.

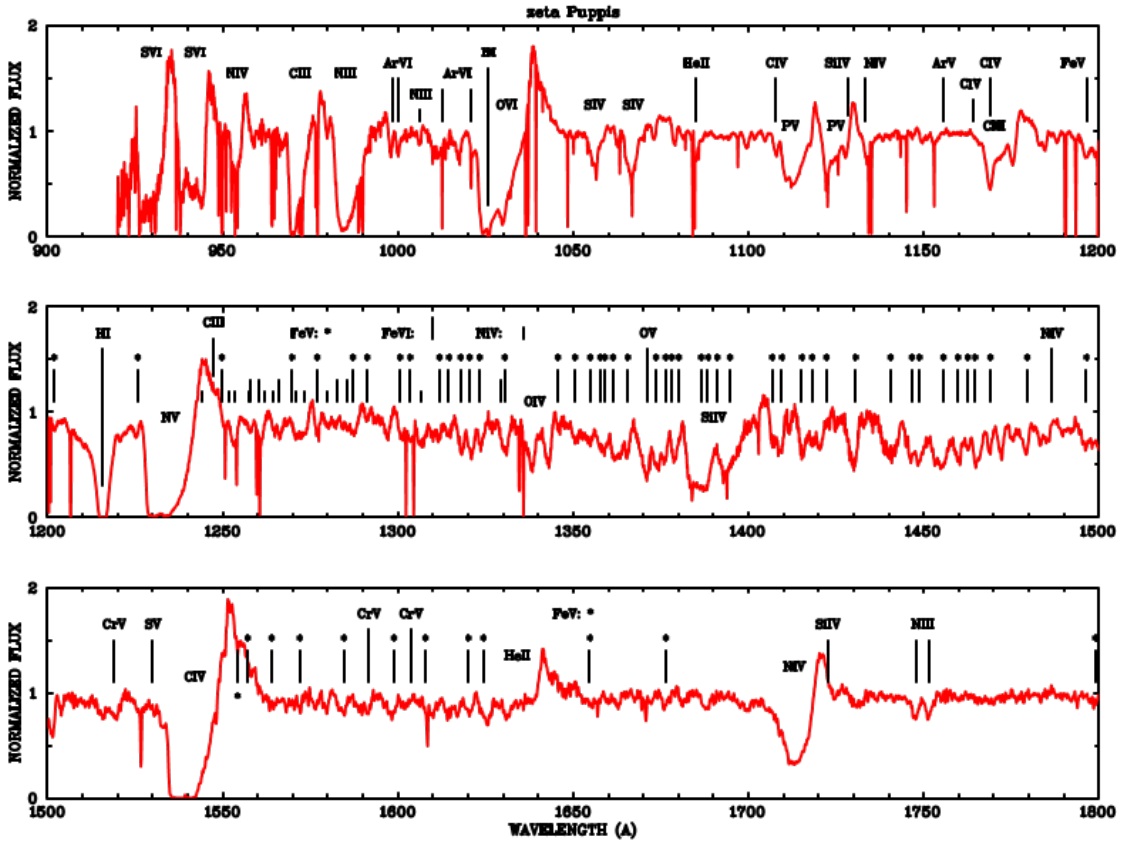


FIGURE 2.9: Credit: Pauldrach et al. 1994. UV spectrum of one of the brightest massive O stars, the O4 supergiant  $\zeta$  Puppis. The spectrum is merged from Copernicus and IUE UV observations, and the prominent lines are marked.

#### 2.1.4.1 Clumping in Stellar Winds

Evidence for clumping in hot star winds comes from a range of sources. Perhaps the most conclusive is from electron scattering wings in emission lines: homogenous models overestimate the strength of these wings, whereas clumpy models produce good agreement with data (Hillier 1984, 1991; Hamann et al. 1992, 1994; Schmutz 1997). Further evidence for clumping comes from line variability (Prinja & Smith 1992) and polarisation (Brown et al. 1995). Clumping is theoretically expected in line-driven winds (see section 2.2.3 and the review by Owocki 2014) and is directly dealt with in this thesis. In chapter 5, I describe the treatment of clumping I have implemented in our radiative transfer code, before presenting results from a clumpy AGN wind model.

### 2.1.5 Outflow Physics

The spectra in figures 2.2, 2.7 and 2.9 show striking similarities – characteristic broad, P-Cygni-like absorption features in UV resonance lines extending to high blueward velocities – despite vast differences in mass and scale. Furthermore, some of the phenomena observed in e.g. stellar winds may naturally solve some of the unanswered questions in other systems. For example, clumping may prevent over-ionization in AGN outflows. It would seem that at least some of the physics of outflows, like accretion physics, is universal, and that lessons learned from smaller-scale systems may be scaleable to AGN and quasars. In order to understand if the similarity extends beyond a cosmetic one, I will discuss some of the underlying physical mechanisms that may be responsible for accelerating these outflows.

## 2.2 Driving Mechanisms

Let us consider a parcel of ideal gas. By imposing nothing more than conservation of mass, energy and momentum on that parcel, and using Maxwell's equations, we can write down three equations of magnetohydrodynamics (MHD):

$$\frac{D\rho}{Dt} + \rho\nabla \cdot \vec{v} = 0, \quad (2.3)$$

$$\rho \frac{D\vec{v}}{Dt} = -\nabla P + \frac{1}{4\pi}(\nabla \times \vec{B}) \times \vec{B} + \rho\vec{g}_{rad} + \rho\vec{g}, \quad (2.4)$$

$$\rho \frac{D}{Dt} \left( \frac{e}{\rho} \right) = P(\nabla \cdot \vec{v}) + \rho\mathcal{L}. \quad (2.5)$$

Here,  $D$  denotes a derivative within the comoving frame of the gas parcel,  $\vec{v}$  is the velocity,  $\rho$  is the gas density,  $\vec{B}$  is the local magnetic field,  $\vec{F}_{rad}$  is the radiation force per unit mass,  $\mathcal{L}$  is the cooling rate of the gas, and  $\vec{g}$  denotes the gravitational acceleration vector.

Equation 2.3 is the *continuity equation* and describes conservation of mass. Equation 2.4 is the *equation of motion* and describes conservation of momentum. Equation 2.5 is the

*equation of energy conservation.* Equation 2.4 can be used to neatly demonstrate how an outflow can be driven. I have deliberately written equation 2.4 so that all the force terms lie on the RHS. For an outflow to be driven from an accreting object, one of the terms on the RHS must dominate over gravity,  $\rho\vec{g}$ . These terms thus signify three potential driving mechanisms.

- Magnetic / Lorentz Forces,  $\frac{1}{4\pi}(\nabla \times \vec{B}) \times \vec{B}$ .
- Radiative Forces,  $\rho\vec{g}_{rad}$ .
- Thermal Pressure,  $-\nabla P$ .

We can now examine under what physical conditions (and in which corresponding astrophysical objects) we might expect these forces to overcome gravity and cause a parcel of mass to escape to infinity. In other words: *what might drive a wind?*

### 2.2.1 Thermal Winds

In a disc in hydrostatic equilibrium (HSE), thermal pressure balances gravity in the vertical direction. The equation of motion in this  $z$  direction can then be written as

$$\rho \frac{Dv_z}{Dt} = -\frac{\partial P}{\partial z} + \rho g_z = 0. \quad (2.6)$$

Clearly, if the thermal pressure is significantly increased, this equilibrium condition no longer holds. This can occur in accretion discs at temperatures in excess of  $\sim 10^7$  K – where other forces are negligible compared to thermal pressure – and where the escape velocities are relatively low (i.e. far out in the disc). Due to the temperature and gravity scalings, this means that XRBs are natural candidates for showing evidence of thermally driven winds. The outer disc can be heated to the Compton temperature by the central X-ray source, potentially driving relatively high mass-loss rate outflows (Begelman et al. 1983; Woods et al. 1996). This driving mechanism has been proposed as a natural explanation for the ever-present equatorial outflows in soft state XRBs (Ponti et al. 2012). However, they are much less likely candidates in CVs and AGN, because there the escape velocity tends to greatly exceed the thermal velocity.

### 2.2.2 Radiatively Driven Winds

Under spherical symmetry and for opacities dominated by electron scattering, one simply obtains the Eddington limit discussed in section 1.1.1 when  $\rho\vec{F}_{rad} = \rho\vec{g}$ . Hence, sources must be fairly close to the Eddington luminosity in order to drive an outflow purely from radiation pressure on electrons. There are a number of accreting systems that may drive super-Eddington (or close to Eddington) outflows, such as AGN with UFOs (e.g. Reeves et al. 2002; Pounds et al. 2016), NLSIs (Done & Jin 2015) and ultra-luminous X-ray sources (ULXs; Walton et al. 2013). However, high-state CVs are significantly below the Eddington limit (Warner 2003), and at least some BALQSOs have low Eddington fractions ( $\sim 25\%$  have  $L/L_{\text{Edd}} < 0.1$ ; Grupe & Nousek 2015). These systems may nevertheless be capable of radiatively driving strong outflows due to the influence of line opacity.

### 2.2.3 Line-driven Winds

Under the right ionization conditions, radiation pressure mediated by spectral lines can be a significant acceleration term in a partially ionized plasma (Castor et al. 1975, hereafter CAK). The most common way to parameterise the cumulative effect of lines on the radiation force is via the *CAK force multiplier*,  $\mathcal{M}(t)$ , which modifies the equation for the acceleration due to radiation pressure on electrons to give (Castor 1974, CAK)

$$\vec{g}_{rad} = \frac{\sigma_T F}{\mu cm_p} \mathcal{M}(t), \quad (2.7)$$

where  $F$  is the flux, and  $\mu$  is the mean atomic weight.  $\mathcal{M}(t)$  can be approximated by (Abbott 1982)

$$\mathcal{M}(t) = t^{-\alpha} \left( \frac{n_e}{10^{11} \text{ cm}^{-3}} \right)^\delta, \quad (2.8)$$

where  $t$  is the dimensionless optical depth, given by

$$t = \frac{\sigma_T \rho v_{th}}{m_p |d(v_i)/ds|}. \quad (2.9)$$

Here,  $k$ ,  $\alpha$  and  $\delta$  are parameters with best-fit values of 0.28, 0.56 and 0.90, respectively, in O-star winds (Abbott 1982), and  $v_i$  is the component of the velocity field in the direction being considered. This is normally a line between the source of radiation and any given location in the wind. It is possible to show (CAK, Owocki et al. 1988) that the

maximum force multiplier,  $\mathcal{M}_{\max}(t)$ , is around 2000–4000. This is already an interesting result, as it tells us that line-driven outflows can be accelerated when accretion rates / luminosities are much lower than the Eddington limit. Indeed, using equation 2.7 we can see that a radiatively driven wind can be accelerated when  $L > L_{\text{Edd}}/M(t)$ , where  $M(t)$  will depend in detail on the spectral lines in question and their relative ionization and excitation fractions. Line-driven winds are present in O-stars and Wolf-Rayet stars, and the theory produces good matches with observations (e.g. Friend & Abbott 1986; Pauldrach et al. 1986, 1994; Hamann et al. 2008). It is also a strong candidate for driving the winds seen in high-state CVs when the accretion disc is UV bright (Pereyra et al. 1997; Proga et al. 1998; Proga 2005, see also section 2.3.4).

Line driving may be a promising mechanism to explain BAL outflows as well, since the strong UV resonance lines seen in absorption in O stars are also present in BALQSOs. The presence of ‘line-locked’ features (Bowler et al. 2014) and the ‘ghost of Ly $\alpha$ ’ (Arav et al. 1995; Arav 1996; North et al. 2006) in the spectra of some BALQSOs also suggests that line-driving is at least contributing to the acceleration of the wind (but see also Cottis et al. 2010). However, the presence of an X-ray source complicates matters. I have already briefly touched on the ‘over-ionization’ problem in AGN outflows, but it now has another consequence. Not only will strong X-rays prevent the right features forming in the spectrum, but, if the outflow is line-driven, they may prevent the wind existing in the first place. Despite these problems, some hydrodynamic simulations of line-driven AGN winds have been successful in producing high mass-loss rates (see section 2.3.4).

Line-driving is subject to a strong instability known as the line deshadowing instability (LDI; Lucy & Solomon 1970; MacGregor et al. 1979; Owocki & Rybicki 1984, 1985). The basic idea is that any velocity perturbation in a line-driven flow can cause a ‘deshadowing’ effect, as the fluid element will now be in resonance with a region of the spectrum that is less absorbed. Thus, an increase in the line force will occur in proportion with this velocity perturbation, and the instability can grow. Time-dependent numerical modelling of the LDI has shown that it can produce a clumpy flow (Owocki et al. 1988; Feldmeier 1995; Šurlan et al. 2012; Owocki 2014) that may explain the observational characteristics of clumping in stellar winds (see section 2.1.4.1). The LDI is also of interest in CV and AGN winds, as it may affect the ionization state of the flow and possibly the inferred mass-loss rates.

### 2.2.4 Magnetic Winds

There is still great uncertainty over the magnetic fields in accretion discs and the physics of these magnetic processes. However, the MRI is one of the leading candidates for explaining angular momentum transport in accretion discs, implying that magnetic processes are important in their dynamics. Thus, in many senses, magnetic driving is an attractive wind driving mechanism. There are two main ways in which magnetic forces can drive an accretion disc wind, which are best explained by writing down an alternative form for the Lorentz force,

$$\vec{F}_m = \frac{1}{4\pi} \vec{B} \cdot \nabla \vec{B} - \nabla \frac{B^2}{8\pi}. \quad (2.10)$$

The first term can be thought of as a magnetic *tension* associated with the field lines and the second as an isotropic magnetic *pressure*.

Historically, the most popular magnetic wind model has been the ‘bead on a wire’ mechanism proposed by [Blandford & Payne \(1982\)](#) and [Pelletier & Pudritz \(1992\)](#). In these models, the poloidal magnetic field is dominant and is anchored in the accretion disc. A wind can then be driven by magnetic tension, as the first term in the above equation operates on fluid elements (‘beads’) on the surface of the accretion disc. This can accelerate a wind when the poloidal component of the field makes an angle of  $> 30^\circ$  with the normal to the disc surface. These models are known as magnetocentrifugal winds, as it is the interaction between centrifugal forces and a strong, large-scale, ordered magnetic field threading the disc that drives the wind. Magnetocentrifugal wind models have been proposed for both AGN and YSOs ([Pelletier & Pudritz 1992](#); [Konigl & Kartje 1994](#); [Kudoh & Shibata 1997](#)), and numerical simulations have demonstrated that this mechanism can produce jets and outflows ([Romanova et al. 1997](#); [Ouyed & Pudritz 1997](#); [Ustyugova et al. 1999](#)).

In an alternative MHD model the isotropic magnetic pressure is responsible for driving the outflow ([Proga 2003](#)). In this case the toroidal component dominates over the poloidal component and drives a slow, dense outflow which behaves more like a thermally-driven wind (i.e. it conserves specific angular momentum rather than angular velocity).

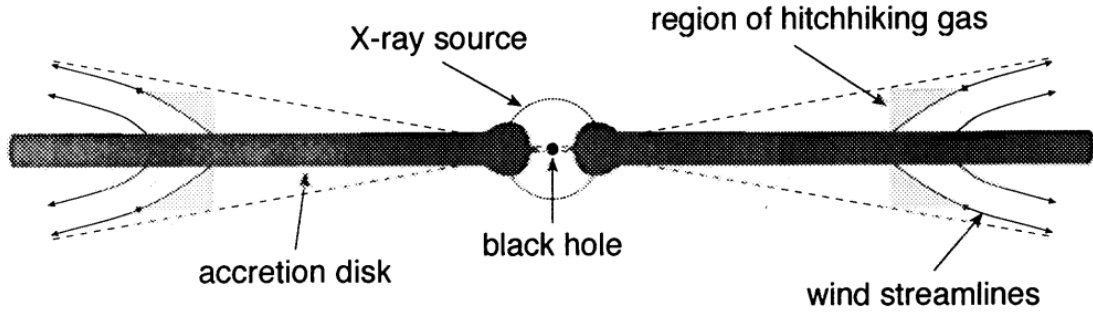


FIGURE 2.10: Credit: Murray et al. 1995. Cartoon showing the geometry of the MCGV95 model.

## 2.3 Accretion Disc Wind Models

A number of different wind models have appeared in the literature over the years, each attempting to explain the different observational characteristics of quasars and CVs with a mixture of conceptual frameworks and underlying physics. In AGN and quasars, the authors behind the models attempt to explain the origins of BELs and BALs, although some extend their remit into the infra-red, radio and X-ray regimes. In CVs, the picture is slightly more straightforward, as the geometry of the outflow is better constrained (see section 2.1.1). Below, I will briefly discuss a few examples that have gained traction over the years, particularly those describing quasars and unification, before outlining the kinematic prescription I have used in the modelling that forms part of this thesis. This prescription has been successfully applied to both CVs and AGN.

### 2.3.1 MCGV95: A Line-driven Wind Model for AGN

MCGV95 proposed a model in which a smooth wind rises from an accretion disc with a launch radius of around  $10^{16}$  cm. The wind is equatorial, with an opening angle of  $5^\circ$ , and is accelerated by line forces up to a terminal velocity of  $0.1c$ . A sketch of the geometry is shown in Fig. 2.10. One of the key features of the model is the presence of a ‘shield’ of hitchhiking gas, which protects the outflow from X-ray over-ionization and allows radiation pressure on UV resonance lines to efficiently accelerate the flow.

MCGV95 found that BAL profiles were seen for an observer looking into the wind cone, and significant collisionally excited line *emission* emerged at low inclinations. This line emission came from a relatively small BLR ( $r_{BLR} \sim 10^{16}$  cm) at the base of the wind, where densities were high ( $n_e \approx 10^{10}$  cm $^{-3}$ ). The MCGV95 model was one

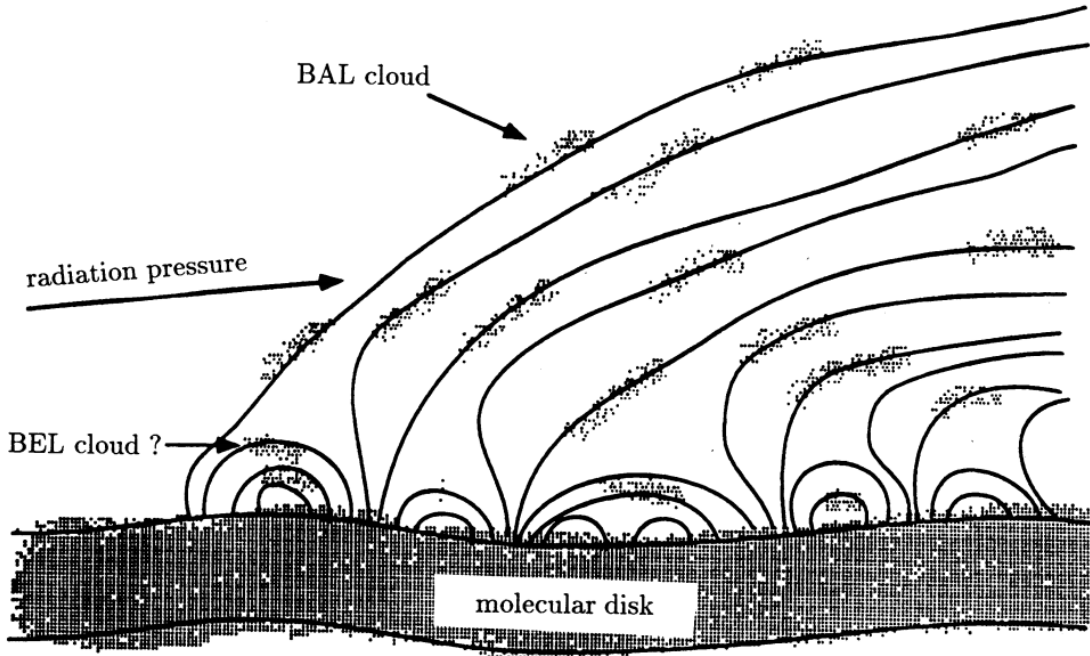


FIGURE 2.11: Credit: De Kool & Begelman 1995. A cartoon showing the components in the De Kool & Begelman model.

of the first successful disc-wind unification models. It is especially impressive as it includes photoionization calculations and quantitative estimates of the resultant line EWs. However, the effects of multiple scattering and complex radiative transfer effects could not be included in the calculations (see chapter 5).

### 2.3.2 De Kool & Begelman: A Radiatively Driven, Magnetically Confined Wind

It is, of course, possible that radiation and magnetic fields are both important in determining the outflow characteristics. In the [de Kool & Begelman \(1995\)](#) model, radiation pressure drives an outflow from an accretion disc and also compresses the magnetic field lines that are dragged along with the flow. This causes the magnetic field strength in certain regions to be comparable to the gas pressure, meaning that clouds can be magnetically confined in the flow. A diagram is shown in Fig. 2.11. The authors find that such a model would naturally emerge at a fairly equatorial angle with a covering factor of around 10%, and that lower ionization material would be intercepted when the system was viewed from higher inclinations, potentially explaining some of the properties of LoBALQSOs.

### 2.3.3 Elvis 2000: A Structure for Quasars

[Elvis \(2000\)](#) expanded on the work of MCGV95 by proposing a simple disc wind model, empirically designed to explain as much of quasar phenomenology as possible within one unifying framework. The geometry of Elvis' is shown in Fig. 2.12. As in the two previous models, observers looking into the wind cone will see a BALQSO, whereas observers looking down onto the wind will see a type 1 quasar. Initially, the wind rises vertically, so that observers looking underneath the flow will see NALs, due to the small range of velocities intercepted by their line of sight.

The flow conserves angular momentum, such that the initial Keplerian velocities determine the BEL widths, before accelerating to BAL-like velocities of  $\sim 0.1c$ . The wind is assumed to be two-phase, with BEL and BAL clouds embedded in a warm, highly ionized medium (WHIM). This WHIM is responsible for WA-like absorption and the X-ray scattering phenomena seen in AGN. It is also responsible for confining the BAL and BEL clouds, allowing high densities and cooler temperatures to exist within the flow. The ionization structure for the wind is stratified, such that the material further out along the disc plane is somewhat shielded from the inner disc and X-rays. This allows the lower ionization BEL profiles to form in the right locations, and also means that LoBAL profiles would be seen at a subset of inclinations.

### 2.3.4 Proga et al.: Line-driven Hydrodynamic Models for AGN and CVs

Around the turn of the century, Daniel Proga and collaborators published a series of important papers in which they conducted hydrodynamic simulations of line-driven disc winds in AGN and CVs. In the first of these, the problem considered was that of disc winds in CVs ([Proga et al. 1998](#)). In their model, the disc was assumed to radiate according to the  $\alpha$ -disc model, and the central WD was also included as a radiating source. They found that when the disc has  $L/L_{\text{Edd}} \gtrsim 1/\mathcal{M}_{\max}(t) \approx 0.001$ , then strong, line-driven outflows are driven from a few WD radii with bending angles of  $\sim 45^\circ$ . This result agreed qualitatively with outflows in CVs, and later efforts to compute synthetic line profiles produced promising results ([Proga et al. 2002a](#)). This was the first successful demonstration of line driving in a full hydrodynamic simulation.

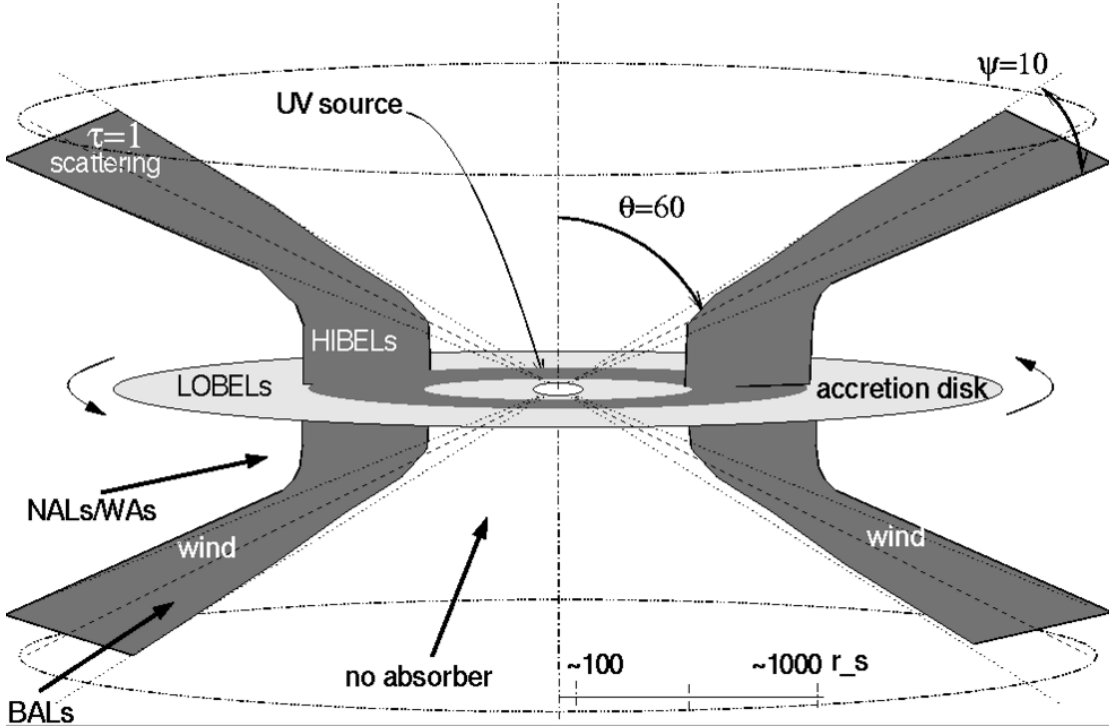


FIGURE 2.12: Credit: Martin Elvis. A schematic showing the main features of the Elvis model. A biconical wind rises from an accretion disc, and the observed spectrum is determined purely by the viewing angle of the observer.

The same principle was then applied to the problem of AGN outflows, with the additional complication of an ionizing X-ray source now included (Proga et al. 2000; Proga & Kallman 2004, hereafter PK04). A snapshot from the PK04 model is shown in Fig. 2.13. An inner ‘failed’ wind forms in this simulation, which initially rises up from the disc before being over-ionized by the central X-rays. Crucially, this acts as a shield, similarly to the hitchhiking gas proposed by MCGV95, and allows a line-driven wind to be accelerated further out in the disc. This outflow can be seen clearly in Fig. 2.13.

One of the interesting results of these simulations is that they tended to produce somewhat unsteady, clumpy flows. In the CV case, this was caused by the interaction between the line force and gravity, as both force terms vary differently with height. In the AGN case, it was instead due to the critical importance of the ionization state on the line force. Parcels of gas can only be accelerated if they have the ‘right’ ionization state, and this depends critically on both their density and the radiation field they see. This causes a coupling between the dynamics of the flow and the path of ionizing radiation. The radiation field also helps determine the geometry of the outflow, as increasing the strength of the radiation interior to the launch radius tends to flatten out the wind and lead to more equatorial outflows (Proga 2005). This is particularly important when

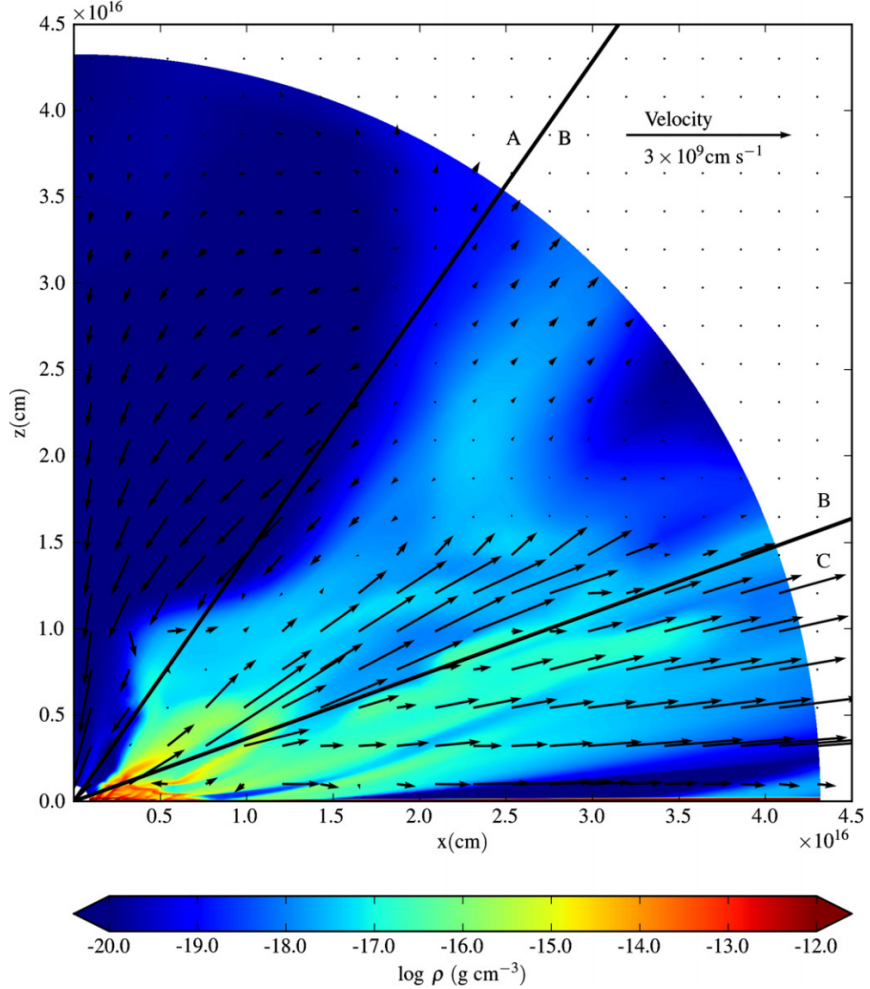


FIGURE 2.13: Credit: Higginbottom et al. 2014.. A snapshot of the PK04 model. Colours shows the density and arrows show the velocity of the flow. The radial lines separate three areas described by H14.

considering quasar unification, as it means the viewing angles of BALQSOs can provide information about where the wind is launched.

It is worth noting that the smaller scale LDI could not be included in this model, partly for computational reasons and partly because of the approximations used to treat the radiation field. Treating the radiation transport is also important for other reasons. [Higginbottom et al. \(2014\)](#), hereafter H14 showed that, in this particular geometry, multiple scattering actually makes shielding ineffective, and radiation will simply find its way around the failed wind to over-ionize the flow beyond. Ideally, full radiative transfer and hydrodynamical simulations would be used to estimate the viability of line-driven winds. Our team is currently working on this problem (see H14 for the first step); however, much can also be learned from simpler, kinematic prescriptions for outflows, which already be modelled with full treatments of radiative transfer and ionization.

## 2.4 A Kinematic Prescription for a Biconical Wind

[Shlosman & Vitello \(1993\)](#), hereafter SV93) expanded on the work of the stellar wind community (e.g. [Abbott & Lucy 1985](#)) in proposing a kinematic model for an accretion disc wind. Unlike hydrodynamical models, this model has no real predictive power in terms of velocities and mass-loss rates. Instead, one sets these quantities in advance and examines the resultant properties of the flow and the emergent spectra. The SV93 prescription is the most common way of describing the outflow in the radiative transfer code PYTHON (see chapter 3) and has been used to simulate spectra for CVs ([Long & Knigge 2002](#); [Matthews et al. 2015](#), chapter 4), AM CVn systems ([Kusterer et al. 2014](#)) and AGN/quasars ([Higginbottom et al. 2013](#); [Matthews et al. 2016](#); [Yong et al. 2016](#), chapter 5). An alternative description was developed by [Knigge et al. \(1995\)](#) and has been used in similar applications ([Long & Knigge 2002](#); [Sim et al. 2008, 2010a](#)), as well as for young-stellar objects (YSOs; [Sim et al. 2005](#)). Kinematic prescriptions have thus been a useful tool in allowing quantitative tests of conceptual models, specifically for assessing their ability to reproduce the observed spectra of a variety of astrophysical systems.

In the SV93 parametrization, a smooth, biconical disc wind emanates from the accretion disc between  $r_{\min}$  and  $r_{\max}$ . A schematic is shown in Fig. 2.14. The covering fraction of the outflow is also controlled by the inner and outer opening angles of the wind,  $\theta_{\min}$  and  $\theta_{\max}$ , and the launch angle of the other streamlines is given by

$$\theta(r_0) = \theta_{\min} + (\theta_{\max} - \theta_{\min}) \left( \frac{r_0 - r_{\min}}{r_{\max} - r_{\min}} \right)^{\gamma}, \quad (2.11)$$

where  $r_0$  is the launch radius of the streamline.

The poloidal (non-rotational) velocity field of the wind,  $v_l$ , is given by

$$v_l = v_0 + [v_{\infty}(r_0) - v_0] \frac{(l/R_v)^{\alpha}}{(l/R_v)^{\alpha} + 1}, \quad (2.12)$$

where  $l$  is the poloidal distance along a particular wind streamline. The terminal velocity along a streamline,  $v_{\infty}$ , is set to a fixed multiple of  $v_{\text{esc}}$ , the escape velocity at the launch point. The terminal velocity will therefore be higher for streamlines closer to the inner disc edge. The launch velocity from the disc surface,  $v_0$ , is assumed to be constant (set to  $6 \text{ km s}^{-1}$ ). Once the wind is launched, it accelerates, reaching half

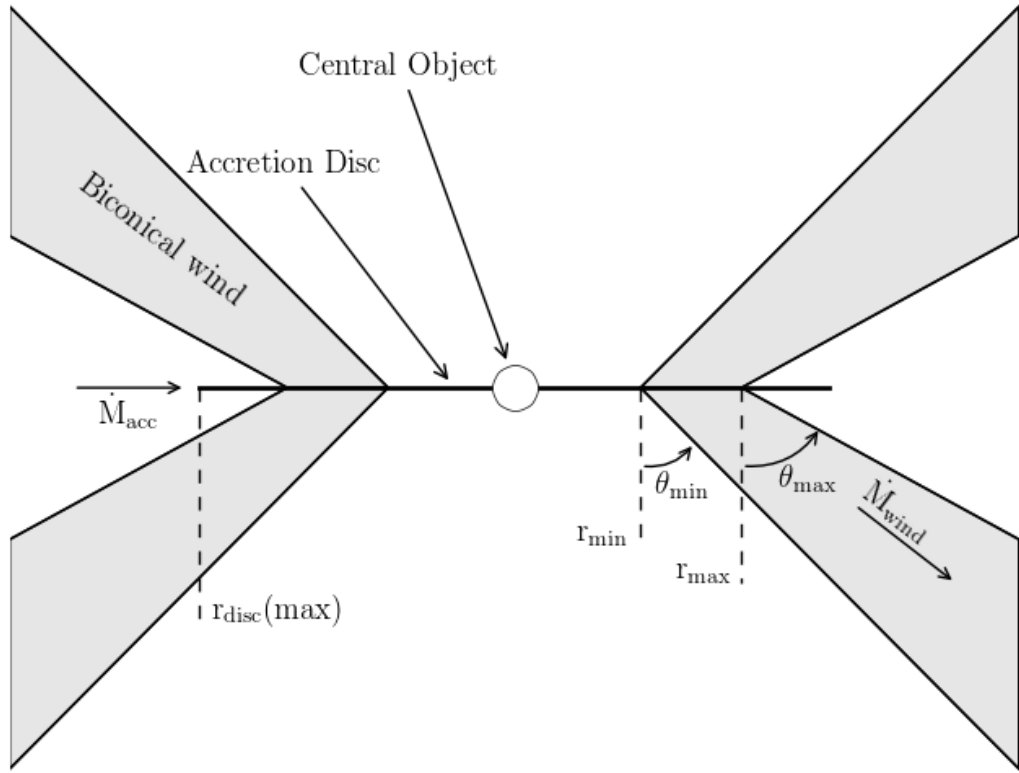


FIGURE 2.14: A schematic showing the geometry and kinematics of the SV93 model.

of its terminal velocity at  $l = R_v$ . The velocity law exponent,  $\alpha$ , controls how quickly the wind accelerates. Larger values of  $\alpha$  cause the main region of acceleration to occur close to  $R_v$ , whereas smaller values correspond to fast acceleration close to the disc (see Fig. 2.15). The rotational velocity,  $v_\phi$ , is Keplerian at the base of the streamline, and the wind conserves specific angular momentum, such that

$$v_\phi r = v_k r_0, \quad (2.13)$$

where  $v_k = (GM_{WD}/r_0)^{1/2}$ . The mass-loss rate per unit surface area,  $\dot{m}'$ , can be controlled by a free parameter,  $\lambda_m$ , such that

$$\dot{m}' \propto \dot{M}_W r_0^{\lambda_m} \cos[\theta(r_0)], \quad (2.14)$$

where  $\dot{M}_W$  is the total mass loss rate in the wind. This equation is normalised so that when integrated over both sides of the disc the correct  $\dot{M}_W$  emerges. I have adopted  $\lambda = 0$  throughout this thesis, which corresponds to uniform mass loss across the disc. The density at a given point can then be calculated by imposing mass conservation and

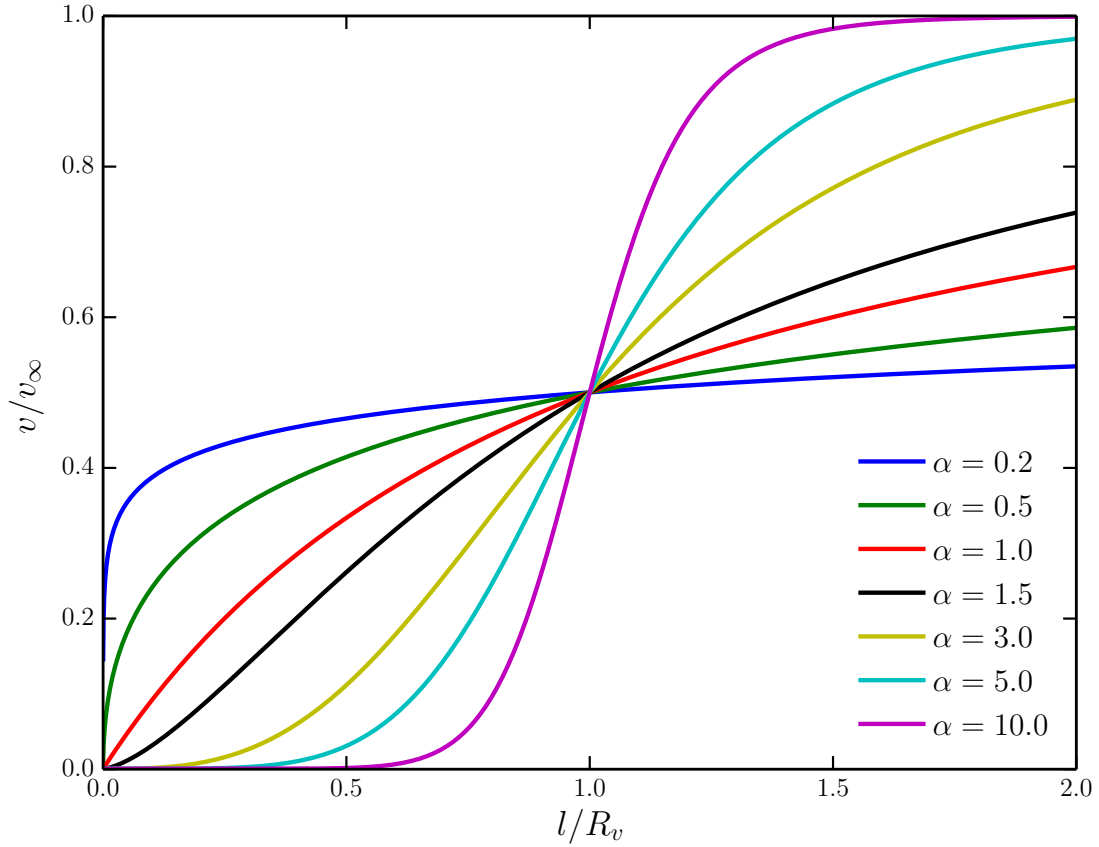


FIGURE 2.15: The SV93 velocity law for various values of the acceleration exponent,  $\alpha$ .

using the velocity law. At the base of the wind, the density is given by

$$\rho(r_0) = \frac{\dot{m}'(r_0)}{v_z(r_0)}. \quad (2.15)$$

At a coordinate  $(r, z)$  in the wind, the density is then

$$\rho(r, z) = \frac{r_0}{r} \frac{dr_0}{dr} \frac{\dot{m}'(r_0)}{v_z(r, z)}, \quad (2.16)$$

where the corresponding  $r_0$  is found by considering the streamline that passes through  $(r, z)$ . These equations govern the kinematics and densities in the wind in the SV93 prescription, which is used extensively throughout this thesis.

## 2.5 The big picture: AGN Feedback

The event horizon of a  $10^9 M_\odot$  BH is approximately  $10^{15}$  cm, a billionth of the radius of a typical galactic bulge. This is roughly the ratio in size between a small coin and

the Earth. Even the sphere of gravitational influence of the BH is roughly 1000 times smaller than the size of the galactic bulge. Despite this vast difference in scale, there is strong evidence that the physics on the scale of the gravitational radius of the BH affects the evolution and dynamics of its host galaxy. This becomes less surprising when considering the *energetics* of accretion. The binding energy of a galactic bulge, with mass  $M_{\text{bulge}}$  and velocity dispersion  $\sigma_*$ , is

$$E_{\text{bulge}} \approx M_{\text{bulge}} \sigma_*^2, \quad (2.17)$$

while the energy released in growing a black hole to a mass  $M'_{BH}$  is (equation 1.3, assuming  $\eta = 0.1$ )

$$E_{BH} \approx 0.1 M'_{BH} c^2. \quad (2.18)$$

By combining these two equations, and substituting in typical numbers ( $\sigma_* = 0.001c$ ,  $M'_{BH}/M_{\text{bulge}} = 10^{-3}$ ), we can show that

$$\frac{E_{BH}}{E_{\text{bulge}}} \approx 10^{-4} \left( \frac{c}{\sigma_*} \right)^2 \sim 10. \quad (2.19)$$

In other words, the energy released when growing a BH can significantly exceed the binding energy of the galactic bulge. This energetic argument is, of course, not sufficient to claim that the accreting BH must affect its host. For example, if the radiated energy never experienced an optical depth of  $\sim 1$ , it could not couple to the galactic bulge. However, we have already seen that many outflows in AGN possess kinetic luminosities that are significant compared to the bolometric luminosity. Thus, outflows (and jets) may provide a mechanism by which the vast accretion energies can be transferred to the BH environment.

### 2.5.1 Observational evidence for feedback

Perhaps the most famous pieces of evidence for some kind of long-distance relationship between a central BH and its host galaxy are the  $M_{BH} - \sigma_*$  (Ferrarese & Merritt 2000; Gebhardt et al. 2000; Gültekin et al. 2009) and  $M_{BH} - M_{\text{bulge}}$  (Magorrian et al. 1998; Häring & Rix 2004; McConnell & Ma 2013) correlations, shown in Fig. 2.16 and Fig. 2.17, respectively. By themselves, these correlations would not necessarily imply that the AGN is having an impact on its environment. Indeed, there are many different theoretical models for the origin of these relations (e.g Somerville et al. 2001; Adams

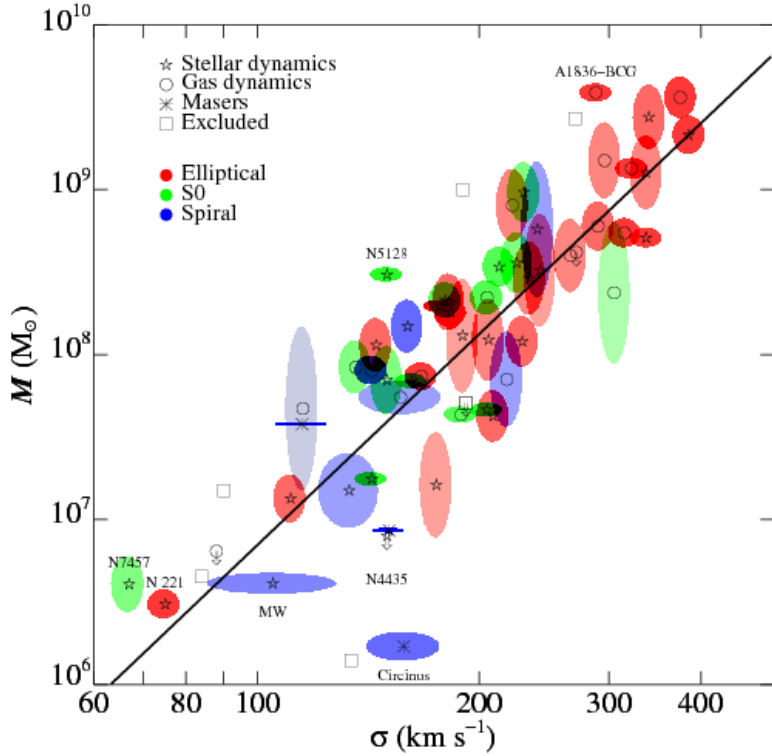


FIGURE 2.16: Credit: Gultekin et al. 2009. The  $M_{BH} - \sigma_*$  correlation.

et al. 2001; Burkert & Silk 2001; King 2003; Croton et al. 2006; Kormendy & Ho 2013). However, there are many other clues that outflows and jets from AGN can affect the host galaxy evolution and morphology.

The galaxy luminosity function describes the number of galaxies as a function of luminosity and is generally modelled with the Schechter (1976) function. Theories of galaxy evolution tend to overpredict the number of galaxies at the high luminosity end, which can be avoided by invoking quenching of star formation by the central AGN (e.g. Read & Trentham 2005; Bongiorno et al. 2016). Galaxies also show bimodality in their colour distributions (Strateva et al. 2001; Bell et al. 2003; Baldry et al. 2004), with a clear separation between a blue, star-forming main sequence, and a red sequence with lower specific star formation rate (sSFR). Furthermore, these two sequences tend to lie in the same regions of colour space as the host galaxies of high and low Eddington fraction AGN, respectively, implying that the AGN may be directly responsible for quenching star formation and moving a galaxy onto the ‘red and dead’ branch. This has been demonstrated in several numerical simulations (e.g. Springel et al. 2005; Croton et al. 2006).

There is also evidence that AGN are energetically significant on scales larger than the

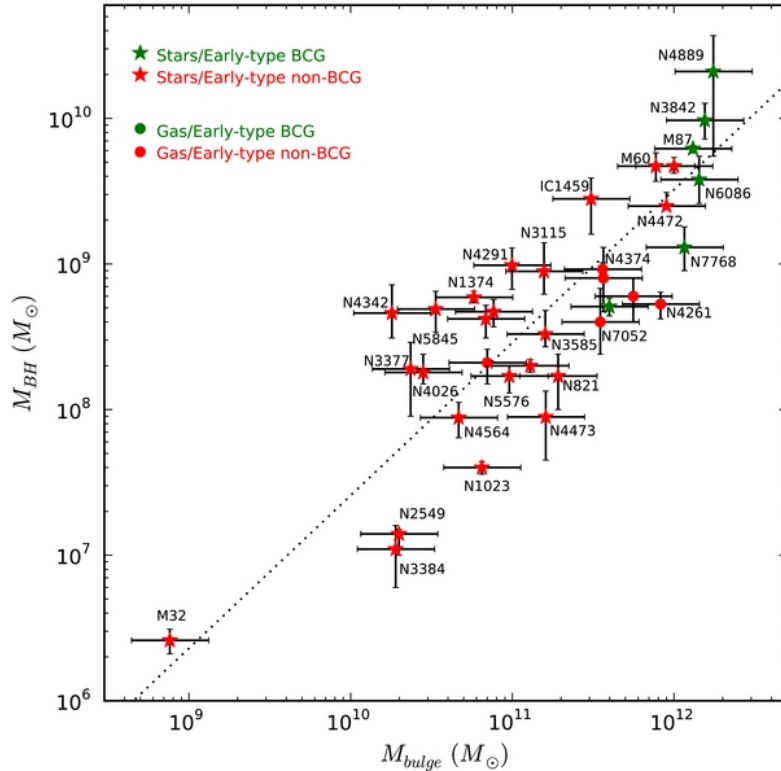


FIGURE 2.17: Credit: McConell & Ma 2013. The  $M_{BH} - M_{bulge}$  correlation.

galactic bulge. X-ray observations of cool core clusters and elliptical galaxies can show dramatic X-ray cavities or bubbles up to 50 kpc across, with a radio-loud AGN at the centre (Randall et al. 2011; Cavagnolo et al. 2011; Fabian 2012, Fig. 2.18). This shows how radio jets can significantly impact the surrounding gas, a flavour of feedback known as ‘radio’ or ‘kinetic’ mode. These cavities also provide an estimate of the kinetic power of a radio jet, as the volume of the bubble and surrounding gas pressure gives a rough estimate of the  $PV$  work done by the jet. This can be divided by an age estimate for the cavity, giving powers of up to  $10^{46}$  erg s $^{-1}$ , which are weakly correlated with the radio luminosity of the source and can be large even for modest radio power (Bîrzan et al. 2008).

However, jets are not the only way for AGN to interact with their environment. I have already briefly discussed in section 2.1.3.3 how fast AGN winds can drive larger-scale molecular outflows. This can be seen spectacularly in the FeLoBALQSO Mrk231, where integrated field spectroscopy shows kiloparsec-scale neutral gas outflows (see Fig. 2.19; Rupke & Veilleux 2011). Furthermore, King (2003) expanded on the ideas of Silk & Rees (1998) and considered a super-Eddington, momentum-driven outflow expanding into the surrounding gas. This model naturally reproduces the observed slope of the  $M_{BH} - \sigma_*$  relation. This line of argument was used to suggest that super-Eddington accretion must

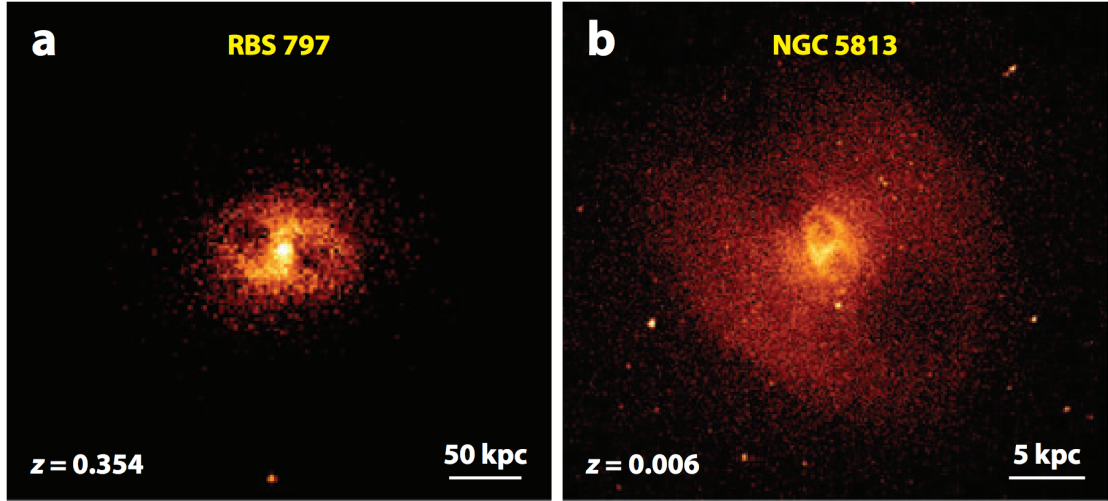


FIGURE 2.18: *Figure adapted from Fabian 2012.* Chandra X-ray images showing two examples of X-ray cavities, illustrating how a radio jet from an AGN can have a dramatic impact on its environment. a) The RBS 797 Cluster (Cavagnolo et al. 2011). b) elliptical galaxy NGC 5813 (Randall et al. 2011).

be common near the end of a quasar cycle, although it is worth noting that line-driving, or non-radiative driving, means that super-Eddington accretion rates are not necessarily required to drive such an outflow. Intriguingly, this means that understanding outflow physics has implications for the Soltan (1982) argument, SMBH spin and the accretion history of the Universe.

### 2.5.2 Alternative Explanations

It cannot yet be proven that AGN are the drivers of the observed galaxy colour evolution, high-end luminosity function discrepancy or BH-bulge correlations. In particular, it is also possible that mergers are responsible for these phenomena. For example, major galaxy mergers may explain the ‘red and dead’ branch of the galaxy colour bimodality (e.g. Somerville et al. 2001; Baldry et al. 2004). However, AGN winds and jets are clearly energetically significant with respect to their host galaxies, so estimating their kinetic powers accurately is important in discriminating between in-situ and ex-situ scenarios.

Having established the astrophysical importance of outflows, I will now move on to discussing how we might go about accurately modelling the ionization states of accretion disc winds and their emergent spectra.

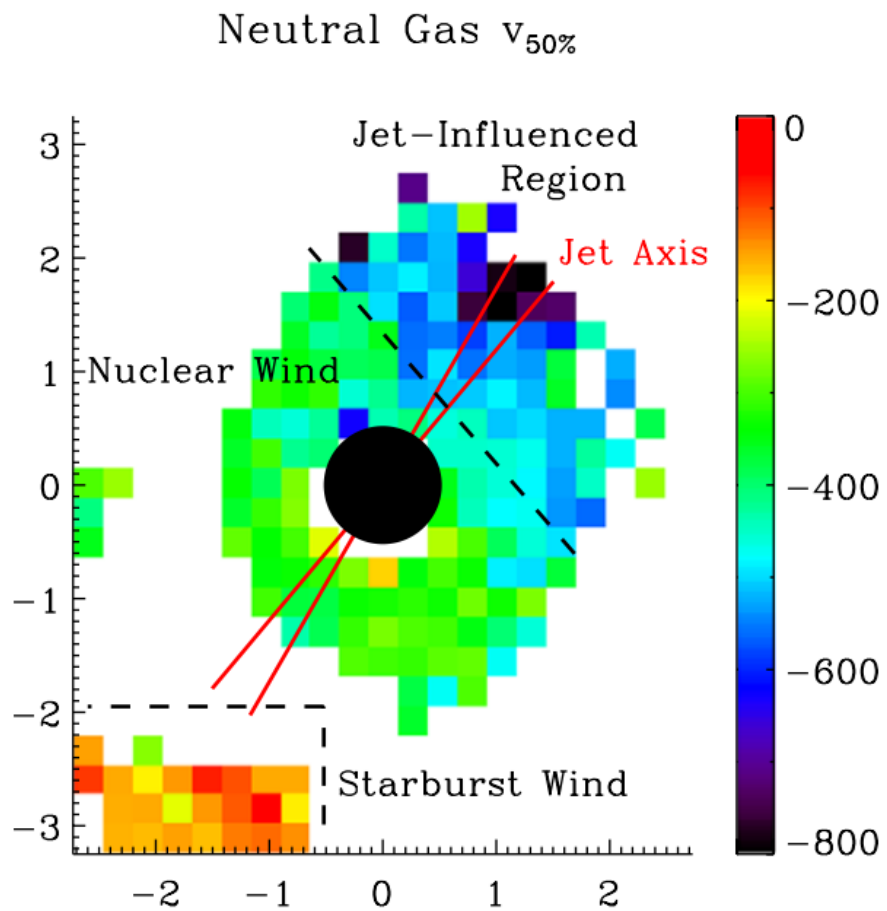


FIGURE 2.19: Credit: Rupke & Veilleux 2011. Results of Gaussian line profile fitting to integral field spectroscopy of Mrk 231. The quantity shown,  $v_{50\%}$ , corresponds to the centre of the fitted Gaussian profile and indicates that high outflow velocities are present in the neutral gas.



# Bibliography

- Abbott D. C., 1982, ApJ 259, 282
- Abbott D. C., Lucy L. B., 1985, ApJ 288, 679
- Adams F. C., Graff D. S., Richstone D. O., 2001, ApJ Letters 551, L31
- Alexander D. M., Bauer F. E., Brandt W. N., Daddi E. et al., 2011, ApJ 738, 44
- Allen J. T., Hewett P. C., Maddox N., Richards G. T., Belokurov V., 2011, MNRAS 410, 860
- Antonucci R., 1988, in M. Kafatos (ed.), Supermassive Black Holes, p. 26
- Antonucci R., 2013, Nature 495, 165
- Antonucci R., Geller R., Goodrich R. W., Miller J. S., 1996, ApJ 472, 502
- Antonucci R. R. J., Miller J. S., 1985, ApJ 297, 621
- Arav N., 1996, ApJ 465, 617
- Arav N., Becker R. H., Laurent-Muehleisen S. A., Gregg M. D. et al., 1999a, ApJ 524, 566
- Arav N., Korista K. T., Barlow T. A., Begelman, 1995, Nature 376, 576
- Arav N., Korista K. T., de Kool M., Junkkarinen V. T., Begelman M. C., 1999b, ApJ 516, 27
- Arévalo P., Uttley P., 2006, MNRAS 367, 801
- Badnell N. R., 2006, ApJs 167, 334
- Balbus S. A., Hawley J. F., 1991, ApJ 376, 214
- Baldi R. D., Capetti A., Robinson A., Laor A., Behar E., 2016, MNRAS
- Baldry I. K., Glazebrook K., Brinkmann J., Ivezić Ž. et al., 2004, ApJ 600, 681
- Baptista R., Silveira C., Steiner J. E., Horne K., 2000, MNRAS 314, 713
- Bartlett E., 2013, Ph.D. thesis, University of Southampton
- Becker R. H., White R. L., Gregg M. D., Brotherton M. S. et al., 2000, ApJ 538, 72
- Begelman M. C., McKee C. F., Shields G. A., 1983, ApJ 271, 70
- Bell E. F., McIntosh D. H., Katz N., Weinberg M. D., 2003, ApJs 149, 289

- Belloni T. (ed.), 2010, The Jet Paradigm, Vol. 794 of *Lecture Notes in Physics*, Berlin Springer Verlag
- Benz A. O., Fuerst E., Kiplinger A. L., 1983, Nature 302, 45
- Beuermann K., Stasiewski U., Schwope A. D., 1992, A&A 256, 433
- Beuermann K., Thomas H.-C., 1990, A&A 230, 326
- Bîrzan L., McNamara B. R., Nulsen P. E. J., Carilli C. L., Wise M. W., 2008, ApJ 686, 859
- Blandford R. D., Payne D. G., 1982, MNRAS 199, 883
- Blandford R. D., Znajek R. L., 1977, MNRAS 179, 433
- Bondi H., 1952, MNRAS 112, 195
- Bondi H., Hoyle F., 1944, MNRAS 104, 273
- Bongiorno A., Schulze A., Merloni A., Zamorani G. et al., 2016, A&A 588, A78
- Bonning E. W., Cheng L., Shields G. A., Salviander S., Gebhardt K., 2007, ApJ 659, 211
- Borguet B., Hutsemékers D., 2010, A&A 515, A22
- Borguet B. C. J., Arav N., Edmonds D., Chamberlain C., Benn C., 2013, ApJ 762, 49
- Borguet B. C. J., Edmonds D., Arav N., Dunn J., Kriss G. A., 2012, ApJ 751, 107
- Boroson T. A., Green R. F., 1992, ApJs 80, 109
- Boroson T. A., Meyers K. A., 1992, ApJ 397, 442
- Bowler R. A. A., Hewett P. C., Allen J. T., Ferland G. J., 2014, MNRAS 445, 359
- Braito V., Reeves J. N., Dewangan G. C., George I. et al., 2007, ApJ 670, 978
- Brandt W. N., Laor A., Wills B. J., 2000, ApJ 528, 637
- Brotherton M. S., De Breuck C., Schaefer J. J., 2006, MNRAS 372, L58
- Brotherton M. S., Singh V., Runnoe J., 2015, MNRAS 454, 3864
- Brotherton M. S., Tran H. D., van Breugel W., Dey A., Antonucci R., 1997, ApJ Letters 487, L113
- Brown J. C., Richardson L. L., Antokhin I., Robert C. et al., 1995, A&A 295, 725
- Burkert A., Silk J., 2001, ApJ Letters 554, L151
- Caccianiga A., Severgnini P., 2011, MNRAS 415, 1928
- Capellupo D. M., Hamann F., Barlow T. A., 2014, MNRAS 444, 1893
- Capellupo D. M., Hamann F., Shields J. C., Rodríguez Hidalgo P., Barlow T. A., 2011, MNRAS 413, 908
- Capellupo D. M., Hamann F., Shields J. C., Rodríguez Hidalgo P., Barlow T. A., 2012, MNRAS 422, 3249

- Capellupo D. M., Netzer H., Lira P., Trakhtenbrot B., Mejía-Restrepo J., 2015, MNRAS 446, 3427
- Cappi M., Mihara T., Matsuoka M., Hayashida K. et al., 1996, ApJ 458, 149
- Cassinelli J. P., 1979, ARAA 17, 275
- Castor J. I., Abbott D. C., Klein R. I., 1975, ApJ 195, 157
- Castor J. L., 1974, MNRAS 169, 279
- Cavagnolo K. W., McNamara B. R., Wise M. W., Nulsen P. E. J. et al., 2011, ApJ 732, 71
- Chamberlain C., Arav N., Benn C., 2015, MNRAS 450, 1085
- Chartas G., Kochanek C. S., Dai X., Poindexter S., Garmire G., 2009, ApJ 693, 174
- Chen B., Dai X., Baron E., 2013a, ApJ 762, 122
- Chen B., Dai X., Baron E., Kantowski R., 2013b, ApJ 769, 131
- Clavel J., Schartel N., Tomas L., 2006, A&A 446, 439
- Cohen M. H., Ogle P. M., Tran H. D., Vermeulen R. C. et al., 1995, ApJ Letters 448, L77
- Cohen R. D., Puetter R. C., Rudy R. J., Ake T. B., Foltz C. B., 1986, ApJ 311, 135
- Connolly S. D., McHardy I. M., Dwelly T., 2014, MNRAS 440, 3503
- Connolly S. D., McHardy I. M., Skipper C. J., Emmanoulopoulos D., 2016, MNRAS
- Coppejans D. L., Körding E. G., Miller-Jones J. C. A., Rupen M. P. et al., 2015, MNRAS 451, 3801
- Cordova F. A., Mason K. O., 1982, ApJ 260, 716
- Cottis C. E., Goad M. R., Knigge C., Scaringi S., 2010, MNRAS 406, 2094
- Crenshaw D. M., Rodriguez-Pascual P. M., Penton S. V., Edelson R. A. et al., 1996, ApJ 470, 322
- Croton D. J., Springel V., White S. D. M., De Lucia G. et al., 2006, MNRAS 365, 11
- Crummy J., Fabian A. C., Gallo L., Ross R. R., 2006, MNRAS 365, 1067
- Cunto W., Mendoza C., Ochsenbein F., Zeippen C. J., 1993, A&A 275, L5
- Dabrowski Y., Fabian A. C., Iwasawa K., Lasenby A. N., Reynolds C. S., 1997, MNRAS 288, L11
- Dai X., Kochanek C. S., Chartas G., Kozłowski S. et al., 2010, ApJ 709, 278
- Dai X., Shankar F., Sivakoff G. R., 2008, ApJ 672, 108
- Dai X., Shankar F., Sivakoff G. R., 2012, ApJ 757, 180
- Davis S. W., Hubeny I., 2006, ApJs 164, 530
- Davis S. W., Woo J.-H., Blaes O. M., 2007, ApJ 668, 682

- de Kool M., Begelman M. C., 1995, ApJ 455, 448
- Denney K. D., De Rosa G., Croxall K., Gupta A. et al., 2014, ApJ 796, 134
- Dere K. P., Landi E., Mason H. E., Monsignori Fossi B. C., Young P. R., 1997, A&As 125, 149
- Dexter J., Agol E., 2011, ApJ Letters 727, L24
- Dhillon V. S., 1996, in A. Evans, J. H. Wood (eds.), IAU Colloq. 158: Cataclysmic Variables and Related Objects, Vol. 208 of *Astrophysics and Space Science Library*, 3
- Dhillon V. S., Rutten R. G. M., 1995, MNRAS 277, 777
- Díaz Trigo M., Boirin L., 2015, ArXiv e-prints
- DiPompeo M. A., Brotherton M. S., Cales S. L., Runnoe J. C., 2012a, MNRAS 427, 1135
- DiPompeo M. A., Brotherton M. S., De Breuck C., 2012b, ApJ 752, 6
- Done C., Davis S. W., Jin C., Blaes O., Ward M., 2012, MNRAS 420, 1848
- Done C., Jin C., 2015, ArXiv e-prints
- Drew J., Verbunt F., 1985, MNRAS 213, 191
- Echevarria J., 1988, MNRAS 233, 513
- Edelson R., Gelbord J. M., Horne K., McHardy I. M. et al., 2015, ApJ 806, 129
- Edge D. O., Shakeshaft J. R., McAdam W. B., Baldwin J. E., Archer S., 1959, MmRA 68, 37
- Eggleton P. P., 1983, ApJ 268, 368
- Ehman J. R., Dixon R. S., Kraus J. D., 1970, AJ 75, 351
- Ekers J. A., 1969, Australian Journal of Physics Astrophysical Supplement 7
- Elitzur M., 2012, ApJ Letters 747, L33
- Elitzur M., Ho L. C., Trump J. R., 2014, MNRAS 438, 3340
- Elvis M., 2000, ApJ 545, 63
- Elvis M., Wilkes B. J., McDowell J. C., Green R. F. et al., 1994, ApJs 95, 1
- Emmanoulopoulos D., Papadakis I. E., Dovčiak M., McHardy I. M., 2014, MNRAS 439, 3931
- Emmanoulopoulos D., Papadakis I. E., McHardy I. M., Arévalo P. et al., 2012, MNRAS 424, 1327
- Eracleous M., Halpern J. P., 1994, ApJs 90, 1
- Evans P. A., Hellier C., Ramsay G., Cropper M., 2004, MNRAS 349, 715
- Fabian A. C., 2012, ARAA 50, 455

- Fabian A. C., Kunieda H., Inoue S., Matsuoka M. et al., 1994, PASJ 46, L59
- Fabian A. C., Nandra K., Reynolds C. S., Brandt W. N. et al., 1995, MNRAS 277, L11
- Fath E. A., 1909, Lick Observatory Bulletin 5, 71
- Feldmeier A., 1995, A&A 299, 523
- Fender R. P., 2001, MNRAS 322, 31
- Fender R. P., Belloni T. M., Gallo E., 2004, MNRAS 355, 1105
- Fender R. P., Gallo E., Russell D., 2010, MNRAS 406, 1425
- Ferland G., 2002, ArXiv Astrophysics e-prints
- Ferland G. J., 2005, Hazy, A Brief Introduction to Cloudy 05.07
- Ferland G. J., Porter R. L., van Hoof P. A. M., Williams R. J. R. et al., 2013, RMXAA 49, 137
- Ferrarese L., Merritt D., 2000, ApJ Letters 539, L9
- Filiz Ak N., Brandt W. N., Hall P. B., Schneider D. P. et al., 2012, ApJ 757, 114
- Filiz Ak N., Brandt W. N., Hall P. B., Schneider D. P. et al., 2014, ApJ 791, 88
- Flohic H. M. L. G., Eracleous M., Bogdanović T., 2012, ApJ 753, 133
- Foltz C. B., Weymann R. J., Morris S. L., Turnshek D. A., 1987, ApJ 317, 450
- Frank J., King A., Raine D., 1992, Accretion power in astrophysics.
- Frank J., King A. R., 1981, MNRAS 195, 227
- Friend D. B., Abbott D. C., 1986, ApJ 311, 701
- Fukumura K., Tombesi F., Kazanas D., Shrader C. et al., 2015, ApJ 805, 17
- Gabriel E., Fagg G. E., Bosilca G., Angskun T. et al., 2004, in Proceedings, 11th European PVM/MPI Users' Group Meeting, Budapest, Hungary, p. 97
- Gaetz T. J., Salpeter E. E., 1983, ApJs 52, 155
- Gallagher S. C., Brandt W. N., Chartas G., Garmire G. P., 2002, ApJ 567, 37
- Gallagher S. C., Brandt W. N., Chartas G., Priddey R. et al., 2006, ApJ 644, 709
- Gallagher S. C., Brandt W. N., Sambruna R. M., Mathur S., Yamasaki N., 1999, ApJ 519, 549
- Gallo E., Fender R. P., Pooley G. G., 2003, MNRAS 344, 60
- Gandhi P., Höning S. F., Kishimoto M., 2015, ApJ 812, 113
- Gandhi P., Terashima Y., Yamada S., Mushotzky R. F. et al., 2013, ApJ 773, 51
- Ganguly R., Bond N. A., Charlton J. C., Eracleous M. et al., 2001, ApJ 549, 133
- Ganguly R., Sembach K. R., Tripp T. M., Savage B. D., Wakker B. P., 2006, ApJ 645, 868
- Gardner E., Done C., 2016, ArXiv e-prints

- Gayet R., 1970, A&A 9, 312
- Gebhardt K., Bender R., Bower G., Dressler A. et al., 2000, ApJ Letters 539, L13
- Ghosh K. K., Punshy B., 2007, ApJ Letters 661, L139
- Gibson R. R., Jiang L., Brandt W. N., Hall P. B. et al., 2009, ApJ 692, 758
- Gierliński M., Done C., 2004, MNRAS 349, L7
- Gierliński M., Done C., 2006, MNRAS 371, L16
- Giustini M., Cappi M., Chartas G., Dadina M. et al., 2011, A&A 536, A49
- Gofford J., Reeves J. N., Braito V., Nardini E. et al., 2014, ApJ 784, 77
- Gofford J., Reeves J. N., McLaughlin D. E., Braito V. et al., 2015, MNRAS 451, 4169
- Gofford J., Reeves J. N., Tombesi F., Braito V. et al., 2013, MNRAS 430, 60
- Goodrich R. W., 1997, ApJ 474, 606
- Goodrich R. W., Miller J. S., 1995, ApJ Letters 448, L73
- Gough B., 2009, GNU Scientific Library Reference Manual - Third Edition, Network Theory Ltd., 3rd edition
- Green A. R., McHardy I. M., Lehto H. J., 1993, MNRAS 265, 664
- Green P. J., Aldcroft T. L., Mathur S., Wilkes B. J., Elvis M., 2001, ApJ 558, 109
- Green P. J., Mathur S., 1996, ApJ 462, 637
- Greenstein J. L., Oke J. B., 1982, ApJ 258, 209
- Groot P. J., Rutten R. G. M., van Paradijs J., 2004, A&A 417, 283
- Grupe D., Mathur S., Elvis M., 2003a, AJ 126, 1159
- Grupe D., Mathur S., Elvis M., 2003b, AJ 126, 1159
- Grupe D., Nousek J. A., 2015, AJ 149, 85
- Gu M., Cao X., 2009, MNRAS 399, 349
- Gültekin K., Richstone D. O., Gebhardt K., Lauer T. R. et al., 2009, ApJ 698, 198
- Hōshi R., 1979, Progress of Theoretical Physics 61, 1307
- Haardt F., Maraschi L., 1991, ApJ Letters 380, L51
- Hall P. B., Anderson S. F., Strauss M. A., York D. G. et al., 2002, ApJs 141, 267
- Hall P. B., Anosov K., White R. L., Brandt W. N. et al., 2011, MNRAS 411, 2653
- Halpern J. P., 1984, ApJ 281, 90
- Hamann F., Chartas G., McGraw S., Rodriguez Hidalgo P. et al., 2013, MNRAS 435, 133
- Hamann W.-R., Koesterke L., 1998, A&A 335, 1003
- Hamann W.-R., Leuenhagen U., Koesterke L., Wessolowski U., 1992, A&A 255, 200

- Hamann W.-R., Oskinova L. M., Feldmeier A., 2008, in W.-R. Hamann, A. Feldmeier, L. M. Oskinova (eds.), Clumping in Hot-Star Winds, 75
- Hamann W.-R., Wessolowski U., Koesterke L., 1994, *A&A* 281, 184
- Häring N., Rix H.-W., 2004, *ApJ Letters* 604, L89
- Harrop-Allin M. K., Warner B., 1996, *MNRAS* 279, 219
- Hartley L. E., Murray J. R., Drew J. E., Long K. S., 2005, *MNRAS* 363, 285
- Hassall B. J. M., 1985, *MNRAS* 216, 335
- Haug K., 1987, *AP&SS* 130, 91
- Hazard C., Mackey M. B., Shimmins A. J., 1963, *Nature* 197, 1037
- Hazard C., Morton D. C., Terlevich R., McMahon R., 1984, *ApJ* 282, 33
- Heap S. R., Boggess A., Holm A., Klinglesmith D. A. et al., 1978, *Nature* 275, 385
- Heil L. M., Vaughan S., Uttley P., 2012, *MNRAS* 422, 2620
- Hessman F. V., Robinson E. L., Nather R. E., Zhang E.-H., 1984, *ApJ* 286, 747
- Higginbottom N., Knigge C., Long K. S., Sim S. A., Matthews J. H., 2013, *MNRAS* 436, 1390
- Higginbottom N., Proga D., Knigge C., Long K. S. et al., 2014, *ApJ* 789, 19
- Hillier D. J., 1984, *ApJ* 280, 744
- Hillier D. J., 1991, *A&A* 247, 455
- Hillier D. J., Miller D. L., 1999, *ApJ* 519, 354
- Hoare M. G., Drew J. E., 1991, *MNRAS* 249, 452
- Hoare M. G., Drew J. E., 1993, *MNRAS* 260, 647
- Hogg J. D., Reynolds C., 2015, ArXiv e-prints
- Honeycutt R. K., Schlegel E. M., Kaitchuck R. H., 1986, *ApJ* 302, 388
- Hönig S. F., Kishimoto M., Tristram K. R. W., Prieto M. A. et al., 2013, *ApJ* 771, 87
- Horne K., 1993, Eclipse Mapping of Accretion Disks: The First Decade, 117
- Horne K., Marsh T. R., 1986, *MNRAS* 218, 761
- Horne K., Marsh T. R., Cheng F. H., Hubeny I., Lanz T., 1994, *ApJ* 426, 294
- Hoyle F., Lyttleton R. A., 1939, *Proceedings of the Cambridge Philosophical Society* 35, 405
- Hubeny I., 2001, in G. Ferland, D. W. Savin (eds.), Spectroscopic Challenges of Photoionized Plasmas, Vol. 247 of *Astronomical Society of the Pacific Conference Series*, 197
- Hubeny I., Agol E., Blaes O., Krolik J. H., 2000, *ApJ* 533, 710
- Hubeny I., Lanz T., 1995, *ApJ* 439, 875

- Humphrey A., Binette L., 2014, MNRAS 442, 753
- Idan I., Lasota J.-P., Hameury J.-M., Shaviv G., 2010, A&A 519, A117
- Ioannou Z., van Zyl L., Naylor T., Charles P. A. et al., 2003, A&A 399, 211
- Iwasawa K., Fabian A. C., Mushotzky R. F., Brandt W. N. et al., 1996a, MNRAS 279, 837
- Iwasawa K., Fabian A. C., Reynolds C. S., Nandra K. et al., 1996b, MNRAS 282, 1038
- Janiuk A., Czerny B., Madejski G. M., 2001, ApJ 557, 408
- Ju W., Stone J. M., Zhu Z., 2016, ArXiv e-prints
- Junkkarinen V. T., Burbidge E. M., Smith H. E., 1983, ApJ 265, 51
- Kaastra J. S., Kriss G. A., Cappi M., Mehdipour M. et al., 2014, Science 345, 64
- Kaastra J. S., Mewe R., Liedahl D. A., Komossa S., Brinkman A. C., 2000, A&A 354, L83
- Kafka S., Honeycutt R. K., 2004, AJ 128, 2420
- Kaspi S., Brandt W. N., Maoz D., Netzer H. et al., 2007, ApJ 659, 997
- Kerzendorf W. E., Sim S. A., 2014, MNRAS 440, 387
- King A., 2003, ApJ Letters 596, L27
- Klein O., Nishina T., 1929, Zeitschrift fur Physik 52, 853
- Knigge C., 1999, MNRAS 309, 409
- Knigge C., Baraffe I., Patterson J., 2011, ApJs 194, 28
- Knigge C., Drew J. E., 1997, ApJ 486, 445
- Knigge C., Long K. S., Blair W. P., Wade R. A., 1997, ApJ 476, 291
- Knigge C., Long K. S., Wade R. A., Baptista R. et al., 1998a, ApJ 499, 414
- Knigge C., Long K. S., Wade R. A., Baptista R. et al., 1998b, ApJ 499, 414
- Knigge C., Scaringi S., Goad M. R., Cottis C. E., 2008, MNRAS 386, 1426
- Knigge C., Woods J. A., Drew J. E., 1995, MNRAS 273, 225
- Kollatschny W., Zetzl M., 2011, Nature 470, 366
- Konigl A., Kartje J. F., 1994, ApJ 434, 446
- Koratkar A., Blaes O., 1999, PASP 111, 1
- Körding E., Rupen M., Knigge C., Fender R. et al., 2008, Science 320, 1318
- Körding E. G., Jester S., Fender R., 2006, MNRAS 372, 1366
- Kormendy J., Ho L. C., 2013, ARAA 51, 511
- Kotani T., Ebisawa K., Dotani T., Inoue H. et al., 2000, ApJ 539, 413
- Kotov O., Churazov E., Gilfanov M., 2001, MNRAS 327, 799
- Kraft R. P., Mathews J., Greenstein J. L., 1962, ApJ 136, 312

- Kriss G. A., Krolik J. H., Otani C., Espey B. R. et al., 1996, ApJ 467, 629
- Krolik J. H., Begelman M. C., 1986, in Bulletin of the American Astronomical Society, Vol. 18 of *BAAS*, 903
- Krolik J. H., Kriss G. A., 2001, ApJ 561, 684
- Krolik J. H., Voit G. M., 1998, ApJ Letters 497, L5
- Kromer M., Sim S. A., 2009, MNRAS 398, 1809
- Kudoh T., Shibata K., 1997, ApJ 474, 362
- Kurosawa R., Proga D., 2009, ApJ 693, 1929
- Kurucz R. L., 1991, in L. Crivellari, I. Hubeny, D. G. Hummer (eds.), NATO ASIC Proc. 341: Stellar Atmospheres - Beyond Classical Models, 441
- Kurucz R. L., Bell B., 1995, Atomic line list
- Kusterer D.-J., Nagel T., Hartmann S., Werner K., Feldmeier A., 2014, A&A 561, A14
- Kuulkers E., Motta S., Kajava J., Homan J. et al., 2015, The Astronomer's Telegram 7647
- La Dous C., 1989a, MNRAS 238, 935
- La Dous C., 1989b, A&A 211, 131
- Lamy H., Hutsemékers D., 2000, A&A 356, L9
- Lamy H., Hutsemékers D., 2004, A&A 427, 107
- Landi E., Del Zanna G., Young P. R., Dere K. P., Mason H. E., 2012, ApJ 744, 99
- Laor A., 1991, ApJ 376, 90
- Laor A., Brandt W. N., 2002, ApJ 569, 641
- Laor A., Davis S. W., 2014, MNRAS 438, 3024
- Lasota J.-P., 2001, NAR 45, 449
- Lazarova M. S., Canalizo G., Lacy M., Sajina A., 2012, ApJ 755, 29
- Liebert J., Stockman H. S., 1985, in D. Q. Lamb, J. Patterson (eds.), *Cataclysmic Variables and Low-Mass X-ray Binaries*, Vol. 113 of *Astrophysics and Space Science Library*, p. 151
- Long K. S., Blair W. P., Davidsen A. F., Bowers C. W. et al., 1991, ApJ Letters 381, L25
- Long K. S., Knigge C., 2002, ApJ 579, 725
- Long K. S., Wade R. A., Blair W. P., Davidsen A. F., Hubeny I., 1994, ApJ 426, 704
- Longmore A. J., Lee T. J., Allen D. A., Adams D. J., 1981, MNRAS 195, 825
- Lucy L. B., 1999a, A&A 344, 282
- Lucy L. B., 1999b, A&A 345, 211

- Lucy L. B., 2002, A&A 384, 725
- Lucy L. B., 2003, A&A 403, 261
- Lucy L. B., Solomon P. M., 1970, ApJ 159, 879
- Lusso E., Worseck G., Hennawi J. F., Prochaska J. X. et al., 2015, MNRAS 449, 4204
- Lynden-Bell D., 1969, Nature 223, 690
- Lyubarskii Y. E., 1997, MNRAS 292, 679
- MacGregor K. B., Hartmann L., Raymond J. C., 1979, ApJ 231, 514
- Madau P., Ghisellini G., Fabian A. C., 1994, MNRAS 270, L17
- Magdziarz P., Blaes O. M., Zdziarski A. A., Johnson W. N., Smith D. A., 1998, MNRAS 301, 179
- Magorrian J., Tremaine S., Richstone D., Bender R. et al., 1998, AJ 115, 2285
- Mangham S. W., Knigge C., Matthews J. H., Long K. S. et al., 2016, in prep.
- Marin F., 2014, MNRAS 441, 551
- Marin F., 2016, ArXiv e-prints
- Marin F., Goosmann R. W., 2013, MNRAS 436, 2522
- Marinucci A., Bianchi S., Matt G., Alexander D. M. et al., 2016, MNRAS 456, L94
- Marscher A. P., 2006, in P. A. Hughes, J. N. Bregman (eds.), Relativistic Jets: The Common Physics of AGN, Microquasars, and Gamma-Ray Bursts, Vol. 856 of *American Institute of Physics Conference Series*, p. 1
- Marsh T. R., Horne K., 1988, MNRAS 235, 269
- Marsh T. R., Horne K., 1990, ApJ 349, 593
- Marziani P., Sulentic J. W., Zwitter T., Dultzin-Hacyan D., Calvani M., 2001, ApJ 558, 553
- Mathur S., Green P. J., Arav N., Brotherton M. et al., 2000, ApJ Letters 533, L79
- Matt G., Guainazzi M., Maiolino R., 2003, MNRAS 342, 422
- Matthews J. H., Knigge C., Long K. S., Sim S. A., Higginbottom N., 2015, MNRAS 450, 3331
- Matthews J. H., Knigge C., Long K. S., Sim S. A. et al., 2016, MNRAS
- Matzeu G. A., Reeves J. N., Nardini E., Braito V. et al., 2016, MNRAS 458, 1311
- Mauche C. W., 1996, ArXiv Astrophysics e-prints
- Mauche C. W., Raymond J. C., 1987, ApJ 323, 690
- Mazzali P. A., Lucy L. B., 1993, A&A 279, 447
- McConnell N. J., Ma C.-P., 2013, ApJ 764, 184
- McHardy I. M., Koerding E., Knigge C., Uttley P., Fender R. P., 2006, Nature 444, 730

- McHardy I. M., Papadakis I. E., Uttley P., 1999, Nuclear Physics B Proceedings Supplements 69, 509
- Menzel D. H., Pekeris C. L., 1935, MNRAS 96, 77
- Merloni A., Heinz S., di Matteo T., 2003, MNRAS 345, 1057
- Meyer F., Meyer-Hofmeister E., 1981, A&A 104, L10
- Mihalas D., 1978, Stellar atmospheres /2nd edition/
- Miller L., Turner T. J., 2013, ApJ Letters 773, L5
- Miller L., Turner T. J., Reeves J. N., 2008, A&A 483, 437
- Misawa T., Charlton J. C., Eracleous M., Ganguly R. et al., 2007, ApJs 171, 1
- Misawa T., Eracleous M., Chartas G., Charlton J. C., 2008, ApJ 677, 863
- Misra R., Kembhavi A. K., 1998, ApJ 499, 205
- Mitsuda K., Inoue H., Nakamura N., Tanaka Y., 1989, PASJ 41, 97
- Morabito L. K., Dai X., Leighly K. M., Sivakoff G. R., Shankar F., 2011, ApJ 737, 46
- Morabito L. K., Dai X., Leighly K. M., Sivakoff G. R., Shankar F., 2013, ArXiv e-prints
- Morgan C. W., Kochanek C. S., Morgan N. D., Falco E. E., 2010, ApJ 712, 1129
- Motta S., Beardmore A., Oates S., Sanna N. P. M. K. A. et al., 2015, The Astronomer's Telegram 7665
- Muñoz-Darias T., Casares J., Mata Sánchez D., Fender R. P. et al., 2016, Nature
- Muñoz-Darias T., Coriat M., Plant D. S., Ponti G. et al., 2013, MNRAS 432, 1330
- Murray N., Chiang J., 1996, Nature 382, 789
- Murray N., Chiang J., 1997, ApJ 474, 91
- Murray N., Chiang J., Grossman S. A., Voit G. M., 1995, ApJ 451, 498
- Nandra K., Pounds K. A., 1994, MNRAS 268, 405
- Narayan R., McClintock J. E., 2012, MNRAS 419, L69
- Narayan R., McClintock J. E., Tchekhovskoy A., 2014, Energy Extraction from Spinning Black Holes Via Relativistic Jets, 523
- Narayan R., Yi I., 1994, ApJ Letters 428, L13
- Narayan R., Yi I., 1995, ApJ 452, 710
- Nardini E., Reeves J. N., Gofford J., Harrison F. A. et al., 2015, Science 347, 860
- Nestor D., Hamann F., Rodriguez Hidalgo P., 2008, MNRAS 386, 2055
- Netzer H., 1990, in R. D. Blandford, H. Netzer, L. Woltjer, T. J.-L. Courvoisier, M. Mayor (eds.), Active Galactic Nuclei, p. 57
- Neugebauer G., Oke J. B., Becklin E. E., Matthews K., 1979, ApJ 230, 79

- Neustroev V. V., Suleimanov V. F., Borisov N. V., Belyakov K. V., Shearer A., 2011, MNRAS 410, 963
- Noebauer U. M., Long K. S., Sim S. A., Knigge C., 2010, ApJ 719, 1932
- Nomura M., Ohsuga K., Takahashi H. R., Wada K., Yoshida T., 2016, PASJ 68, 16
- Nomura M., Ohsuga K., Wada K., Susa H., Misawa T., 2013, PASJ 65, 40
- North M., Knigge C., Goad M., 2006, MNRAS 365, 1057
- O'Dowd M. J., Bate N. F., Webster R. L., Labrie K., Rogers J., 2015, ArXiv e-prints
- Orr A., Molendi S., Fiore F., Grandi P. et al., 1997, A&A 324, L77
- Osaki Y., 1974, PASJ 26, 429
- Osterbrock D. E., 1989, Astrophysics of gaseous nebulae and active galactic nuclei
- Otani C., Kii T., Reynolds C. S., Fabian A. C. et al., 1996, PASJ 48, 211
- Ouyed R., Pudritz R. E., 1997, ApJ 482, 712
- Owocki S., 2014, ArXiv e-prints
- Owocki S. P., Castor J. I., Rybicki G. B., 1988, ApJ 335, 914
- Owocki S. P., Rybicki G. B., 1984, ApJ 284, 337
- Owocki S. P., Rybicki G. B., 1985, ApJ 299, 265
- Pancoast A., Brewer B. J., Treu T., 2014a, MNRAS 445, 3055
- Pancoast A., Brewer B. J., Treu T., Park D. et al., 2014b, MNRAS 445, 3073
- Parmar A. N., Oosterbroek T., Boirin L., Lumb D., 2002, A&A 386, 910
- Patterson J., 1984, ApJs 54, 443
- Patterson J., 1994, PASP 106, 209
- Patterson J., Patino R., Thorstensen J. R., Harvey D. et al., 1996, AJ 111, 2422
- Pauldrach A., Puls J., Kudritzki R. P., 1986, A&A 164, 86
- Pauldrach A. W. A., Kudritzki R. P., Puls J., Butler K., Hunsinger J., 1994, A&A 283, 525
- Pelletier G., Pudritz R. E., 1992, ApJ 394, 117
- Penrose R., Floyd R. M., 1971, Nature Physical Science 229, 177
- Pereyra N. A., Kallman T. R., Blondin J. M., 1997, ApJ 477, 368
- Perley R. A., Dreher J. W., Cowan J. J., 1984, ApJ Letters 285, L35
- Ponti G., Fender R. P., Begelman M. C., Dunn R. J. H. et al., 2012, MNRAS 422, L11
- Potash R. I., Wardle J. F. C., 1980, ApJ 239, 42
- Pounds K., Lobban A., Reeves J., Vaughan S., 2016, MNRAS 457, 2951
- Pounds K. A., Nandra K., Stewart G. C., Leighly K., 1989, MNRAS 240, 769
- Pounds K. A., Reeves J. N., 2009, MNRAS 397, 249

- Pringle J. E., 1981, ARAA 19, 137
- Prinja R. K., Ringwald F. A., Wade R. A., Knigge C., 2000, MNRAS 312, 316
- Prinja R. K., Smith L. J., 1992, A&A 266, 377
- Proga D., 2003, ApJ 585, 406
- Proga D., 2005, in J.-M. Hameury, J.-P. Lasota (eds.), *The Astrophysics of Cataclysmic Variables and Related Objects*, Vol. 330 of *Astronomical Society of the Pacific Conference Series*, 103
- Proga D., Kallman T. R., 2004, ApJ 616, 688
- Proga D., Kallman T. R., Drew J. E., Hartley L. E., 2002a, ApJ 572, 382
- Proga D., Kallman T. R., Drew J. E., Hartley L. E., 2002b, ApJ 572, 382
- Proga D., Stone J. M., Drew J. E., 1998, MNRAS 295, 595
- Proga D., Stone J. M., Kallman T. R., 2000, ApJ 543, 686
- Puccetti S., Fiore F., Risaliti G., Capalbi M. et al., 2007, MNRAS 377, 607
- Puebla R. E., Diaz M. P., Hillier D. J., Hubeny I., 2011, ApJ 736, 17
- Randall S. W., Forman W. R., Giacintucci S., Nulsen P. E. J. et al., 2011, ApJ 726, 86
- Read J. I., Trentham N., 2005, Philosophical Transactions of the Royal Society of London Series A 363
- Reeves J. N., O'Brien P. T., Ward M. J., 2003, ApJ Letters 593, L65
- Reeves J. N., Wynn G., O'Brien P. T., Pounds K. A., 2002, MNRAS 336, L56
- Reichard T. A., Richards G. T., Hall P. B., Schneider D. P. et al., 2003, AJ 126, 2594
- Reynolds C. S., 1999, in J. Poutanen, R. Svensson (eds.), *High Energy Processes in Accreting Black Holes*, Vol. 161 of *Astronomical Society of the Pacific Conference Series*, 178
- Reynolds C. S., Fabian A. C., 1995, MNRAS 273, 1167
- Ringwald F. A., Naylor T., 1998, AJ 115, 286
- Risaliti G., Elvis M., 2010, A&A 516, A89
- Risaliti G., Elvis M., Fabbiano G., Baldi A. et al., 2007, ApJ Letters 659, L111
- Risaliti G., Elvis M., Nicastro F., 2002, ApJ 571, 234
- Risaliti G., Salvati M., Marconi A., 2011, MNRAS 411, 2223
- Romanova M. M., Ustyugova G. V., Koldoba A. V., Chechetkin V. M., Lovelace R. V. E., 1997, ApJ 482, 708
- Ross R. R., Fabian A. C., 2005, MNRAS 358, 211
- Rottenberg J. A., 1952, MNRAS 112, 125
- Rupke D. S. N., Veilleux S., 2011, ApJ Letters 729, L27

- Rutten R. G. M., van Paradijs J., Tinbergen J., 1992, A&A 260, 213
- Rybicki G., 1970, in H. G. Groth, P. Wellmann (eds.), IAU Colloq. 2: Spectrum Formation in Stars with Steady-State Extended Atmospheres, 87
- Rybicki G. B., Hummer D. G., 1978, ApJ 219, 654
- Sabra B. M., Hamann F., 2001, ApJ 563, 555
- Scaringi S., Körding E., Uttley P., Knigge C. et al., 2012, MNRAS 421, 2854
- Scaringi S., Maccarone T. J., Koerding E., Knigge C. et al., 2015, ArXiv e-prints
- Schechter P., 1976, ApJ 203, 297
- Schmidt G. D., Hines D. C., 1999, ApJ 512, 125
- Schmidt M., 1963, Nature 197, 1040
- Schmidt M., 1965a, ApJ 141, 1295
- Schmidt M., 1965b, ApJ 141, 1
- Schmutz W., 1997, A&A 321, 268
- Seaton M. J., 1959, MNRAS 119, 90
- Setti G., Woltjer L., 1989, A&A 224, L21
- Seyfert C. K., 1943, ApJ 97, 28
- Shakura N. I., Sunyaev R. A., 1973, A&A 24, 337
- Shankar F., Calderone G., Knigge C., Matthews J. et al., 2016, ApJ Letters 818, L1
- Shaviv G., Wehrse R., 1991, A&A 251, 117
- Shen Y., Ho L. C., 2014, Nature 513, 210
- Shen Y., Richards G. T., Strauss M. A., Hall P. B. et al., 2011, ApJs 194, 45
- Shi Y., Rieke G. H., Smith P., Rigby J. et al., 2010, ApJ 714, 115
- Shlosman I., Vitello P., 1993, ApJ 409, 372
- Silk J., Rees M. J., 1998, A&A 331, L1
- Silva C., Uttley P., Costantini E., 2015, in The Extremes of Black Hole Accretion, 63
- Sim S. A., 2004, MNRAS 349, 899
- Sim S. A., Drew J. E., Long K. S., 2005, MNRAS 363, 615
- Sim S. A., Long K. S., Miller L., Turner T. J., 2008, MNRAS 388, 611
- Sim S. A., Miller L., Long K. S., Turner T. J., Reeves J. N., 2010a, MNRAS 404, 1369
- Sim S. A., Proga D., Kurosawa R., Long K. S. et al., 2012, MNRAS 426, 2859
- Sim S. A., Proga D., Miller L., Long K. S., Turner T. J., 2010b, MNRAS 408, 1396
- Simon L. E., Hamann F., 2010, MNRAS 409, 269
- Sluse D., Hutsemékers D., Anguita T., Braibant L., Riaud P., 2015, ArXiv e-prints
- Smak J., 1981, ACTAA 31, 395

- Smak J., 1995, ACTAA 45, 259
- Sobolev V. V., 1957, SvA 1, 678
- Sobolev V. V., 1960, Moving envelopes of stars
- Sobolewska M. A., Siemiginowska A., Gierliński M., 2011, MNRAS 413, 2259
- Soltan A., 1982, MNRAS 200, 115
- Somerville R. S., Primack J. R., Faber S. M., 2001, MNRAS 320, 504
- Springel V., Di Matteo T., Hernquist L., 2005, ApJ Letters 620, L79
- Spruit H. C., 1996, in R. A. M. J. Wijers, M. B. Davies, C. A. Tout (eds.), NATO Advanced Science Institutes (ASI) Series C, Vol. 477 of *NATO Advanced Science Institutes (ASI) Series C*, p. 249
- Stalevski M., Fritz J., Baes M., Popovic L. C., 2013, ArXiv e-prints
- Stalin C. S., Srianand R., Petitjean P., 2011, MNRAS 413, 1013
- Stockman H. S., Angel J. R. P., Miley G. K., 1979, ApJ Letters 227, L55
- Strateva I., Ivezić Ž., Knapp G. R., Narayanan V. K. et al., 2001, AJ 122, 1861
- Struve O., 1935, ApJ 81, 66
- Suleimanov V., Hertfelder M., Werner K., Kley W., 2014, ArXiv e-prints
- Sulentic J. W., Zwitter T., Marziani P., Dultzin-Hacyan D., 2000, ApJ Letters 536, L5
- Surdej J., Hutsemekers D., 1987, A&A 177, 42
- Sutherland R. S., 1998, MNRAS 300, 321
- Tatum M. M., Turner T. J., Sim S. A., Miller L. et al., 2012, ApJ 752, 94
- Thorne K. S., 1974, ApJ 191, 507
- Toohline J. E., Osterbrock D. E., 1976, ApJ Letters 210, L117
- Tombesi F., Cappi M., Reeves J. N., Palumbo G. G. C. et al., 2010, A&A 521, A57
- Tombesi F., Meléndez M., Veilleux S., Reeves J. N. et al., 2015, Nature 519, 436
- Tran H. D., 2001, ApJ Letters 554, L19
- Trump J. R., Hall P. B., Reichard T. A., Richards G. T. et al., 2006, ApJs 165, 1
- Turing A. M., 1948, QJMAM 1(1), 287
- Ueda Y., Inoue H., Tanaka Y., Ebisawa K. et al., 1998, ApJ 492, 782
- Urrutia T., Becker R. H., White R. L., Glikman E. et al., 2009, ApJ 698, 1095
- Urry C. M., Padovani P., 1995, PASP 107, 803
- Ustyugova G. V., Koldoba A. V., Romanova M. M., Chechetkin V. M., Lovelace R. V. E., 1999, ApJ 516, 221
- Uttley P., Cackett E. M., Fabian A. C., Kara E., Wilkins D. R., 2014, AAPR 22, 72
- Uttley P., McHardy I. M., 2001, MNRAS 323, L26

- Uttley P., McHardy I. M., Vaughan S., 2005, MNRAS 359, 345
- Šurlan B., Hamann W.-R., Kubát J., Oschinova L. M., Feldmeier A., 2012, A&A 541, A37
- Van de Sande M., Scaringi S., Knigge C., 2015, MNRAS 448, 2430
- van Regemorter H., 1962, ApJ 136, 906
- Verner D. A., Barthel P. D., Tytler D., 1994, A&As 108, 287
- Verner D. A., Ferland G. J., Korista K. T., Yakovlev D. G., 1996a, ApJ 465, 487
- Verner D. A., Verner E. M., Ferland G. J., 1996b, Atomic Data and Nuclear Data Tables 64, 1
- Vestergaard M., Wilkes B. J., 2001, ApJs 134, 1
- Voit G. M., Weymann R. J., Korista K. T., 1993, ApJ 413, 95
- Wade R. A., 1984, MNRAS 208, 381
- Wade R. A., 1988, ApJ 335, 394
- Walker M. F., 1963, ApJ 137, 485
- Walton D. J., Miller J. M., Harrison F. A., Fabian A. C. et al., 2013, ApJ Letters 773, L9
- Wang B., Han Z., 2012, NAR 56, 122
- Warner B., 2003, Cataclysmic Variable Stars
- Weymann R. J., Morris S. L., Foltz C. B., Hewett P. C., 1991, ApJ 373, 23
- Weymann R. J., Turnshek D. A., Christiansen W. A., 1985, in J. S. Miller (ed.), Astrophysics of Active Galaxies and Quasi-Stellar Objects, p. 333
- White N. E., Stella L., Parmar A. N., 1988, ApJ 324, 363
- Woltjer L., 1959, ApJ 130, 38
- Woods D. T., Klein R. I., Castor J. I., McKee C. F., Bell J. B., 1996, ApJ 461, 767
- Woods J. A., 1991, Ph.D. thesis, D. Phil thesis, Univ. Oxford , (1991)
- Yong S. Y., Webster R. L., King A. L., 2016, PASA 33, e009
- Zakamska N. L., Strauss M. A., Krolik J. H., Collinge M. J. et al., 2003, AJ 126, 2125
- Zanstra H., 1929, Publications of the Dominion Astrophysical Observatory Victoria 4, 209
- Zhang S. N., Cui W., Chen W., 1997, ApJ Letters 482, L155
- Zhou H., Wang T., Wang H., Wang J. et al., 2006, ApJ 639, 716
- Zubovas K., King A., 2013, ApJ 769, 51